AN EXPERIMENTAL STUDY OF THE SEPARATION OF COMBUSTION AND ENTROPY NOISE

A THESIS

Presented to

The Faculty of the Division of Graduate Studies

By

M. Muthukrishnan

In Partial Fulfillment

of the Requirements for the Degree

Doctor of Philosophy

in the School of Aerospace Engineering

Georgia Institute of Technology

August, 1977

AN EXPERIMENTAL STUDY OF THE SEPARATION OF

COMBUSTION AND ENTROPY NOISE

Approved:

Warren C. Strahle, Chairman

Don P. Giddens

Alvin G. Pierce

Date approved by Chairman: 8/19/77

Dedicated to

My late father

ACKNOWLEDGMENTS

It gives me a great pleasure to express my deep gratitude to my teacher and advisor Dr. Warren C. Strahle for suggesting the problem and for his sustained guidance throughout the course of this research program. His ever-willingness to discuss various aspects of the investigation is sincerely appreciated.

I also thank Drs. Don P. Giddens, Alvin G. Pierce, George M. Rentzepis and Prof. Edward W. Price for their careful examination of the manuscript and for their constructive comments.

My thanks are due to Dr. Douglas H. Neale and Dr. John C. Handley for their valuable assistance during the experimental phase of the research program.

The financial assistance provided by the School of Aerospace Engineering and the National Aeronautics and Space Administration, under Grant No. NSG 3015, is gratefully acknowledged.

My sincere thanks go to Mrs. Peggy Weldon for her skillful typing of the manuscript.

Finally, I am grateful to my wife, Lakshmi Krishnan, for her patience, understanding and encouragement during my graduate work.

TABLE OF CONTENTS

TABLE OF CONTENTS (Continued)

LIST OF TABLES

LIST OF ILLUSTRATIONS

LIST OF ILLUSTRATIONS (Continued)

LIST OF ILLUSTRATIONS (Continued)

LIST OF ILLUSTRATIONS (Continued)

SUMMARY

Acoustic experiments have been conducted on a combustor taken from a Boeing 502-7D gas turbine unit. The purpose was to determine the relative importance of combustion and entropy noise in the core noise problem encountered in turbopropulsion systems. The measurements have been made on two types of exit terminations. In one configuration, the burner discharges the hot gases directly into the atmosphere, and no strong pressure gradient is encountered by exhaust gases. This facilitates a good study of combustion noise radiation characteristics. In the other case, a pressure gradient is imposed on the hot gases by attaching a nozzle or orifice plate to the burner exit. Combustion generated hot spots interacting with the pressure gradient give rise to entropy noise in addition to the existing combustion noise. In the present program, the airflow rates have been varied between 7 and 19.8 m^3/min. with overall fuel/air ratio varying between 0.008 and 0.016. The test conditions cover a wide range of exit Mach numbers from 0.05 to 1.0. Measurements consist of combustor interior pressure fluctuations, exterior radiated sound pressures and burner exit plane mean as well as fluctuating temperature. Analysis techniques include spectral, cross-correlation and ordinary as well as partial coherence estimates of the measurements.

The results indicate that hydrodynamic noise, which is non-propagational pseudo-sound, dominates combustion generated noise in the interior of the combustor below 150 Hz. The most important conclusion

of the present investigation is that at low exit Mach numbers, the core engine noise is mostly attributable to combustion noise whereas at high Mach numbers, entropy noise overtakes and dominates combustion noise. This entropy noise domination seems to result from a combination of high level of temperature fluctuations existing at the nozzle entrance plane and large pressure gradients being imposed on them. The present results also lead to a speculation on the possible existence of another propagational noise source, namely, vorticity-nozzle interaction noise, which deserves investigation in a future program.

CHAPTER I

INTRODUCTION

Literature Review

General

In recent years, considerable efforts have been directed towards aircraft noise reduction, with a good degree of success. In the early stages, the aircraft propulsion system was a main target. As far as aircraft engines are concerned, fan noise and jet noise were the easily identifiable sources and hence received a great deal of attention in noise reduction programs for modern turbopropulsion systems. Striking progress has been achieved in fan noise reduction through the incorporation of new fan designs as well as acoustic treatments of fan inlets and exhaust ducts, whereas jet noise has been minimized by the use of high by-pass ratio engines. With the introduction of these improvements, modern aircraft engines have met the present noise certification requirements. However, considering the stringent requirements which may be enforced in the future, it is becoming evidently clear that many noise sources, situated inside the engine core and hitherto considered as secondary, may gain prominence. It is also predicted that these new noise sources will soon constitute a threshold and thus offset the benefits that may be derived by future application of more advanced techniques in fan and jet noise reduction. It is this reasoning that motivated research workers to have a fresh look at these noise sources,

called "core engine noise." According to the most acceptable definition, core engine noise is referred to as the total noise generated by all the components situated inside the engine core and exhaust systems such as combustor, turbines, nozzles, etc.

The subject of core engine noise is of recent origin and, until today, it is poorly understood and inadequately controlled. The existence of core engine noise has been confirmed by experimental evidence. Bushell[1] measured the noise radiated by a number of jet engines at various jet velocities. His results showed a good comparison of the measured noise levels with the familiar jet noise eighth power scaling law at higher velocities. However, at low velocities, his measurements revealed higher noise levels than dictated by jet noise scaling laws. This led to the strong belief that, at low velocities, some other noise sources, not encompassed in the eighth power scaling law and located inside the engine,also contribute significantly to the exterior radiated noise. These were later designated "core engine noise" sources. References 2, 3, 4, 5 and 6 present a brief survey of the possible core engine noise sources and prediction methods for the observed noise levels.

Research work concerning core engine noise was carried out at two different levels. On one hand, the aircraft industry conducted experiments on full size engines with sophisticated instrumentation. They were mainly interested in obtaining overall core engine noise levels and their correlations with engine operating parameters.[4,5] On the other hand, academic institutions were concentrating their efforts in understanding the basic source mechanisms involved in core engine noise

radiation. They relied heavily on the component testing for their primary source of data. Simple configurations were used for rational interpretation of their analytical results.

A narrow band analysis of the core engine noise exhibits a broad band spectrum at low and medium frequencies while containing turbine tones, corresponding to blade passing frequencies in the higher frequency regime. It has been recently established that direct combustion noise (hereafter referred to as combustion noise) and indirect combustion noise (hereafter referred to as entropy noise) are the main sources responsible for the observed low frequency core engine noise radiation. The present research topic is concerned only with the low frequency core engine noise and, hence, a brief survey of the state of the art pertaining to combustion and entropy noise is presented below.

Combustion Noise

Combustion noise, attributable to the turbulent combustion process, is discussed in the literature in great detail. Combustion noise is generated due to fluid dilatation which, in turn, is caused by heat release rate fluctuations. The fluctuating heat release rate owes its origin to turbulence. Recently, Strahle[7,8,9] has carried out extensive theoretical studies on the noise generated by open flames. He has assumed that the combustion noise is noise caused by a velocity source and arrived at a wave equation resulting from the fluctuating heat release rate in a turbulent flame. He was also successful in developing theoretical scaling laws for the radiated acoustic power by open flames. Chiu et al.[10] concluded from their theoretical studies that the acoustic power radiated by the combustion process is proportional

to a product of combustion sound number and flame structural factor which contains the detailed structure of the flame.

On the experimental side, Shivashankara et al.[11] have reported extensive data on the directionality patterns and acoustic spectra of the noise generated by open flames anchored at the ends of burner tubes. Reference 11 also contains reliable scaling laws for the acoustic power radiated and the frequency of maximum radiated power. Continuing the work of Reference 11, Muthukrishnan et al.[12] conducted noise measurements on open flames anchored at various flameholders to study the effects of flame retention techniques on the noise radiation characteristics of open flames.

The above analytical and experimental studies have led to the conclusions that in the case of open flames, combustion noise dominates jet noise even up to velocities of 600 ft/sec., and the combustion noise spectrum is a broadband one with a single broad peak in the frequency range of 200 - 1000 Hz. The far field measurements of the radiated acoustic power characterize the combustion noise as a monopole type regardless of the different flame stabilization techniques employed.

However, in practical cases, like turbopropulsion systems, combustion takes place in a confined space. Hence, there was a strong need for understanding the characteristics of the noise radiated by enclosed flames.

Chiu et al.[13] made analytical and experimental studies on the acoustic interaction between the combustion process and the enclosure system in the case of ducted flames. They concluded that the confinement of the flame has induced strong oscillations leading to duct

resonances which cause an increase in the noise levels when compared with open flames.

Abdelhamid et al.[14] have conducted tests on the noise radiation by subsonic jets discharging from a combustion chamber. Through cross-correlation techniques, they established a correspondence between chamber pressure oscillations and observed far field noise characteristics and attributed the origin of much of the radiated noise to the inside of the combustor. They also concluded that radiated noise levels were heavily dependent on fuel/air ratio, geometry of the combustor and overall mass flow through the combustor.

Strahle and Shivashankara[15] have also reported augmentation of the radiated acoustic power in the case of enclosed flames, attributing it to the change in the radiation impedance of the flame.

Very recently, Strahle and Shivashankara[16] have carried out noise measurements on a single gas turbine combustor exhausting to the atmosphere. They concluded that for a fixed fuel type, the acoustic power output had a very weak dependence on fuel/air ratio, but strongly depended on the total air flow rate. The spectral analysis of their measurements has exhibited familiar combustion noise characteristics with several weak peaks resulting from ground reflections.

Entropy Noise

With the attainment of significant progress in the understanding of the combustion process as a direct source of noise generation, attempts were made to study the indirect contributions of combustion to the overall noise generated. This is called entropy noise which arises

due to combustor generated non-uniformities, such as temperature fluctuations, interacting with downstream components of the engine like the turbine or nozzle. When these non-uniformities (hot spots) pass through regions with a mean pressure gradient, they are accelerated differently than the surrounding fluid. To maintain continuity, unsteady pressure waves are created which are termed "entropy noise." There is a strong speculation that entropy noise may be a chief competitor to combustion noise.

Tracing the literature of entropy noise, Cuadra[17] solved the problem of acoustic wave generation due to the convection of an entropy wave past an infinitesimal area change. Crocco and Sirignano,[18] in relation to the combustion instability problem, analyzed the behavior of supercritical nozzles under three dimensional oscillatory flow conditions and obtained admittance coefficients at the nozzle entrance.

Candel[19] has presented an analytical treatment for the case of noise generation due to convection of upstream generated simple harmonic entropy and pressure fluctuations through a choked nozzle. He has discussed a novel noise source mechanism arising from the partial conversion of entropy fluctuations into pressure fluctuations by a non-homogeneous velocity field present in the nozzle.

Wahbah[20] has made a theoretical study of internal noise generation due to the passage of entropy waves in a constant area duct terminated with a choked nozzle. He has assumed a model of transient entropy waves, created by the injection of an additional fluid at a temperature different from that of main flow inside the duct. Pickett[21] has claimed success in calculating the low frequency core engine noise levels

analytically by analyzing the acoustic waves created due to the interactions of upstream generated vorticity and temperature fluctuations with an actuator disc, modelling the turbine blade row.

Cumpsty[22] has assumed a model which attributes the observed low frequency core engine noise to the interactions of temperature fluctuations in the gas with the turbine. A theory is developed based on the above mechanism to calculate the acoustic power output from the actual engines.

Strahle[23] has recently investigated the possibility of entropy noise generation in turbopropulsion systems brought about by the variations either in the molecular weight or heat capacity, associated with variable mixture ratios.

Regarding the suspected sources of core engine noise, the literature contains contradicting claims. While Grande[24] and Mathews et al.[25] have reported correlations of the observed low frequency core engine noise based on combustion noise, References 21 and 22 claim successful correlations by attributing it to entropy noise. This is not too surprising reviewed from the fact that both these noise sources have the combustion process as their origin. It is clear from the above statements that identifying the dominant interior source responsible for the exterior core engine noise radiation will be clouded with uncertainty until experiments designed solely for separating combustion and entropy noise effects are performed. Until now, no work has been reported with this objective. In short, the literature survey points out a need for further study in understanding the relative importance of the various noise sources involved in low frequency core engine noise radiation.

Objectives of the Research

The main objective of the present research program is to perform acoustic experiments on a given combustor with a view to isolate qualitatively the individual effects of two suspected sources of core noise, namely, combustion and entropy noise. Also intended is a study of their relative importance to the core noise problem. This is feasible only if one can relate the processes taking place inside the combustor to the exterior radiated sound over a wide range of operating conditions. This leads to the following tasks:

1. To conduct pressure fluctuation measurements both interior and exterior to the given combustor at various operating conditions, with hot exhaust gases encountering different pressure gradients. The presence of a strong pressure gradient is important for the generation of entropy noise whereas combustion noise is present under all exit conditions.

2. To obtain details of temperature fluctuations of hot gases at the burner exit plane to characterize entropy noise. This is necessary because the temperature fluctuations, convected through a mean pressure gradient, give rise to entropy noise.

3. To perform spectral analysis of the measurements mentioned in tasks 1 and 2 and also obtain coherence estimates between interior and exterior measurements.

It is believed that spectral and coherence results obtained from various operating conditions will yield enough information to assess the degree of influence exerted by the individual noise sources, namely, combustion and entropy noise, on the core engine noise radiation.

CHAPTER II

EXPERIMENTAL PROCEDURES

An Outline of Approach

The noise experiments, mentioned in this program have been conducted on a can-type gas turbine combustor. The measurements were made separately for two different exit terminations of the above combustor. In one configuration, the burner discharges the hot gases directly into the atmosphere and this facilitates the study of combustion noise characteristics mostly. In the other case, a pressure gradient is introduced on the hot gases, by attaching a nozzle or an orifice plate to the burner exit. As mentioned in the previous chapter, this leads to the generation of entropy noise, in addition to the existing combustion noise. In both cases, the interior pressure fluctuations, the exterior radiated sound pressures and the temperature fluctuations at the burner exit plane have been measured. The signals are then analyzed for spectral content and coherence estimates. The results pertaining to both the exit terminations are compared and these comparisons are used to bring out the dominant noise sources at various operating conditions and their radiation characteristics.

Combustor Details

The combustor, used in the present investigation, is of can-type, taken from a Boeing 502-7D gas turbine engine unit. The original air inlet has been modified to suit the experimental set-up. Figure 1 shows

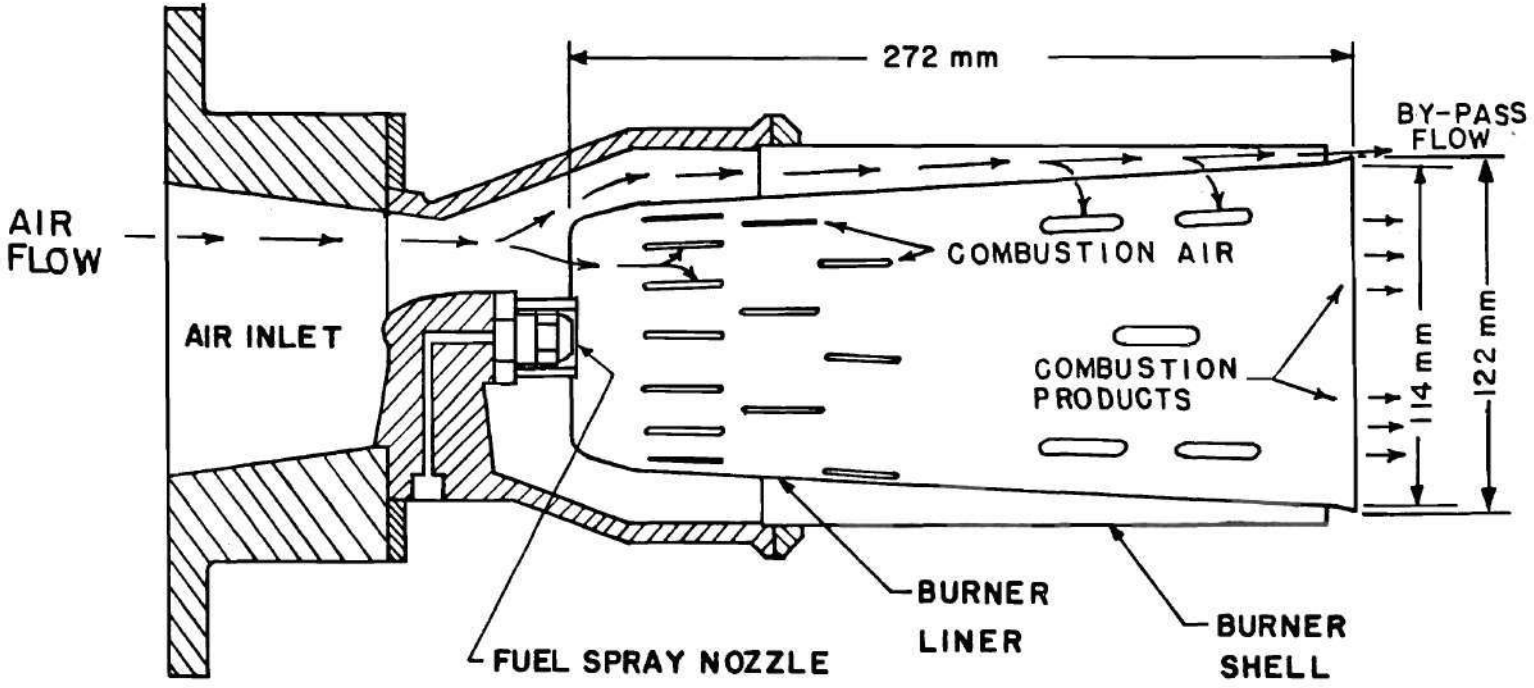

Figure 1. Combustor Details.

a cross-sectional view of the combustor. Liquid fuel is sprayed into the burner liner through a fuel nozzle. Air for combustion enters through the slots in the head end and walls of the liner. The by-passed air leaves the combustor through the annular space between the liner and the burner shell. The geometry and the arrangement of the slots is shown in Figure 1. A spark plug is used to ignite the fuel/air mixture. Stable operation limits for this combustor were determined in a previous program (Reference 16). The by-pass air flow rate is measured to be 26% of total air supplied. Pitot pressure distribution and mean temperature distribution of the hot gases at the burner exit plane are reported in Reference 26.

Flow Systems

The schematic lay-out of the flow system is shown in Figure 2. Air for the combustor is supplied from an 861 KPa air reservoir, regulated by a valve and metered by an orifice meter. A muffler is provided in the line, upstream of the combustor, to reduce the flow noises. Fuel is pumped from a tank to the fuel spray nozzle by nitrogen pressurization. A turbine flow meter measures the fuel flow rate through the system. The muffler, the fuel tank and the combustor are all mounted on a test stand outside the laboratory at an open site while the flow control valves, the flow meter displays and the data acquisition systems are situated inside the laboratory.

Measurement Techniques

Pressure Fluctuation Measurements

The main task of separating combustion and entropy noise

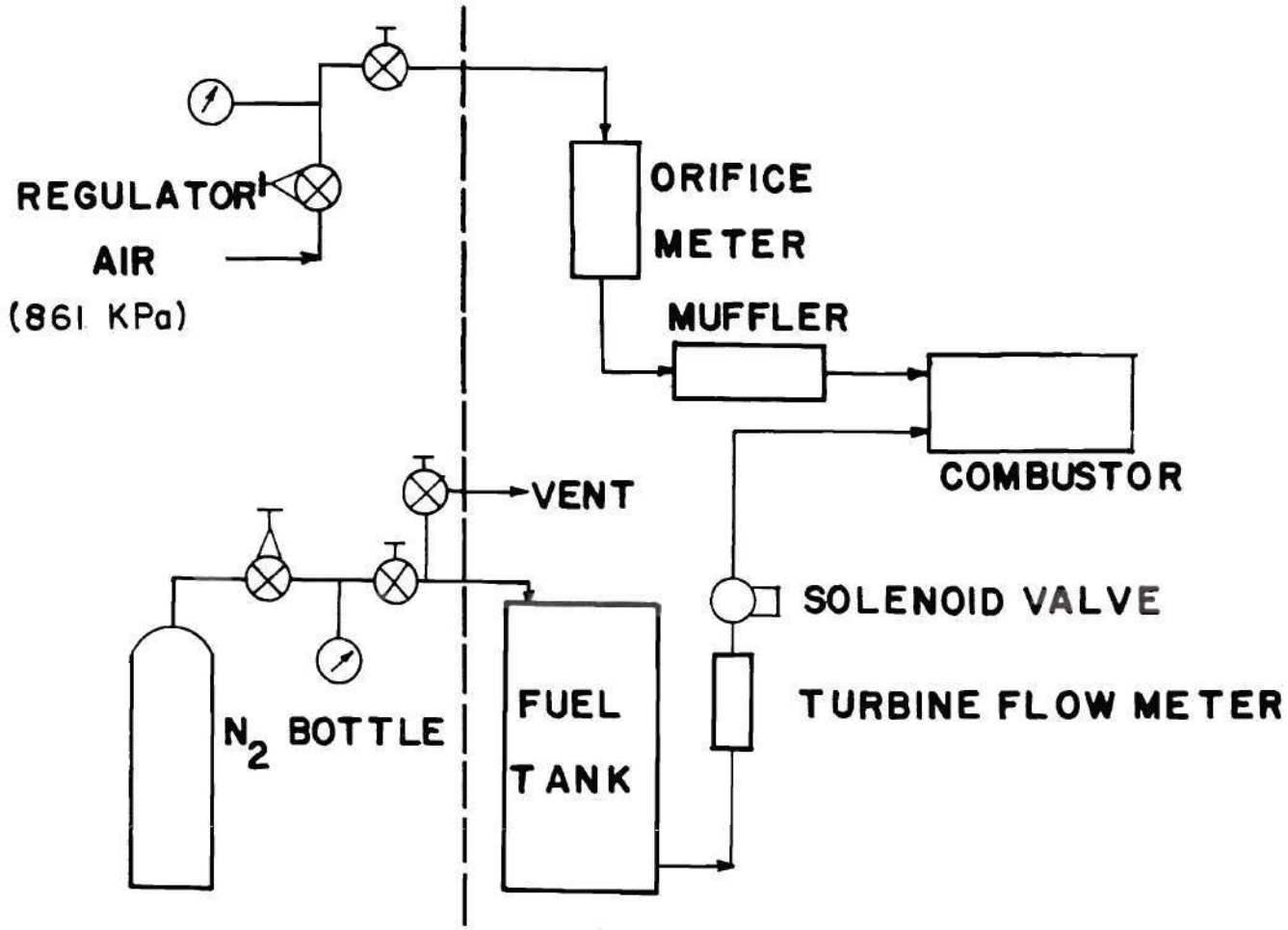

Figure 2. Flow System Schematic.

characteristics can be made easier if proper links are established between the combustor interior events and the associated exterior effects. The interior pressure fluctuations are measured either by an AVL pressure transducer or a photocon transducer depending on the measurement objectives. The AVL transducer is flush mounted in the burner can walls and directly exposed to the flame. Hence, this is water-cooled to withstand the high temperature of the flame. The AVL transducer works on a piezoelectric principle. For reasons to be explained in the next chapter, the photocon transducer is mounted in a location slightly displaced away from flow field through an infinite tube assembly. Hence, this does not need water cooling. The photocon transducer can extract signals above 130 dB referred to 2×10^{-5} N/m^2 compared to that of 135 dB by the AVL transducer. The near and far field radiated sound pressures are monitored by two Brüel and Kjaer type 4134, 12 mm condenser microphones. The relative positions of these transducers are shown in Figure 3. All these pressure transducers are calibrated by a Whittaker type Pc-125 acoustic calibrator.

Temperature Fluctuation Measurements

As stated earlier, the entropy noise study requires the details of combustion generated hot spots; and hence, temperature fluctuation measurements of the hot gases at the burner exit plane have been carried out. This is accomplished using fast response Chromel-Alumel thermocouples. The choice of proper wire diameter for the thermocouple junction is made under a compromise between two contrasting requirements. While a larger diameter thermocouple junction increases the longevity, it is well known that the speed of response is improved by using a

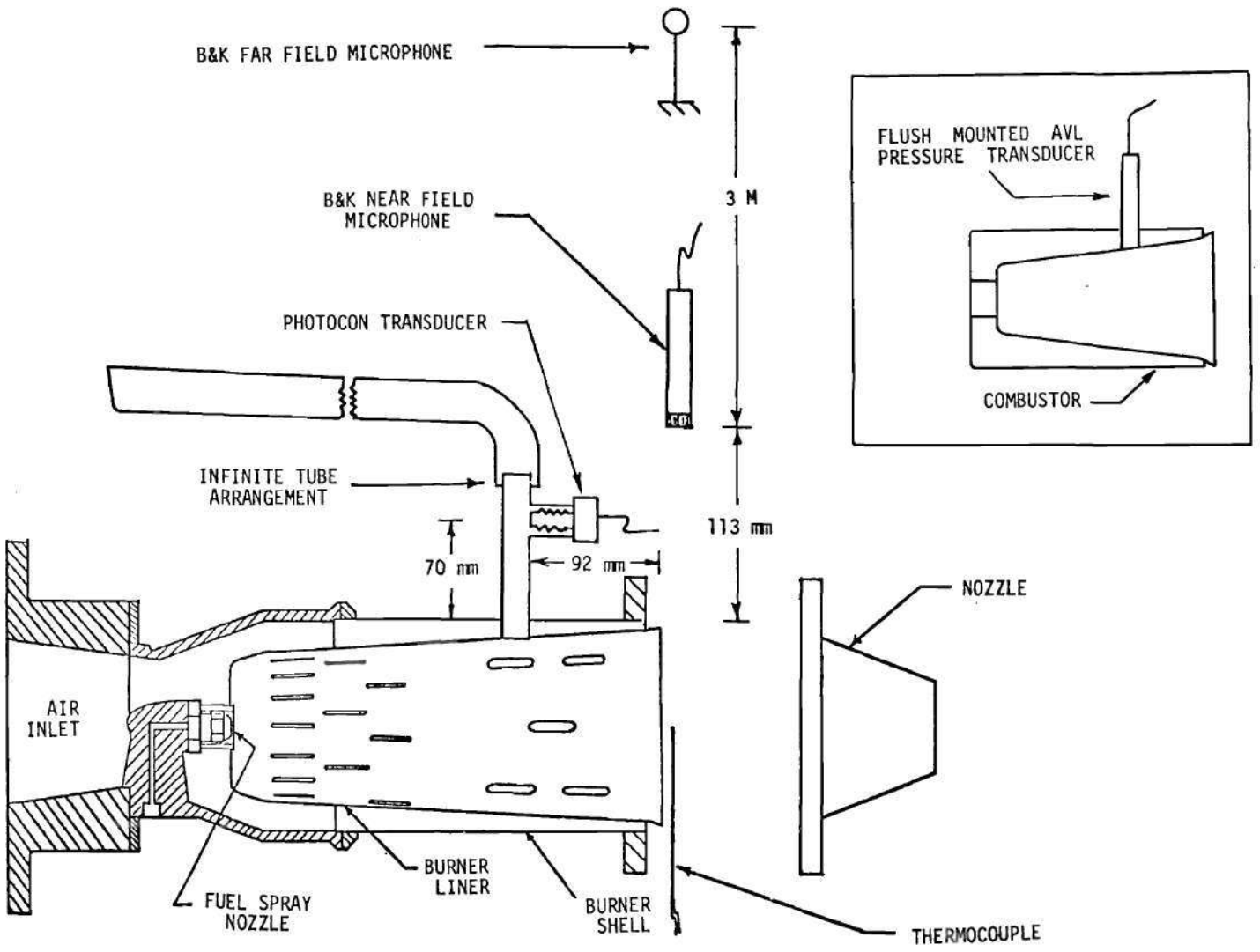

Figure 3. Schematic of Experimental Set-up with Relative Positions of Transducer Locations.

smaller diameter thermocouple junction. In the present program, a thermocouple junction constructed from wire of diameter 0.025 mm is selected to serve the requirements based on its operational characteristics and cost. According to the manufacturer (HY-Cal Engineering Company), these specific thermocouples have response times less than 10 msec.

When a thermocouple is used as the primary element for rapidly fluctuating temperature measurements, the thermal lag of the element, caused by the slow rate of heat transfer between the element and the surrounding gas, limits the ability of the element to follow such fluctuations truly. This thermal lag is quantified by a parameter called the "time constant" of the thermocouple. The value of the time constant depends mostly on the properties of the thermocouple junction and the fluid dynamic environment in which the element is used. It is important to note that the thermocouple output has to be properly compensated for its time constant to yield accurate results. This leads to the primary task of finding the time constants of the thermocouples, preferably under operating conditions.

Methods usually described in the literature[27] consist of either subjecting the thermocouple to sudden changes in the temperature, using cold and hot streams, and noting its subsequent impulse response, or turning off an initial current through the wire and watching the temperature decay to the temperature of the environment. These conventional methods have their own limitations. When the response time of the thermocouple is much shorter than the time involved in the mechanical switching operations, reliable results cannot be guaranteed. Secondly, there is also a great concern as to accepting the time constant,

determined under simulated surroundings, as valid under operating conditions also. This has motivated the search for a reliable method of determining the time constants of the thermocouples. In this program, an experiment has been designed towards this goal based on a recent theory developed by Strahle.[28] The theory involves the cross power spectra of the signals, obtained from two thermocouples of differing junction sizes, simultaneously exposed to the actual test conditions. The experimental procedure and the theoretical support pertaining to this new method of time constant determination are described in Appendix A. It is found from experience that any two thermocouples, even if constructed from the same diameter wire, are likely to have different time constants. Though this difference is very small, it is found to change spectral levels slightly. Hence, each time a new thermocouple is used, its time constant is obtained separately. Thus, the time constants of the various 0.025 mm wire diameter thermocouple junctions used in this program, varied between 3.6 to 4.5 msec. It is also observed that the differences in time constants of a particular thermocouple over the range of test conditions are negligibly small. Once the time constant is determined, the next step is to correct the thermocouple signals for this thermal lag. In conventional methods, the thermocouple signal is compensated for the time constant by adding suitable electrical compensation networks at the test site itself. But in the present program, the signals are corrected later during data analysis by suitable modification of Fourier Analyzer programming, as explained in Appendix A. To summarize, this new method not only allows the time constant to be determined under actual test conditions but also yields

a simpler compensation procedure.

The temperature measurements of interest in the present program are the mean temperature of the hot gases, the spectral details and spatial correlation length scales of the temperature fluctuations at the burner exit plane. The first two can be obtained by using a single thermocouple whereas the correlation study requires two thermocouples simultaneously. One of the thermocouples will be monitoring temperature fluctuations at a fixed place in the burner exit plane while the other one will be registering the signals at various locations moving radially away from the former. This radial traverse is repeated for various angular positions to check the axisymmetric nature of the correlation length scales. Thermocouples of junction size 0.025 mm have been used in all these cases.

Data Acquisition Scheme

The pressure and temperature fluctuation data are obtained through the instrumentation scheme shown in Figure 4. The overall sound pressure levels, registered by microphones, are read out on a Brüel and Kjaer type 2606 microphone amplifier, one at a time. The mean temperature of the hot gases at the burner exit plane is measured with a digital voltmeter included in the thermocouple line. A 20 Hz high pass filter following the digital voltmeter removes the d.c. component of the thermocouple signal corresponding to the mean temperature which would otherwise saturate the tape recorder due to high amplifications involved in the later stages. All the pressure transducer and thermocouple signals are amplified by an array of four NEFF type 122 amplifiers and recorded

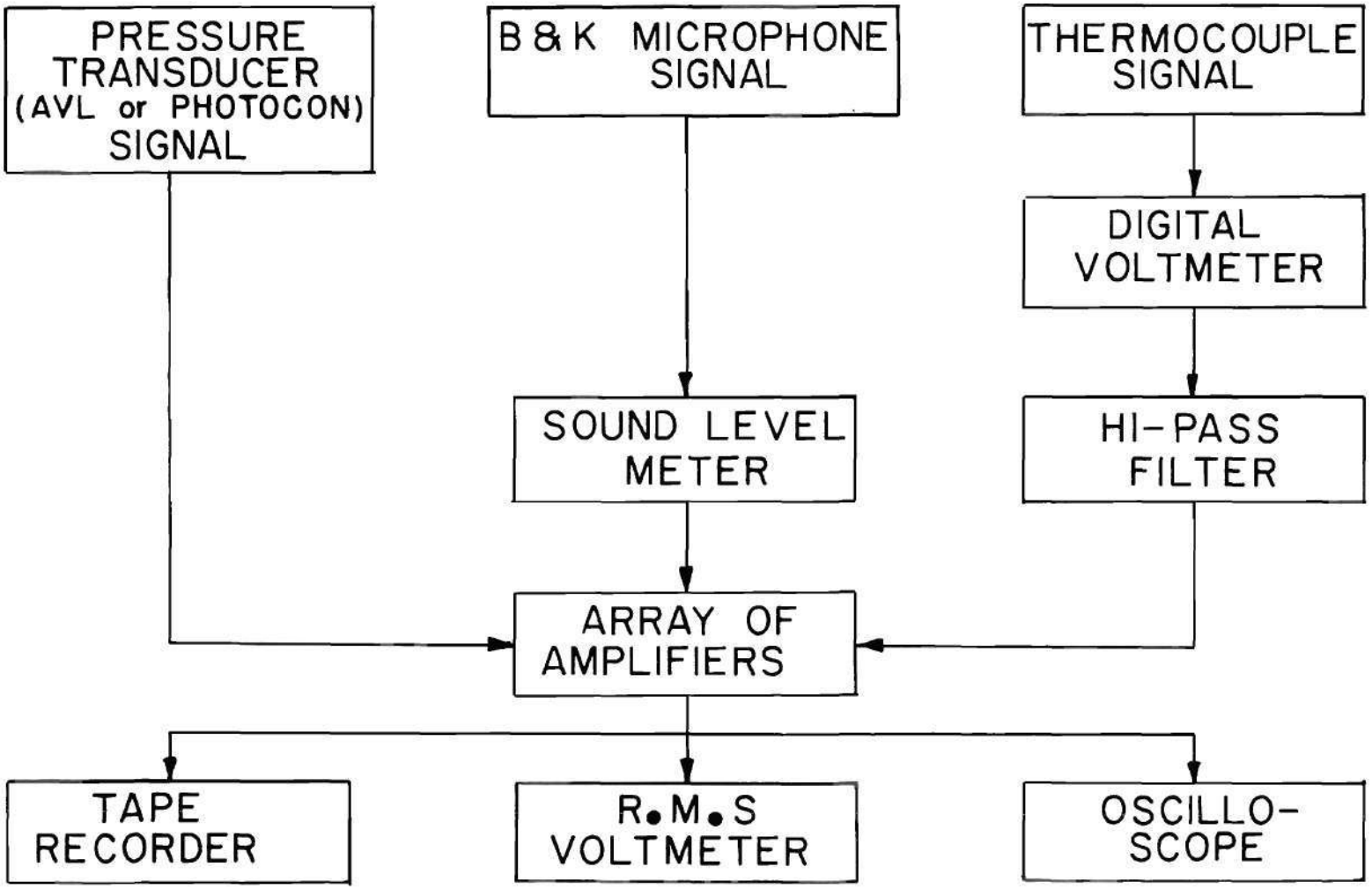

Figure 4. Measurement System Schematic.

on four channels of an ampex FR 1300, 14 channel magnetic tape recorder at 30 ips tape speed. The r.m.s. levels of the amplified signals are indicated by a true r.m.s. voltmeter whereas their visual display is available on the oscilloscope screen.

Data Reduction Procedures

The data reduction schematic is shown in Figure 5. The Fourier Analyzer system 5451A plays a key role in the data analysis. This system consists of a 5465A 10 bit 2 channel analog to digital converter and a Hewlett-Packard 2100A computer with 16K memory. The system has facilities for various forms of data input and output. The recorded signals on the magnetic tape are played back at 1 7/8 ips and these analog signals are sampled through the analog to digital converter. These digitized data are then subjected to different time series analyses with the help of the built-in fast Fourier transform algorithms. A brief description of the various signal processing techniques involved in the present data reduction program is given below.

Spectral Analysis

Spectral analysis is a frequency domain analysis and describes the way the energy of a signal is distributed over the frequency range of interest. The auto spectrum of a single signal or the cross spectrum of two signals can be obtained by keyboard programming of the Fourier analyzer. A low pass filter, as shown in Figure 5, is introduced to prevent the aliasing phenomenon. It is well known in the signal processing techniques that if the sampling rate for an incoming signal is not greater than twice the highest frequency of any component in the signal,

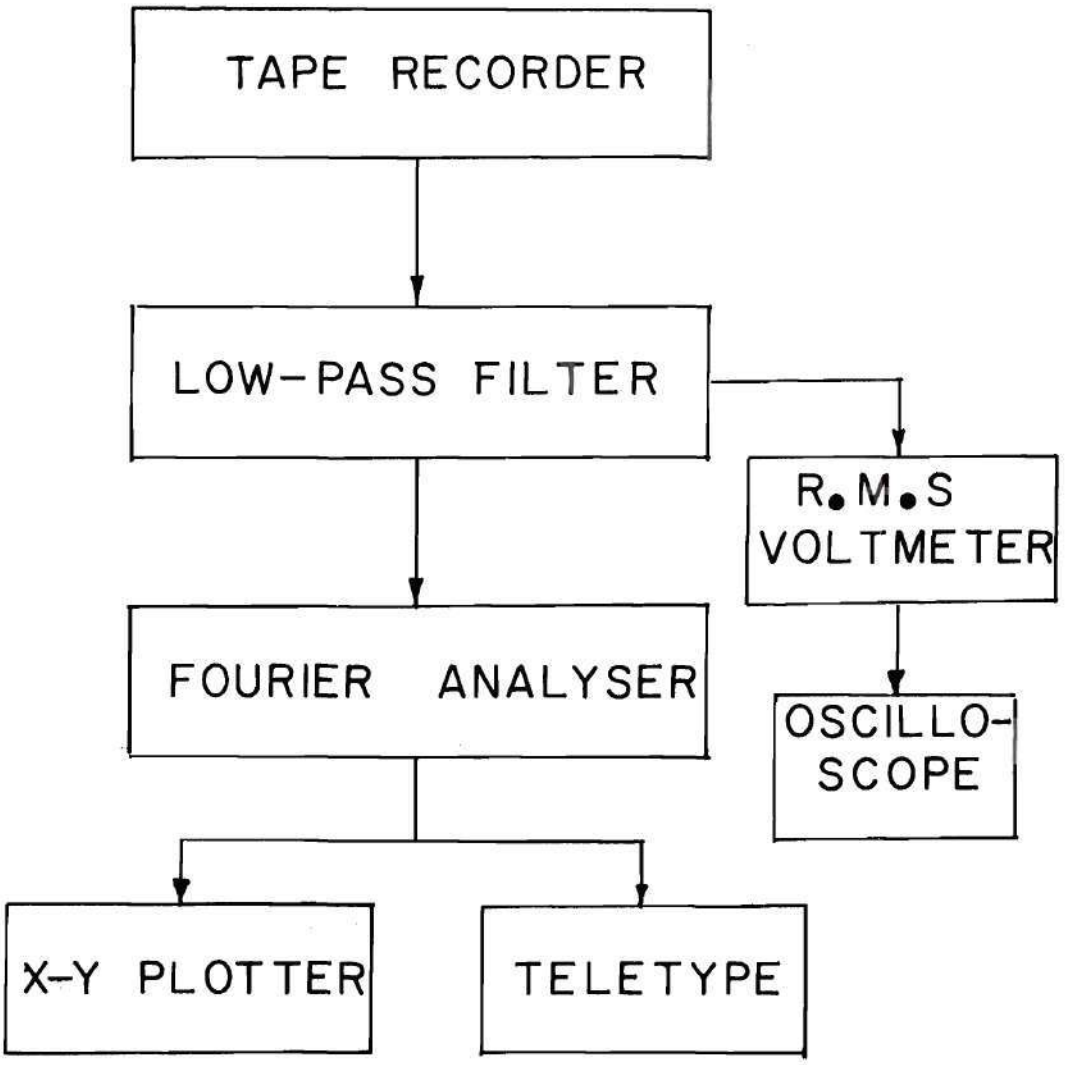

Figure 5. Data Reduction Schematic.

then some of the high-frequency components of the signal will be translated down to be less than one-half the sampling rate, causing serious problems by way of interference of high and low frequency components. This folding action is called aliasing. This can be avoided in two ways. One method requires the sampling of the incoming signal at a sufficiently high rate; the other one is to filter off the frequencies above the range of interest since this enables the use of a lower sampling rate. In the present spectral analysis program, the latter method has been used.

Another common problem in signal processing is the window effect.[29] The window here refers to the time window which is the duration through which the signal is observed. A rectangular time window has an abrupt rise and fall at the ends. When a continuous signal is analyzed through a finite rectangular window, the discontinuities at the ends of the sample frame leads to an unwanted set of spectral components in the analysis, interfering with the components of interest. This action is sometimes termed the "leakage effect." This effect is greatly minimized by using a suitable window shape and a commonly used one is the "Hanning window" which has a smooth transition from zero to the maximum value and back to zero. It is important to note that when a Hanning window is used for analysis, the spectral results have to be properly corrected for the reduction in the window area.[29]

Coherence Estimates

In the present investigation, coherence analysis is expected to play a key role in separating the effects of combustion noise from entropy noise. This is a frequency domain function and has a more

usable form than its time domain counterpart, namely the correlation function. Mathematically, the coherence function γ^2 between two signals 1 and 2 is expressed as

$$\gamma^2 = \frac{|\overline{S}_{12}|^2}{\overline{S}_{11}\overline{S}_{22}}$$

where $|\overline{S}_{12}|^2$ is the square of the magnitude of the many-sample-averaged cross power spectrum formed between two signals 1 and 2 and $\overline{S}_{11}$ and $\overline{S}_{22}$ are the many-sample-averaged auto spectra of the signals 1 and 2 respectively. Stated in simple words, this function establishes the degree to which the output is solely caused by the input for linear systems. This function is normalized in such a way that it has a value between 0 and 1 at all frequencies. A coherence value of 1 means that there is a perfect coherence between the two signals. It will be less than one if one of the signals is influenced by not only the other signal but also by any other uncorrelated signal. The coherence results are not affected by the transmission paths and the transducer gains.

In the present program, two types of coherence techniques are used, namely ordinary and partial coherence estimates. The ordinary coherence technique is employed only when a single input and a single output is involved. In the present investigation, under some operating conditions, the near field microphone receives contributions from two interior noise sources and thus a case of a multiple input problem arises. In such cases, the degree of linear relationship between any single cause and effect is best revealed through the partial coherence function

analysis. This is achieved by computing the partial coherence between the two variables, when the effects of other extraneous variables have been subtracted out through a linear least-square prediction procedure. The theory and the calculation procedures involved in the partial coherence estimates are explained in detail in Reference 30. The modeling of the present problem to exploit the partial coherence analysis is explained in the next chapter.

Correlation Techniques

Correlation is a time domain analysis and brings out the extent of similarity between two signals. When a signal is compared with itself, the result is the auto-correlation whereas two different signals are compared in the case of cross-correlation. Mathematically, the cross-correlation function R_{xy} between two signals $x(t)$ and $y(t)$ is expressed as

$$R_{xy}(\tau) = \lim_{T \to \infty} \frac{1}{T} \int_{-T/2}^{+T/2} x(t)y(t+\tau)dt$$

where T is the observation time and τ is the time delay between two signals. It is well known that the maximum value of the auto-correlation function occurs at zero time delay while the cross-correlation function maximizes at some time delay which has some physical significance in some applications.

In the present program, the main interest is to obtain the spatial correlation length scales for the temperature fluctuations. As already explained in the measurement section, two thermocouples of the same wire diameter (0.025 mm) are used to monitor the temperature fluctuations

at the burner exit plane. One of them will be registering the temperature fluctuations at a fixed place while the other one, moving radially away from the former, registers the fluctuations. The cross-correlation technique is applied between the fixed thermocouple signal and the moving thermocouple signal. The value of the cross-correlation function corresponding to zero time delay is picked up and normalized by the product of their corresponding root mean square values to obtain the cross-correlation coefficient. Thus, cross-correlation coefficient values as a function of separation distance between the two thermocouples are obtained. These results are discussed in the next chapter.

It is important to note that the results of the correlation analysis are affected by wrap-around error,[29] which arises due to the misrepresentation of the original signal during the finite window Fourier transform analysis. When the Fourier analyzer takes in a portion (a frame) of the original signal, the standard Fourier transform uses the duration of the frame as the basic period for the analysis and in doing so it assumes a signal that is the original frame continuously repeated. This assumed signal has a wave form which is different from that of the original one and this leads to the erroneous results. This problem is remedied by clearing the end portions of the frame and then carrying out the subsequent operations, as explained in Reference 29.

Error Analysis and Spectrum Averaging

Often, there is a practical restraint that measurements can be made on only one sample function or on only a few sample functions from an infinite ensemble. Furthermore, it will be physically possible to analyze only a limited length of any given sample function. These two

factors introduce errors in the measured spectra. A detailed analysis of these errors is given in Reference 30. An often encountered one is the variance error, also labelled as "random error." When a stationary random signal of effective bandwidth B_e and a total record length T_{tot} is divided into n_f frames each of individual length T and spectrally analyzed and averaged, the normalized random error ε_r for such an average power spectral estimate is given as below.[30]

$$\varepsilon_r = \frac{1}{\sqrt{B_e T_{tot}}} = \frac{1}{\sqrt{n_f}}$$

where $B_e = \frac{1}{T}$ and $T_{tot} = n_f T$.

In the present program, in many cases, a 100 frame average has been found to be sufficient to obtain statistically stable results. In some cases, the estimates even after many frame averaging, were so low that they were in the range of statistical error bounds. This situation has been remedied by a technique called spectral smoothing. In this process, the spectral estimates corresponding to a number of adjacent bands have been averaged. Because of the increased bandwidth, this procedure improves the statistical accuracy of the results, imposing at the same time a penalty on the frequency resolution.

CHAPTER III

RESULTS AND DISCUSSION

As stated in the earlier chapter, the noise experiments have been carried out on a combustor with different exit terminations. In one configuration, the hot gases are discharged into the atmosphere directly and no strong pressure gradient is encountered by hot gases. In the other one, a nozzle or an orifice plate is attached to the burner exit, thereby forcing a pressure gradient on the hot gases. In this chapter, first the results of the nozzle-off tests are reported and later a comparison of nozzle-off and nozzle-on test results is made.

Separation of Combustion and Hydrodynamic Noise

The first series of tests have been carried out with only the burner can operating and the hot gases being discharged into the atmosphere directly. In this series of tests, internal pressure fluctuations are monitored by a flush mounted AVL pressure transducer, whereas near and far field sound pressures are measured by Brüel and Kjaer microphones. The measurements are repeated over a wide range of test conditions with total airflow rates varying between 14.2 and 28.4 m^3/min. and fuel/air ratios between 0.006 and 0.016. Fixed bandwidth spectra of internal, near field and far field signals have been obtained.

Figure 6 shows the spectra of interior pressure fluctuations, corresponding to the extreme test conditions. In all cases, the spectra can be broadly divided into two regimes; below about 200 Hz, the spectra

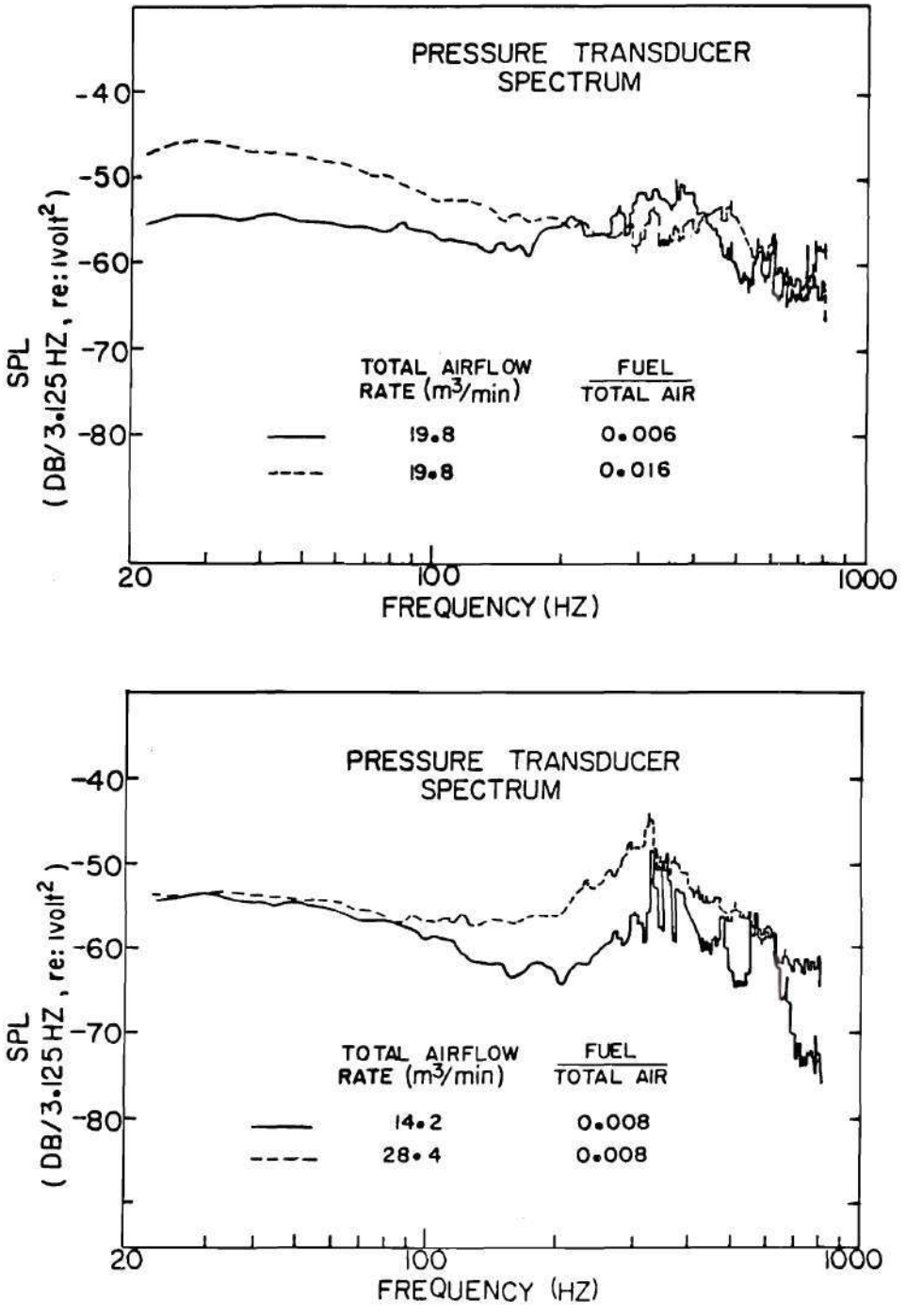

Figure 6. Interior AVL Spectra as a Function of Airflow Rate and Overall Fuel/air Ratio.

are almost flat and above 200 Hz, a hump appears in all cases. Also, a weak quarter wave resonance of the burner can is seen in all the spectra in the vicinity of 400 Hz, depending upon the fuel/air ratio.

The near field spectra for various test conditions are shown in Figure 7. All spectra display similar behavior. At low frequencies, below 200 Hz, the near field spectra fall off rapidly at about 13 db/ octave in contrast to an almost flat interior spectrum. However, above 200 Hz, the near field spectrum has behavior very similar to the interior one. A broad band combustion noise peak, around 200 Hz, is seen in all near field spectra. A peak around 400 Hz is due to the quarter wave resonance of the burner can and should not be mistaken for a combustion noise peak. This is confirmed through Figure 8 which shows a typical near field spectrum, covering a wider frequency range, wherein 1/4, 3/4 and 5/4 wave resonance peaks can be seen clearly. These resonance peaks are not strong thereby suggesting that the burner can walls are highly absorbing.

A typical far field spectrum, shown in Figure 7, seems to be affected by severe ground reflection effects. This makes it difficult to pick up the resonance peaks from the far field spectrum. This is the main reason for choosing the near field microphone for spectral diagnostic purposes. Interestingly, an overlay of near and far field microphone spectra will clearly separate the resonance peaks from ground reflection effects. Stated otherwise, there is a good similarity between near and far field spectra in the overall behavior. However, it is important to note that the use of the near field microphone,

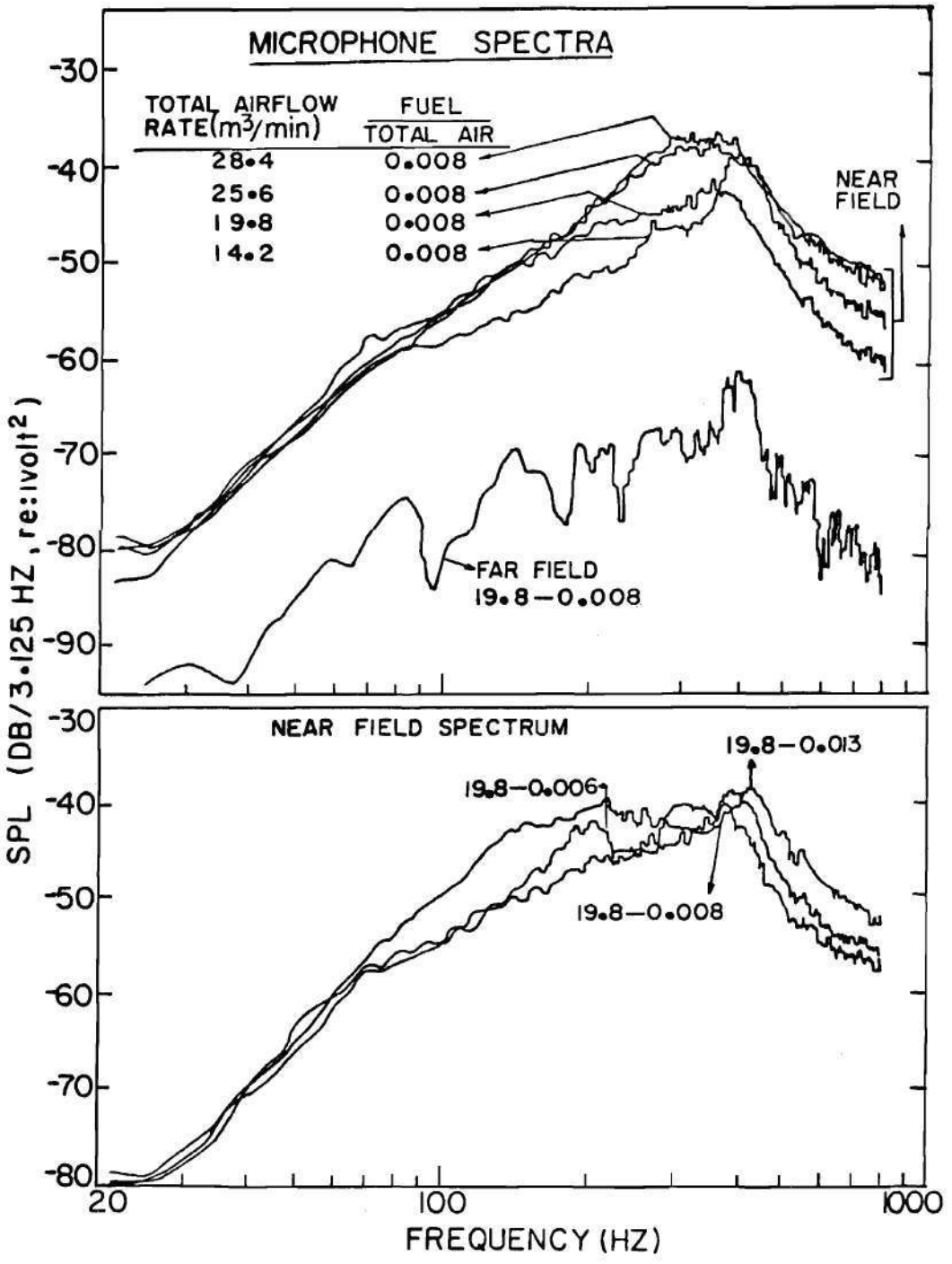

Figure 7. Near Field Microphone Spectra as a Function of Airflow Rate and Overall Fuel/air Ratio. Also Shown is a Typical Far Field Spectrum.

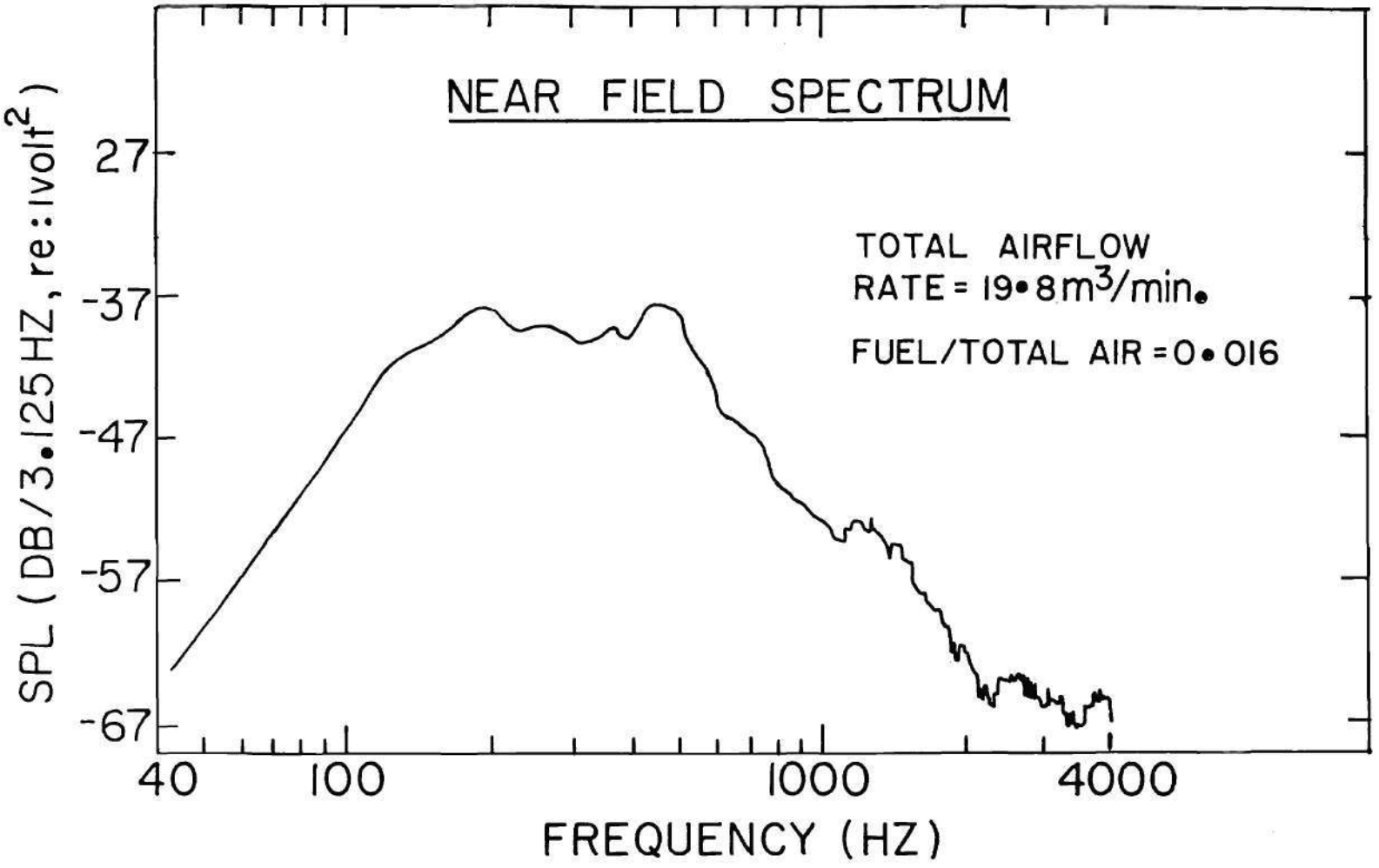

Figure 8. Near Field Spectrum Exhibiting Burner Can Resonances.

instead of the far field one, to represent the exterior radiated sound pressure is valid only if the coherence between near and far field signals is very good, at least in the frequency range of interest. This condition is indeed satisfied, as explained later.

While spectral analysis brings out the nature of the frequency content of the signals, the cause-effect relationship is best illustrated through the coherence estimates. As stated in the previous chapter, the coherence has a value between 0 and 1 at all frequencies. It must be equal to 1 if there exists a perfect linear casual relation between two signals. It will be less than unity if one of the signals is not only related linearly to the other signal but also influenced by any other uncorrelated signal. Figures 9 and 10 show the coherence between interior and near field microphone signals for several run conditions. In all cases, the coherence behavior is similar. It can be seen from Figures 9 and 10 that below 150 Hz, the coherence drops to very low values and above 150 Hz, it rises gradually toward unity in the frequency of 150-600 Hz, again falling off above 600 Hz. The very low coherence below 150 Hz is indicative of the poor casual relationship between interior and near field signals. It is worth stating again that below 150 Hz, the interior and near field spectra exhibit different characteristics as shown in Figures 6 and 7. The low coherence, coupled with dissimilarity in spectral shapes between interior and near field signals leads to the speculation that below 150 Hz, hydrodynamic noises (flow noises), generated inside by local vortical motions of the turbulence might have dominated the combustion noise contributions

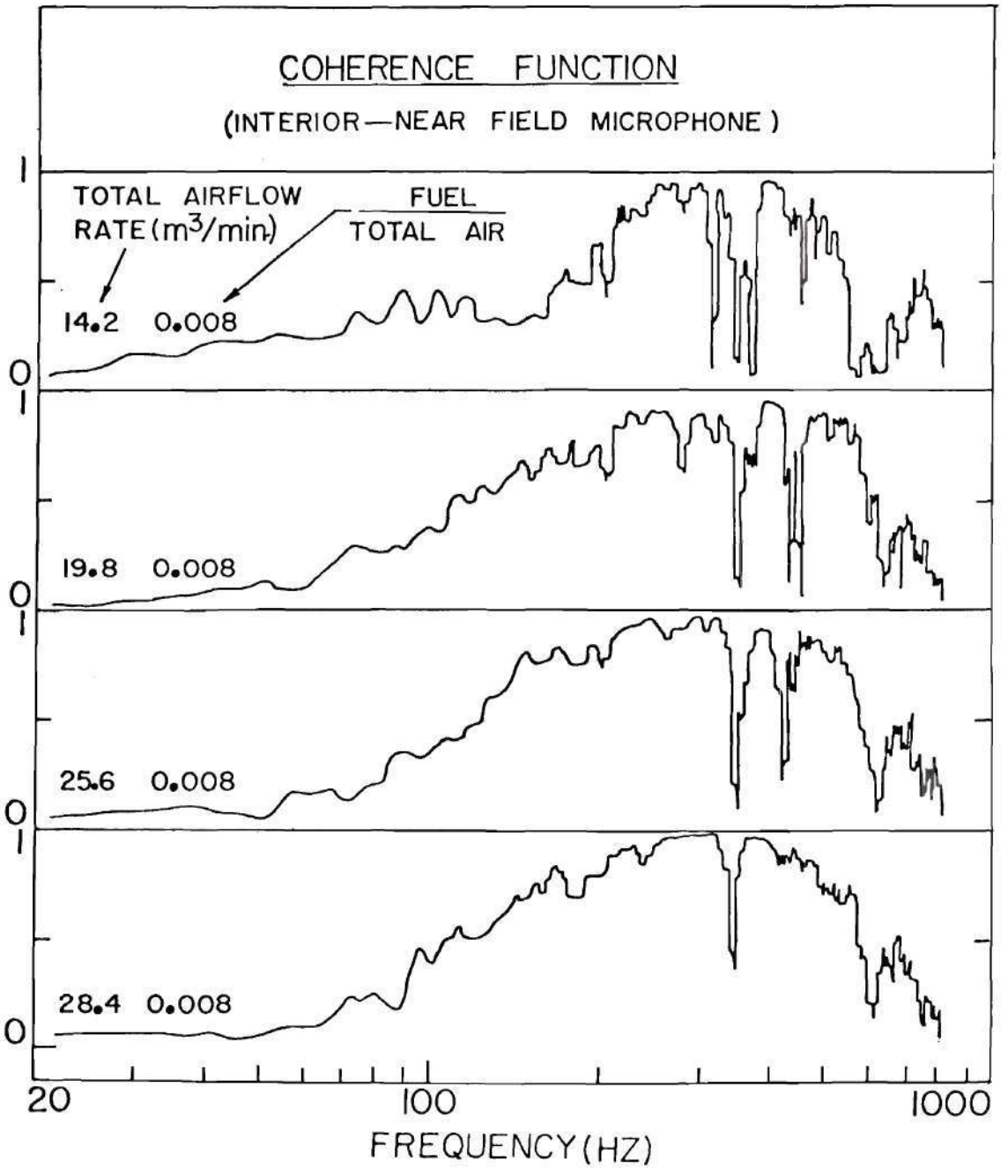

Figure 9. Ordinary Coherence Estimates Between Interior AVL and Near Field Microphone Signals for Varying Airflow Rates and a Fixed Overall Fuel/air Ratio.

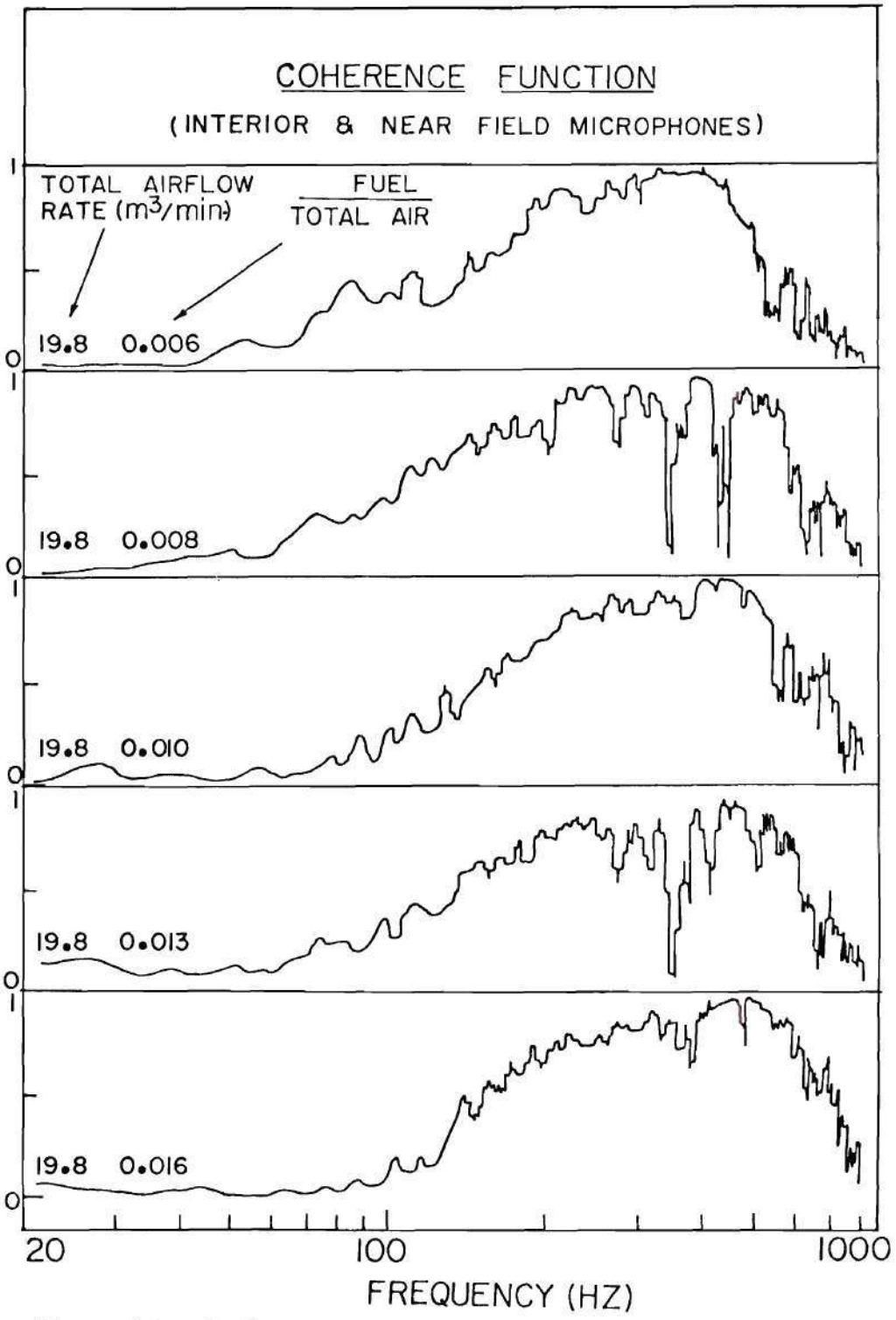

Figure 10. Ordinary Coherence Estimates Between Interior AVL and Near Field Microphone Signals for a Fixed Airflow Rate and Varying Overall Fuel/air Ratios.

to the interior pressure transducer. A theoretical study by Strahle et al.[31] lends support to the above suspicion. The pressure fluctuations leading to the hydrodynamic noise are not propagational in nature because they are merely convected with the mean flow. This is confirmed through the coherence analysis of cold flow tests, explained later in this paragraph. A coherence value of near unity in the frequency range of 150-600 Hz indicates that both interior and near field signals have major contributions from combustion noise. Above 600 Hz, the coherence again drops to low values. Because of the rapid fall off in the spectral levels at higher frequency range, a suspicion arises whether or not this poor coherence above 600 Hz is due to a dynamic range problem encountered by any of the pressure transducers. To check this, a spectral comparison of a typical cold flow and the corresponding hot flow conditions is made as shown in Figure 11. The figure shows no difference in the levels of the two interior spectra above 600 Hz whereas near field spectra clearly show a difference in the levels. This could mean either a dynamic range problem with interior pressure measurements or a high dominance of hydrodynamic noise over combustion noise. However, a very poor coherence between interior and near field signals for the cold flow test, as shown in Figure 11, even at low exit velocities (because jet noise interference is low) establishes the non-propagational nature of hydrodynamic noise to the exterior. Hence, the rise in the near field spectral level, shown in Figure 11, must be due to combustion noise only. The absence of a corresponding rise in the interior spectral levels can only be attributed

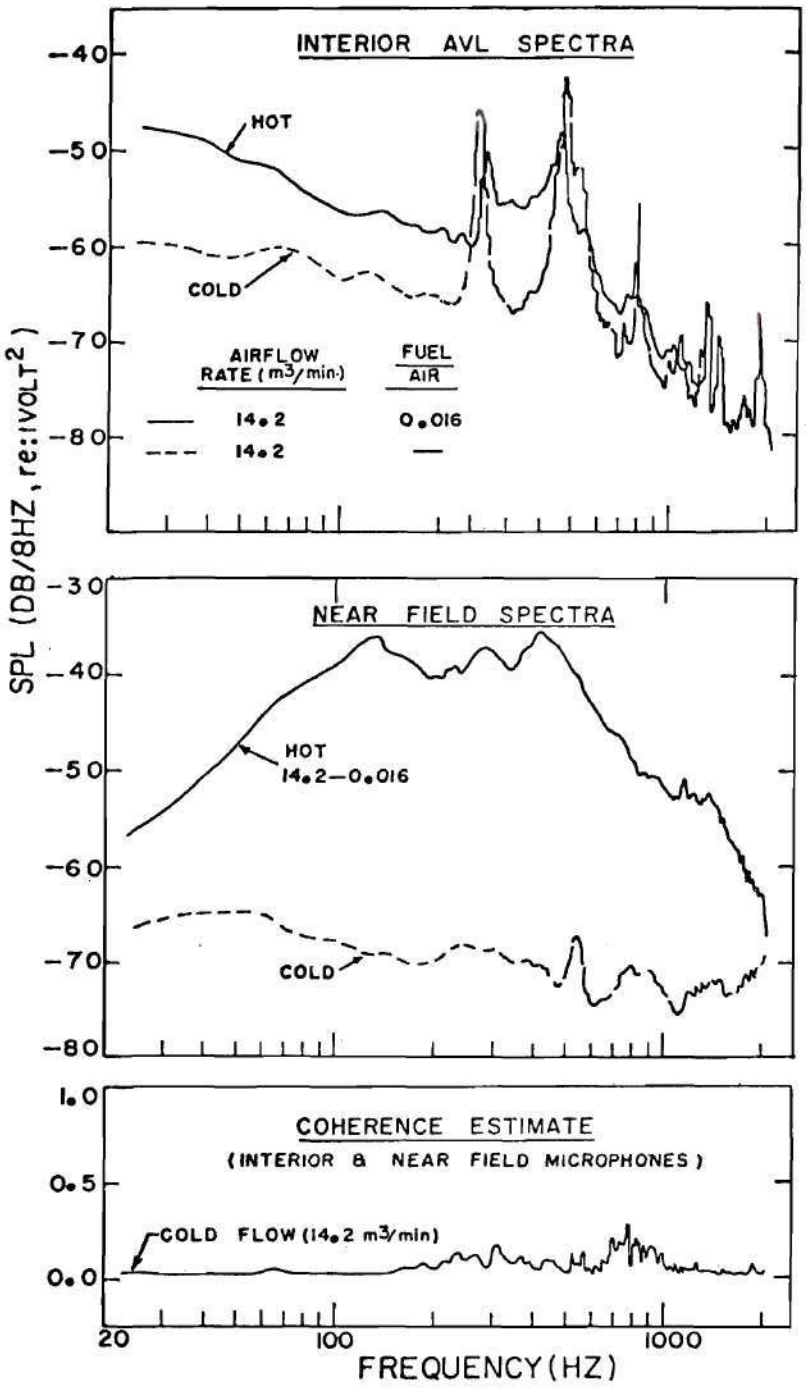

Figure 11. Comparison of Cold and Combustion-on Spectra. Also Shown is the Coherence Estimate Between Interior and Near Field Microphones for Cold Flow Test.

to the fact that in the above series of tests, the interior spectral level, above 600 Hz, falls below the sensitive range of the AVL transducer and hence does not correspond to the true interior pressure fluctuations. This leads to the observed low coherence between interior and near field signals, above 600 Hz. Figures 9 and 10 also show sharp drops in the coherence levels at some frequencies. A look at the interior spectra reveals sharp changes at these corresponding frequencies while the near field spectra are smooth. This leads to the suggestion that these sharp drops in coherence might have been due to either spurious electronic noise associated with the interior pressure transducer instrumentation or the small differences in the mounting of the interior pressure transducer on different test days.

It is clear from the above discussion that there is a need to use a more sensitive pressure transducer for internal measurements to extract the combustion noise spectrum above 600 Hz. Further, the primary aim of the present investigation centers around relating the processes taking place inside the combustor to the exterior radiated sound. This necessitates an accurate measurement of the propagational internal pressure fluctuations. As discussed earlier, due to the flush mounting of AVL pressure transducer, the internal pressure measurement is contaminated by non-propagational noise sources, such as hydrodynamic noise, at least in the low frequency regime. It seems possible to gain more understanding of the sources and the transmission patterns of the propagational sound provided a measurement technique is devised to keep the contamination of the internal pressure measurements by hydrodynamic noises to a minimum. This two-fold objective has been achieved by conducting

another series of tests, using a photocon transducer to monitor the internal pressure fluctuations. The photocon transducer can extract signals above 130 dB referred to 2 x 10^{-5} N/m^2 compared to that of 135 dB by AVL pressure transducer. It is important to note that the photocon is still located in the same axial position as that of AVL transducer, but radially displaced away from the flow field by a small distance through an infinite tube assembly as shown in Figure 3. This arrangement helps the photocon transducer to pick up mostly propagational pressure fluctuations and the contamination by hydrodynamic noise is expected to be very minimal. The near and far field sound pressures are measured through Brüel and Kjaer 12 mm condenser microphones as before. The airflow rates are varied between 9.8 and 19.8 m^3/min. with fuel/air ratios varying between 0.008 and 0.016.

A narrow band spectral analysis of interior pressure fluctuations and near and far field sound pressures has been carried out. To test the reliability of the measurements with the photocon transducer, again a spectral comparison of cold and hot flow conditions is made as shown in Figure 12. A significant rise in the level of the hot spectrum over the cold one in the entire frequency range of interest gives confidence in the photocon pressure measurements.

Figure 13 shows the spectra of interior pressure fluctuations, obtained with the photocon transducer, corresponding to the extreme test conditions. A similar spectral behavior is observed in all cases. The spectra are almost flat up to 50 Hz and then gradually rise, exhibiting a familiar combustion noise peak around 200 Hz. A quarter wave resonance of the burner can appears in all the spectra in the vicinity

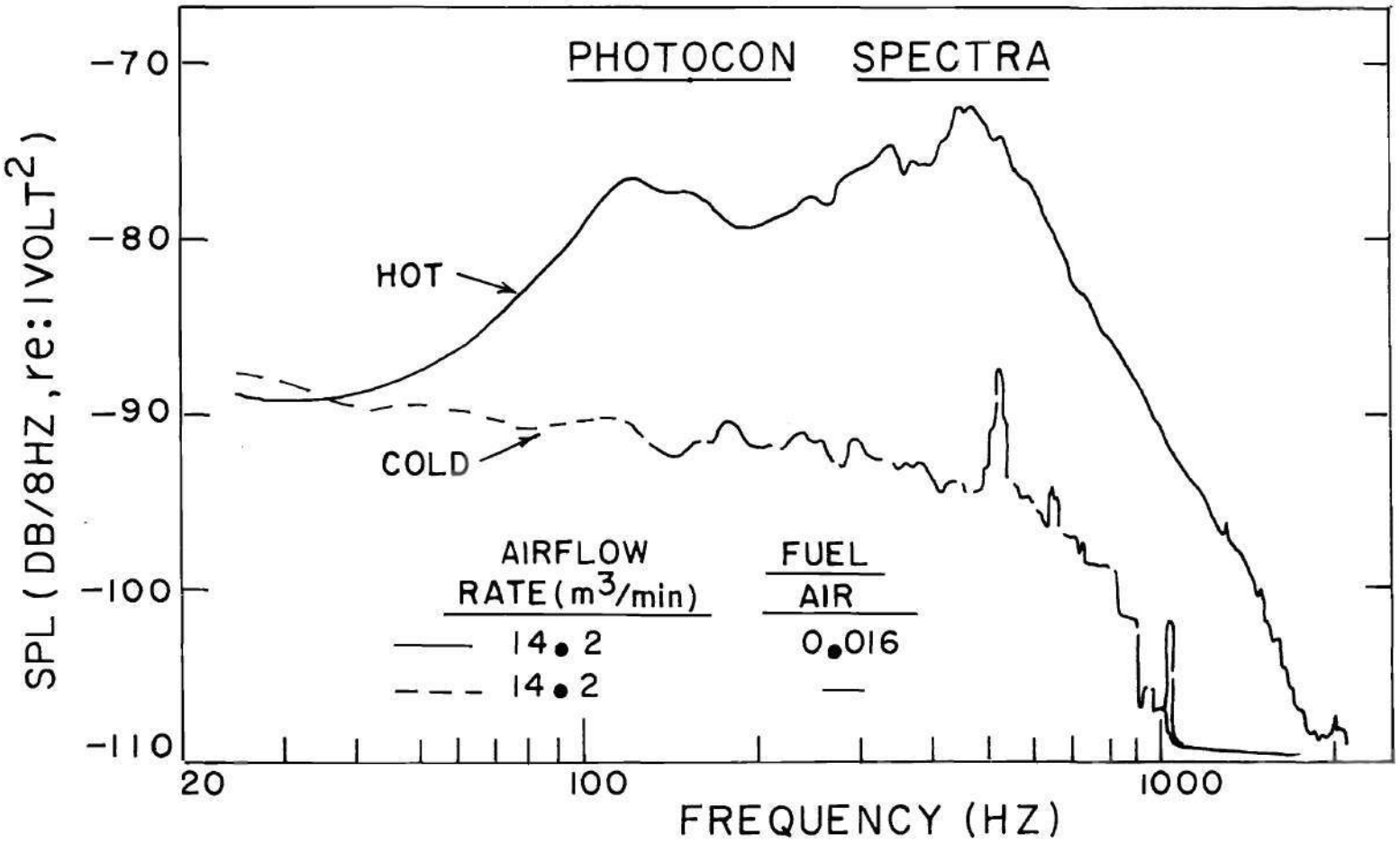

Figure 12. Comparison of Interior Photocon Spectra for Cold and Combustion-on Conditions.

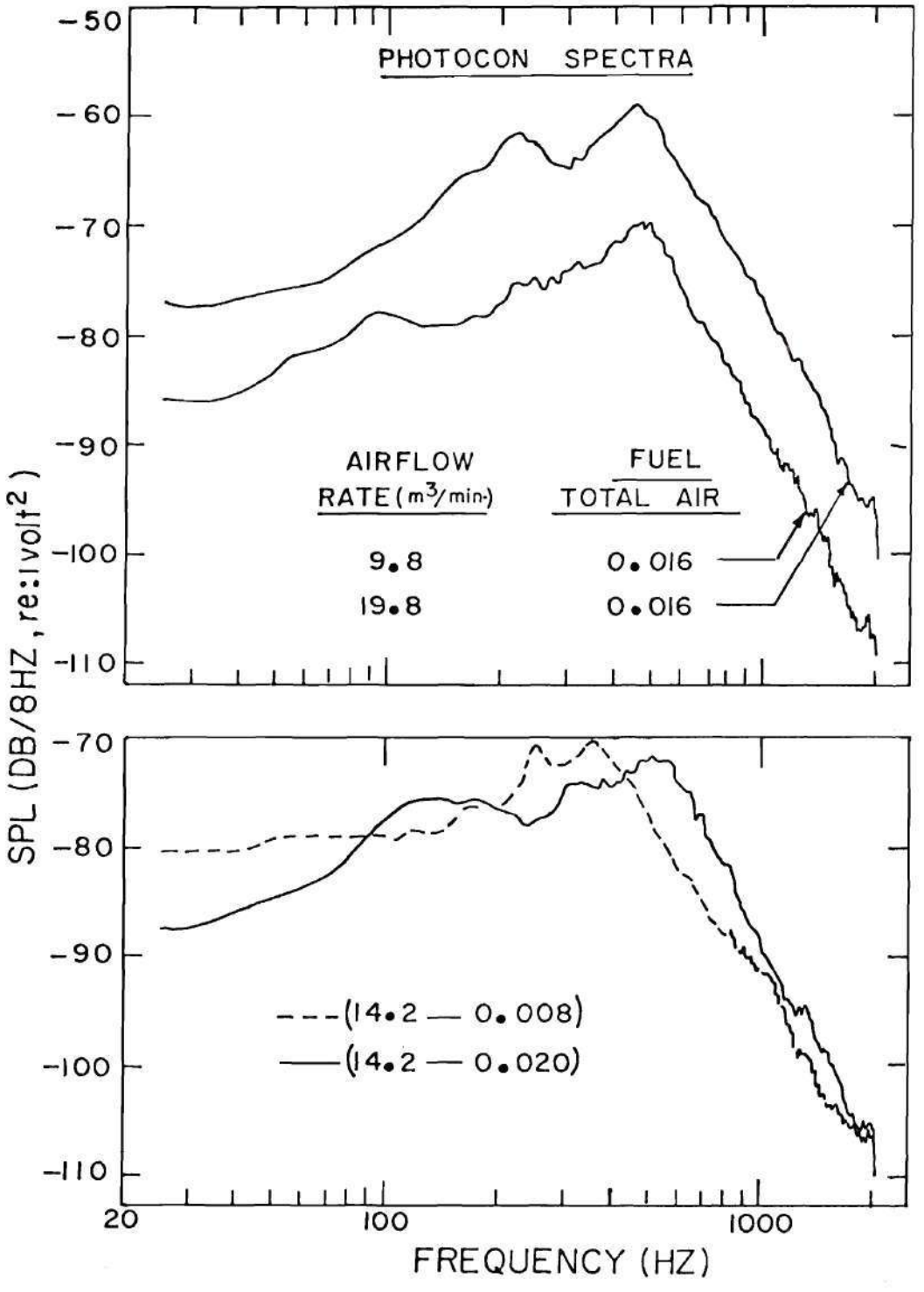

Figure 13. Interior Photocon Spectra as a Function of Airflow Rate and Overall Fuel/air Ratio.

of 500 Hz depending upon the fuel/air ratio. Above 600 Hz, the spectra fall off rapidly.

The near field spectra for the same test conditions are shown in Figure 14. All the spectra exhibit similar characteristics. The general features of the near and far field spectra, such as a broad band combustion noise peak around 200 Hz, quarter wave resonance of the burner can around 500 Hz and ground reflection effects, have been discussed in the previous paragraphs in connection with the previous series of tests. It is interesting to observe a very good similarity in the shapes above 50 Hz between interior and near field spectra.

Figure 15 brings out the coherence between interior (photocon) and near field microphone signals. In all the cases, the coherence behavior is similar. There is a poor coherence in the lower frequency range of 0 - 50 Hz, followed by a gradual rise to near unity around 150 Hz. A comparison of interior and near field spectra reveals that below 50 Hz the interior spectra remain flat while near field spectra keep decreasing. Above 50 Hz, the interior spectra rise at a rate comparable to that of near field ones. The dissimilarity in the spectral shapes below 50 Hz, coupled with low coherence, indicates that the internal measurements by photocon transducer are contaminated with hydrodynamic noise up to 50 Hz. A rising coherence and a correspondence in the spectral shapes above 50 Hz suggest an increasing contribution by combustion noise to the interior pressure measurements. A coherence of near unity in the range of 150 - 1200 Hz reveals that both interior and near field microphone signals are largely dominated by combustion noise in this frequency range. Above 1200 Hz, the coherence drops rapidly to

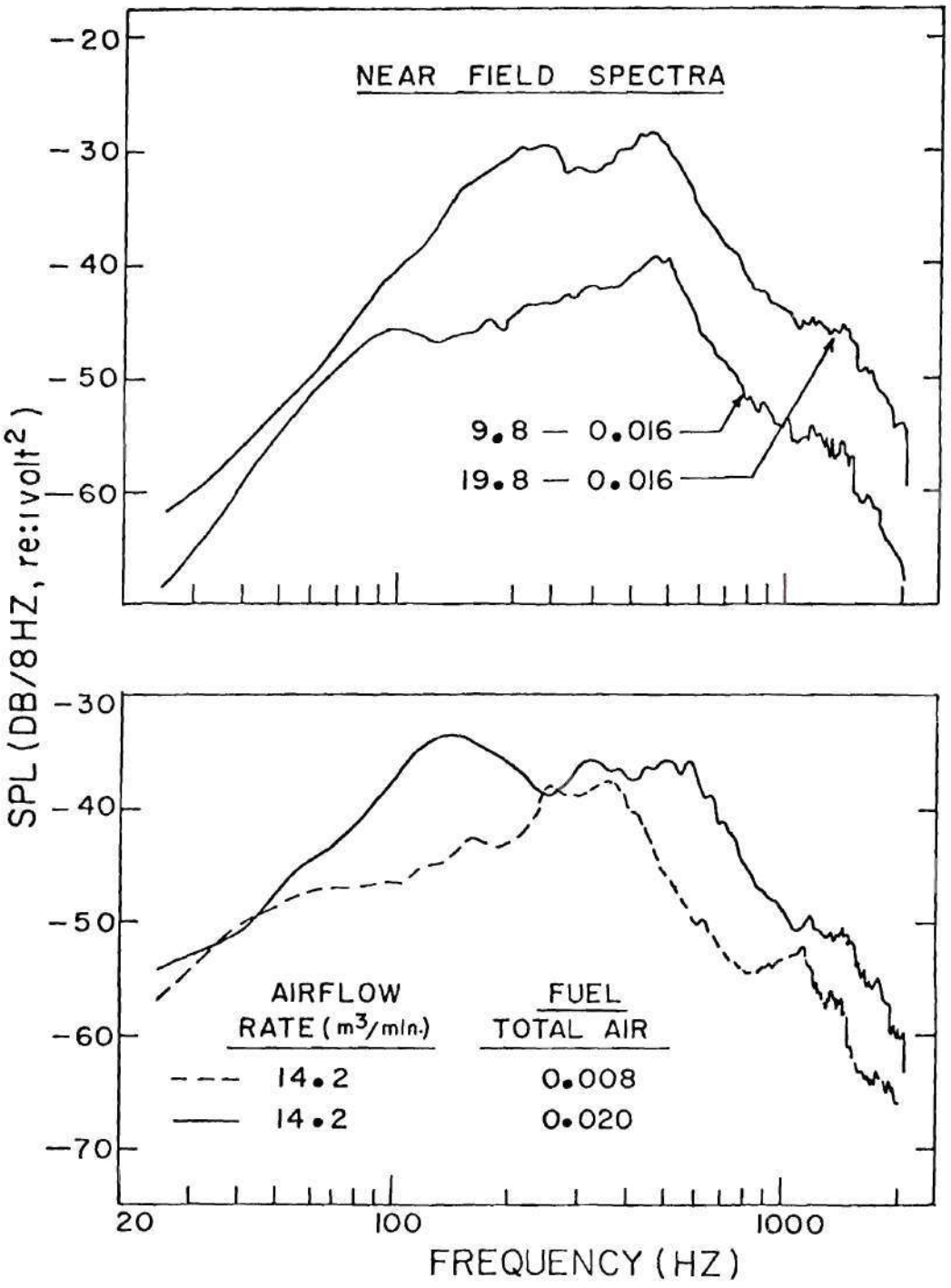

Figure 14. Near Field Microphone Spectra as a Function of Airflow Rate and Overall Fuel/air Ratio.

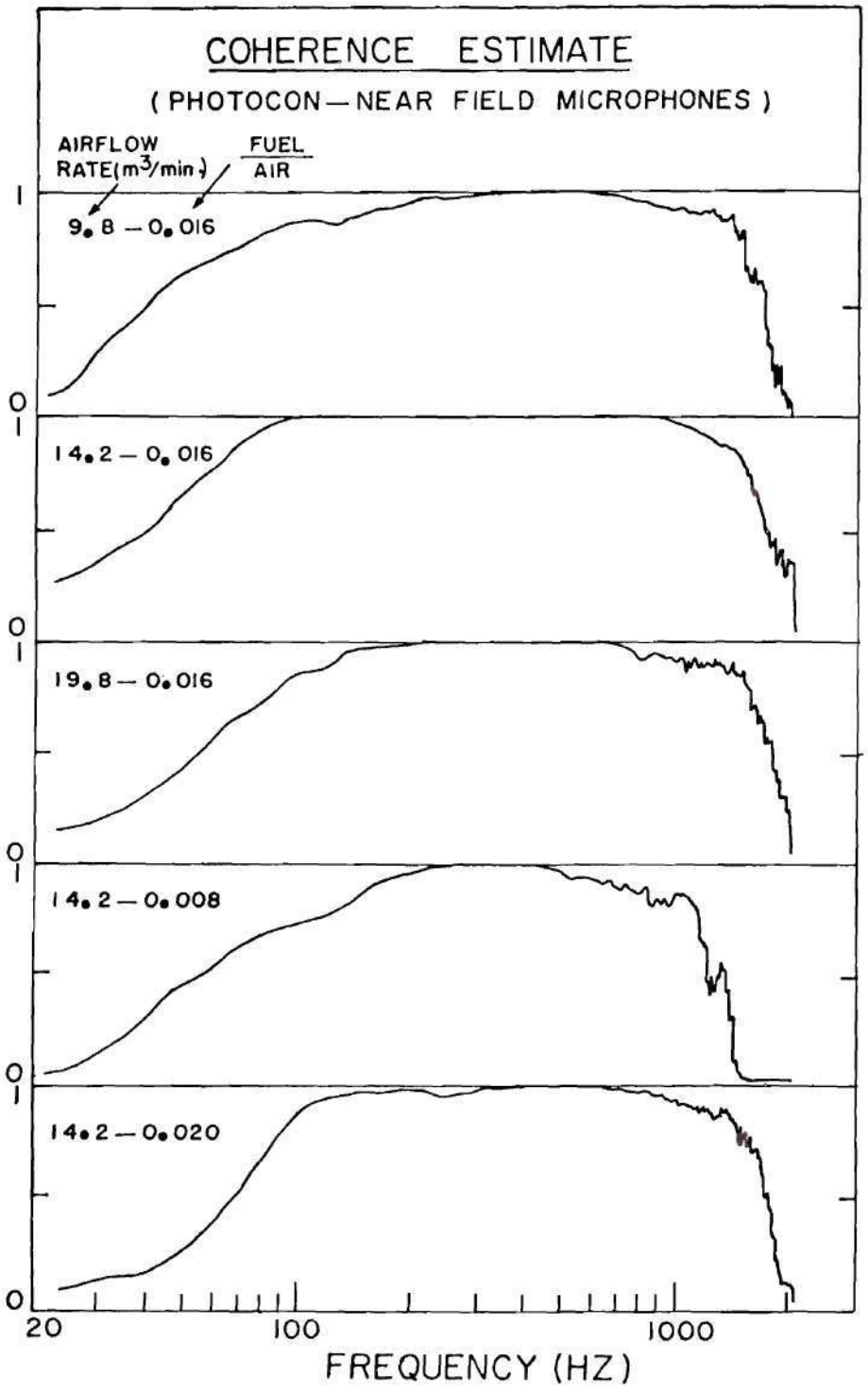

Figure 15. Ordinary Coherence Estimates Between Interior Photocon and Near Field Microphone Signals as a Function of Airflow Rate and Overall Fuel/air Ratio.

very low values. This is because above 1200 Hz, the scattering from the burner hardware becomes more pronounced, destroying the monopole behavior of combustion noise radiation pattern. At this stage, a single near field measurement is not sufficient to characterize the entire radiation pattern and this causes a very low coherence between interior and near field signals above 1200 Hz.

The coherence between near and far field signals for a few typical cases is shown in Figure 16. A similar coherence behavior is found in the other cases also. It is important to note that the measured coherence estimates between near and far field microphones have to be corrected for the separation distance between the two microphones. The *true coherence* $\hat{\gamma}^2$ *is related* to the measured value γ^2 as,

$$\hat{\gamma}^2 = \gamma^2/(1 - \tfrac{\tau}{T})^2$$

where τ is the time delay between near and far field microphone signals and T is the sample record length. The coherence estimate, shown in Figure 16, is a true one. In the frequency range of 100 - 1200 Hz, the coherence level is found to be almost unity and below 100 Hz also it maintains a sufficiently high level. This is mainly because in this frequency range, up to 1200 Hz, the burner can is behaving as a monopole radiator. It is important to note that the coherence level is not affected by ground reflection effects, present in the far field spectrum because the ground reflections can be considered as a linear transform operation to recover the far field signal from the near field one. It can be proved that a mere linear transform operation is cancelled

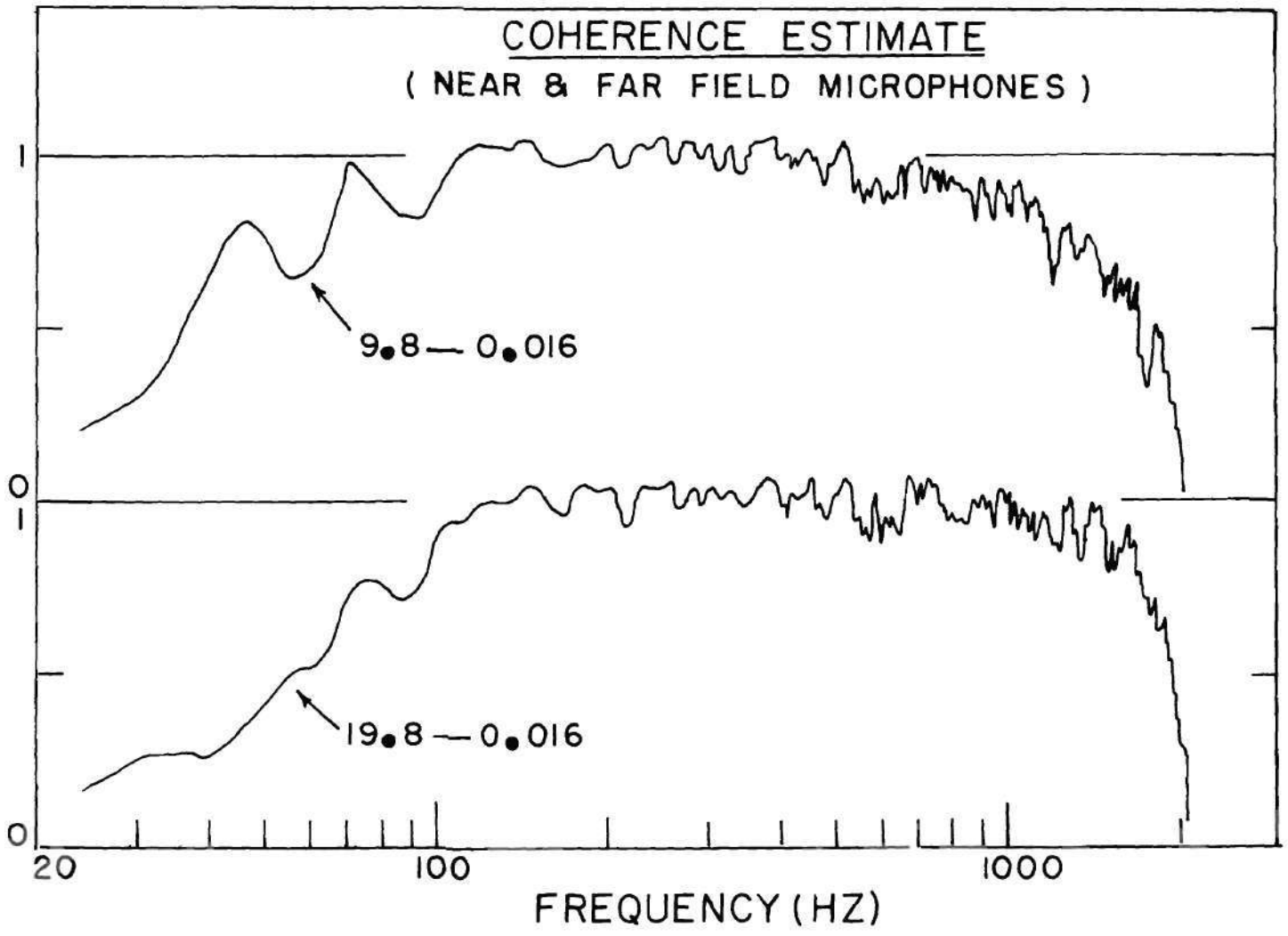

Figure 16. Ordinary Coherence Estimates Between Near and Far Field Microphone Signals as a Function of Airflow Rate and Overall Fuel/air Ratio.

out in the coherence function analysis and does not affect the coherence estimates. Above 1200 Hz, as mentioned earlier, the monopole radiation pattern is destroyed by the burner hardware scattering and the far field radiation characteristics cannot be adequately described by a single point measurement in the near field. This brings down the coherence level between near and far field signals to very low values, above 1200 Hz.

Summarizing the above discussion, it can be stated that two different series of tests have been carried out. The main difference between them is that in one case a flush mounted AVL pressure transducer is used to measure the interior pressure fluctuations whereas in the other case a photocon transducer monitors the same from a location displaced from the flow field. Comparing the results obtained from both cases, it can be said that the flush mounted AVL measurements are dominated by hydrodynamic noise below 150 Hz, thereby leading to a poor coherence between interior and near field signals. The major point to be stressed here is that this low coherence resulting from hydrodynamic noise contamination of the interior signal should not be mistaken for the absence of combustion noise. The fact that combustion noise is present both interior and exterior to the combustor even at frequencies as low as 50 Hz is confirmed by the photocon interior measurements, which are hydrodynamic noise free to a great extent, by virtue of its location and the non-propagational nature of hydrodynamic noise. A very good coherence and spectral similarities in the range of 60 - 1200 Hz between photocon and near field microphone measurements indicate that the core engine noise, in the above frequency range, is mostly attributable to

combustion noise sources inside the combustor for the range of conditions investigated here. It is also shown that a coherence level of unity exists between near and far field signals up to 1200 Hz because the given combustor behaves like a monopole radiator in the above frequency range. Above 1200 Hz, the scattering from burner hardware destroys monopole behavior and hence coherence between near and far field signals drops to very low values. Finally, it can be said that in the above low Mach number cases, the jet noise contamination of the exterior combustion noise signal is insignificant due to very low jet noise levels. This has been confirmed in a previous program (Reference 16) wherein the radiated acoustic power, at low Mach numbers, has been found to scale with exit velocity with an exponent of 2.6. This is far below the jet noise exponent of 8. Further, in the present investigation, a very poor coherence is noticed between interior and near field microphones for cold flow tests whereas combustion-on tests yield a very high coherence between the same. This clearly indicates that in all the above hot flow tests, the combustion noise contribution to the exterior sound far exceeds the jet noise levels.

Separation of Combustion and Entropy Noise

This section deals with combustion and entropy noise radiation characteristics and the experimental procedures for separating them. Entropy noise is generated in turbopropulsion systems when combustion generated hot spots are accelerated through a region of mean pressure gradient. In the present program, such a pressure gradient is imposed on the hot gases by attaching to the burner exit a convergent nozzle of

area reduction 3:1 or an orifice plate with 9 holes of 14 mm diameter each and having an effective area reduction of 10.5:1. An exit Mach number, M_2 = 0.20, is obtained with the above nozzle whereas at high Mach numbers, M_2 = 0.6, 0.8 and 1.0, the jet is exhausted through a multi-hole orifice plate, rather than a single opening nozzle, to keep the jet noise levels low. It has been established in jet noise reduction programs[32] that a multiple jet exhaust will yield lower jet noise levels compared to that of a single jet of equivalent thrust. The experimental set-up with the relative locations of the transducers is the same as shown in Figure 3. The pressure fluctuations inside the combustor and the near field and the far field radiated sound pressures have been measured with a photocon pressure transducer and Brüel and Kjaer type 4134, 12 mm condenser microphones respectively. The reason for including a near field microphone in the measurement scheme is two-fold. At higher exit Mach numbers, the jet noise is expected to contaminate the exterior radiated core noise signals. In that case, the near field microphone by virtue of its location, will receive more contribution from core noise radiation with a lesser degree of contamination from a small local area of the jet. However, the far field microphone signal may be dominated by jet noise as it sees the whole jet. This means that the near field signal, rather than the far field one, can be used with more confidence to represent the exterior radiated core engine noise. The second reason is that the far field microphone spectrum is masked by severe ground reflection effects, as shown earlier in Figure 7, whereas the near field microphone, by virtue of its close

location to the burner exit, is free from these effects. Since the entropy noise study requires the details of the combustion generated hot spots, a measurement program has been carried out to obtain the temperature fluctuation characteristics. Fast response chromel-alumel thermocouples of wire diameter 0.025 mm are used to record the temperature fluctuations at the burner exit plane as shown in Figure 3. The time constants of the thermocouples are determined as explained in Appendix A, and the thermocouple signals are compensated for these time constants later during data analysis by suitable modification of the Fourier Analyzer programming. Fixed bandwidth spectra of interior, near and far field microphones as well as thermocouple signals have been obtained. Also, coherence estimates between them have been evaluated. These results are discussed below.

Spectral Characteristics: An exit Mach number, $M_2 = 0.05$, represents the burner can operating without a nozzle while $M_2 = 0.20$ corresponds to the convergent nozzle case and $M_2 = 0.6$, 0.8 and 1.0 are obtained by using the orifice plate. The airflow rates vary between 7.0 and 19.8 m^3/min., with the overall fuel/air ratio maintained constant at 0.016 for all cases. Out of a wide range of test runs, only the above conditions are selected for the purpose of comparison of results. Other exploratory test runs and their results are documented in Appendix B for additional information. Figure 17 shows the spectra of interior pressure fluctuations. The upper frequency limit is chosen as 2000 Hz because the information of interest falls below this limit. Figure 17a illustrates the spectral changes with the increasing pressure drop across the combustor as the exit termination is changed for a fixed

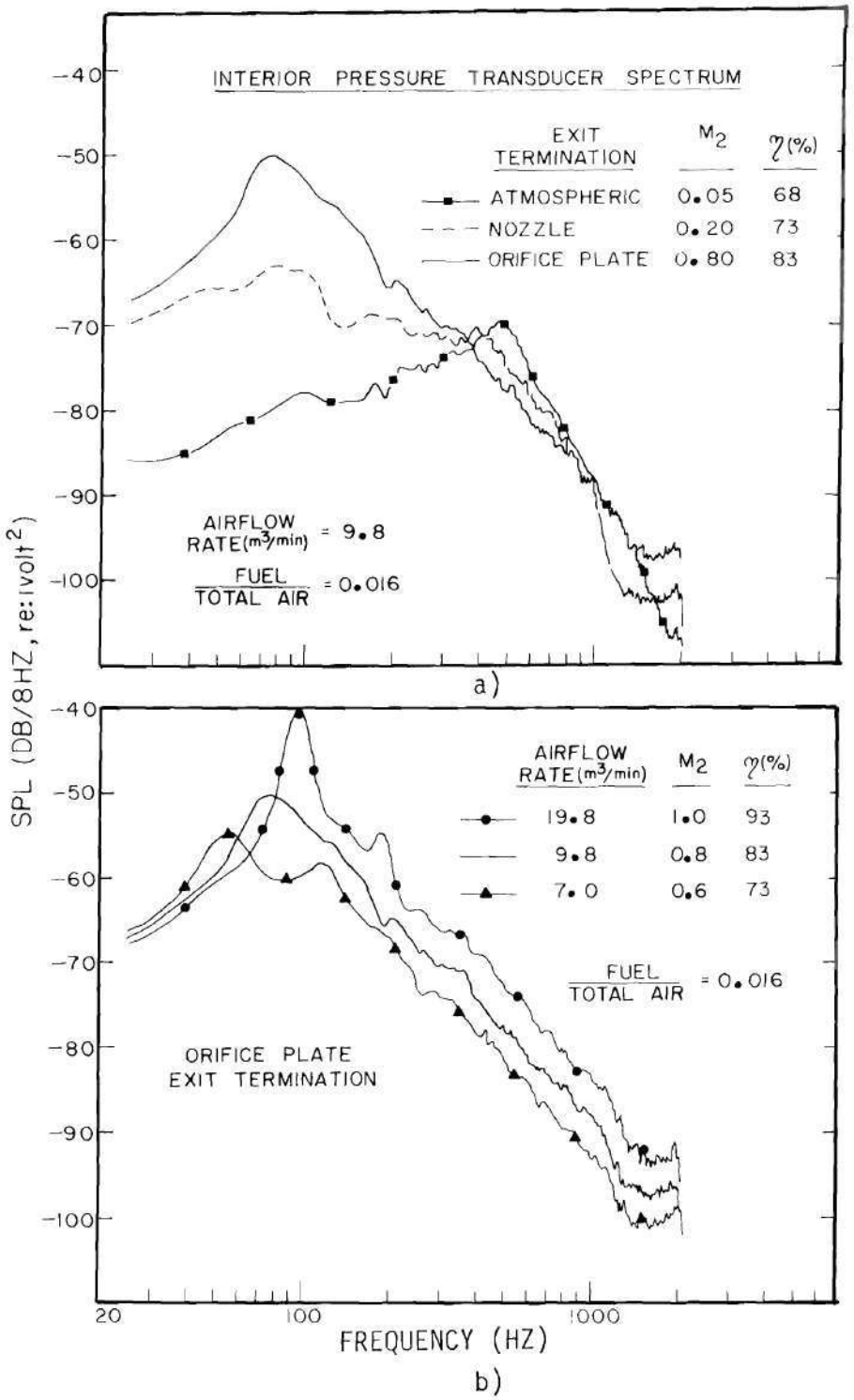

Figure 17. Interior Photocon Spectra for Various Exit Mach Numbers.

airflow rate and overall fuel/air ratio, whereas Figure 17b shows the spectral behavior with increasing pressure drop across the orifice plate for varying airflow rates and a fixed overall fuel/air ratio. The efficiency, shown in Figure 17, refers to combustion efficiency computed as a ratio of actual temperature rise of exhaust gases to the adiabatic flame temperature rise; and the details of measurement are given in Reference 26. It can be seen from Figure 17a that, as the exit contraction ratio is increased, the spectral level rises significantly with an increase in the exit Mach number in the lower frequency range of 0 - 300 Hz. Around 300 Hz, all attain almost the same level, and then they fall off rapidly at the same rate (10 dB/octave) with increasing frequency. Another observation made here is that the interior spectrum corresponding to the exit Mach number, $M_2 = 0.05$, exhibits a quarter wave resonance peak around 500 Hz. With an increase in the exit contraction ratio corresponding to high Mach number cases, this resonance peak should shift to a higher frequency range (800 - 1000 Hz), tending towards a half wave resonance. On the contrary, these peaks have disappeared in the high Mach number cases. However, a similar set of tests, conducted with the flush-mounted AVL transducer monitoring interior pressure fluctuations, exhibits such resonance peaks; and these results are reported in Appendix B. The occurrence of a peak around 100 Hz in the case of high Mach numbers is explained at the end of this section.

Figure 18 shows the near field spectra for the same run conditions. While at low exit Mach numbers, there is a familiar combustion noise hump, high Mach number cases exhibit no such characteristics. The near field spectra, pertaining to high Mach number cases, do not resemble the

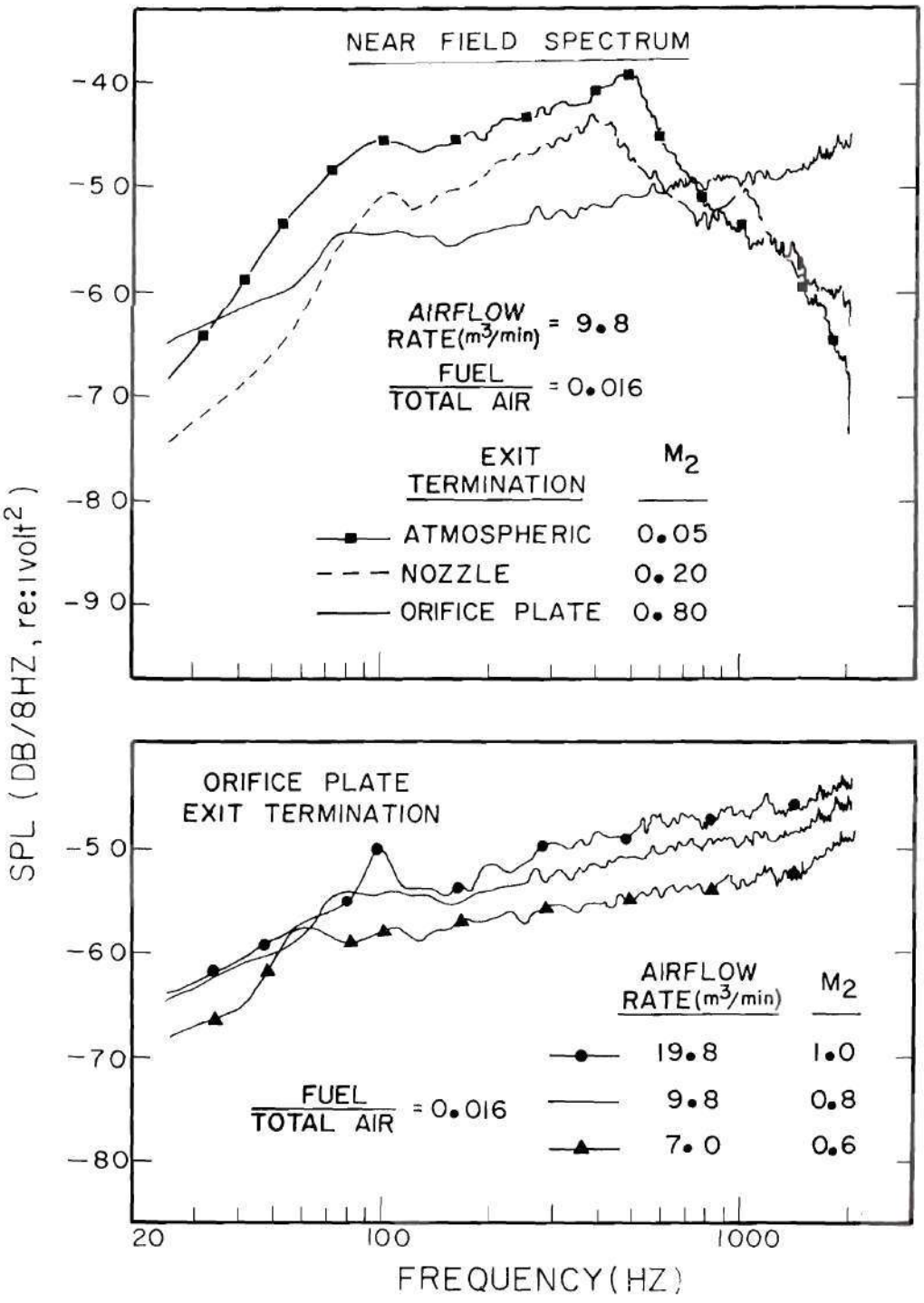

Figure 18. Near Field Microphone Spectra for Various Exit Mach Numbers.

usual combustion noise spectra. The change in the spectral shapes at high Mach numbers could mean either entropy noise domination or jet noise contamination of the near field signal. To investigate the above speculation, two checks have been made. Table 1 shows the overall sound pressure level registered by the near field microphone for various test conditions. From these numbers, the exponent on velocity in high Mach number cases has been computed to be 2.5 which is far below the jet noise exponent of 8. This means that the near field microphone receives a greater contribution from core noise radiation although there is jet noise contamination to a lesser degree. Secondly, a spectral analysis of the near field signals has been carried out. Figure 19 shows a comparison of the near field spectra of the hot exhaust at M_2 = 0.6 with the cold flow of identical exit velocity. It can be seen that the spectrum level with the combustion-on is higher than that of the exit-velocity-matched cold flow by at least 3 to 4 dB in the frequency range of 150 - 1000 Hz. This gives some confidence that the core engine noise dominates the jet noise, at least in the frequency range of interest to the present investigation. Later in this section, it is shown through coherence function analysis that it is indeed the entropy noise that contributes significantly to the near field signal at high exit Mach numbers.

Typical spectra of the temperature fluctuations at the burner exit plane are shown in Figure 20. The spectral shapes of the temperature fluctuations, corresponding to different exit terminations, are seen to be very similar. The temperature fluctuation spectrum is a broad band one and low frequency in nature. The spectrum gradually

Table 1. Overall Sound Pressure Levels and R.M.S. Temperature Fluctuations at Various Operating Conditions

Type of Exit Termination	Exit Mach Number (M_2)	Overall Sound Pressure Level (Referred to 2×10^{-5} N/m^2) At Near Field Microphone (DB)	R.M.S. Temperature Fluctuations as a % age of Mean Temperature
Direct Discharge	0.05	117.5	10.75
Short Nozzle	0.20	113.5	9.02
Orifice Plate	0.60	123.0	9.64
Orifice Plate	0.80	127.8	11.62
Orifice Plate	1.00	130.0	13.84

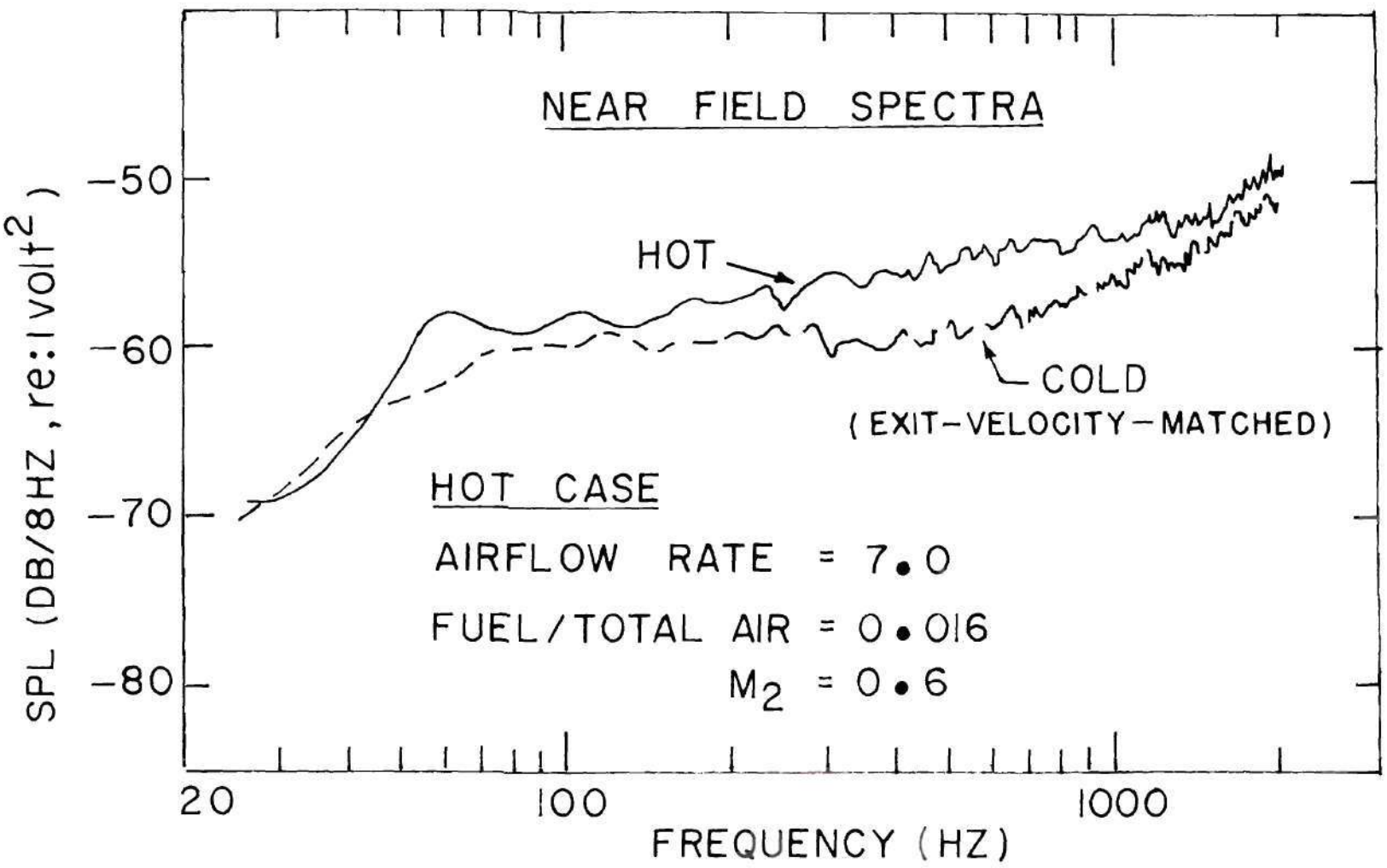

Figure 19. Comparison of Near Field Microphone Spectra for Hot and Exit-Velocity-Matched Cold Flow Conditions.

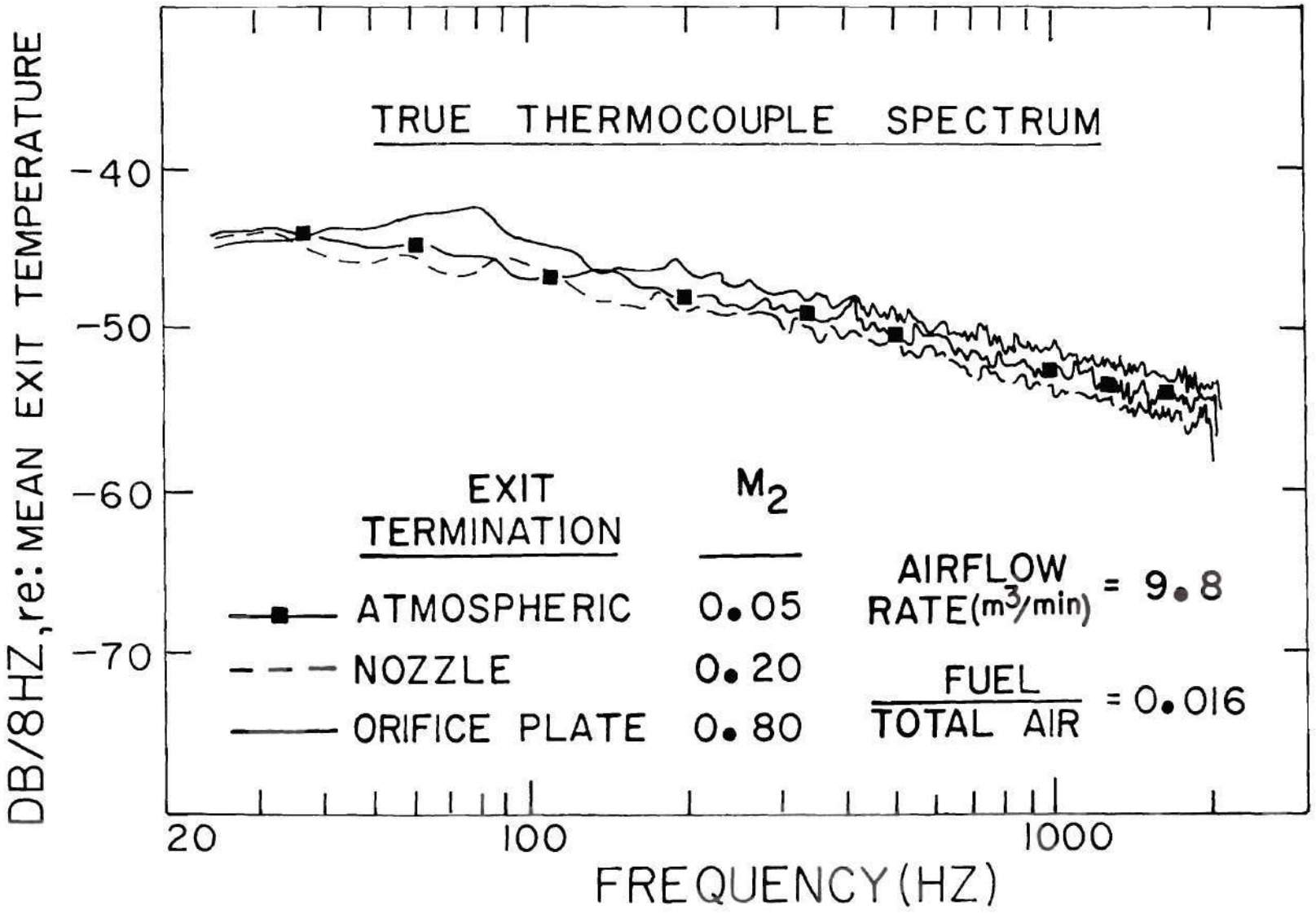

Figure 20. Temperature Fluctuation Spectra for Various Exit Mach Numbers.

falls off with an increase in frequency. The r.m.s. temperature fluctuations are found to vary within a range of 9 to 14% of the mean temperature for various cases, as shown in Table 1.

The theoretical evaluation of entropy noise requires a knowledge of the spatial correlation length scales of the temperature fluctuations. Two thermocouples of the same size (0.025 mm wire diameter) have been used for this correlation study. One of the thermocouples monitors the temperature fluctuations at a fixed place at the burner exit plane while the other one registers the signals at various locations, moving radially away from the former. The fixed and the moving thermocouple signals have been cross-correlated and normalized to obtain the cross-correlation coefficients. The cross-correlation coefficient, as a function of the separation distance between the two thermocouples, is shown in Figure 21 for two cases corresponding to the thermocouple traverses along two different radial directions. In both cases, the temperature fluctuations seem to be correlated over a distance of about 12 mm (half inch) at the burner exit plane, thereby suggesting a temperature eddy of about 12 mm in size. The constancy of the correlation length scales in various radial directions demonstrates the axi-symmetric nature of the thermal eddies. The similarity in the correlation analysis results for two different test conditions is brought out in Figure 22. In all the above cases, the cross-correlation is found to be positive everywhere, with a long tail.

It is important to note that the spectral characteristics of the temperature fluctuations mentioned in the above paragraphs have been obtained through single point thermocouple measurements at the burner

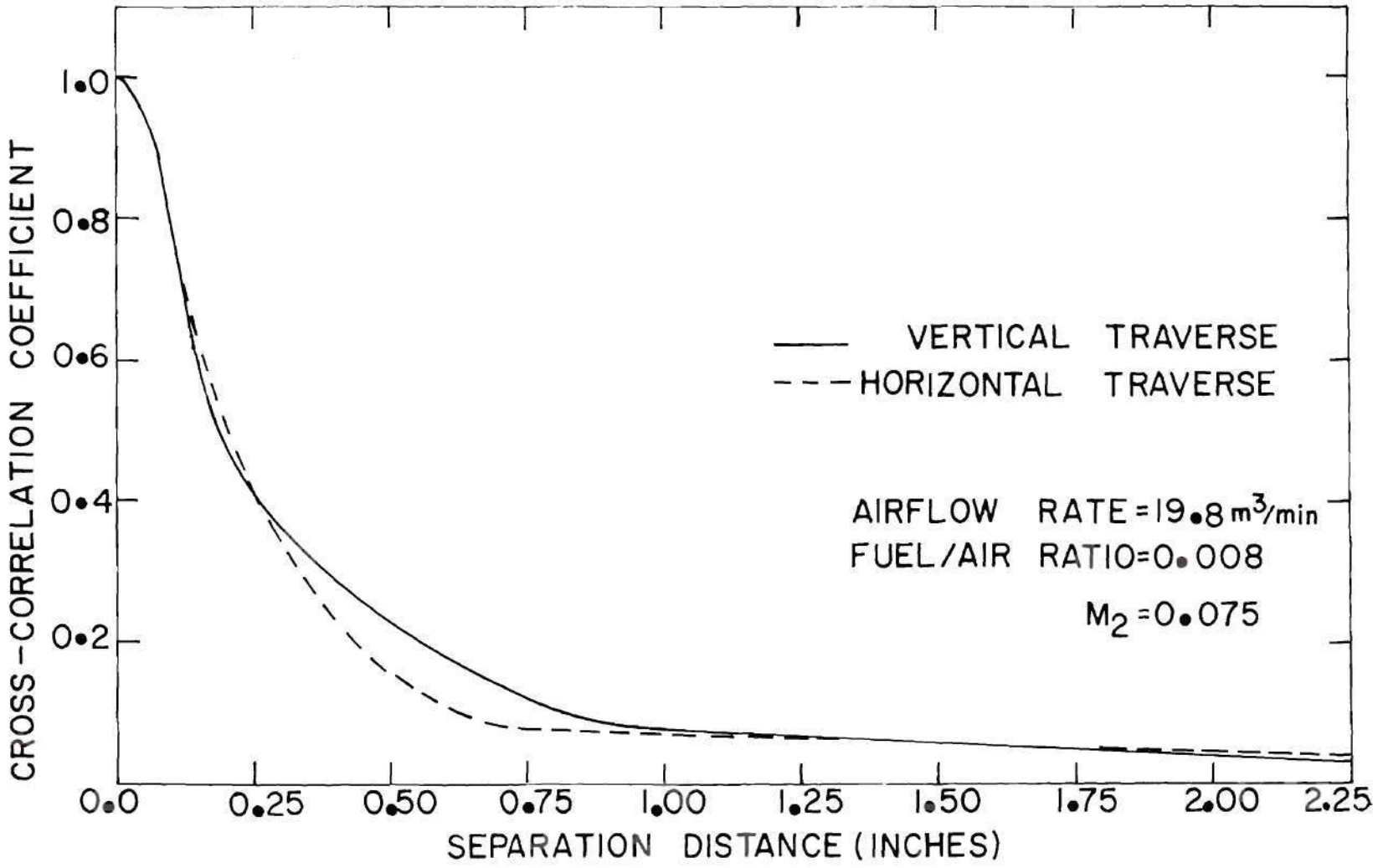

Figure 21. Cross-correlation Coefficients as a Function of Separation Distance Between Two Thermocouples for Different Traverse Directions.

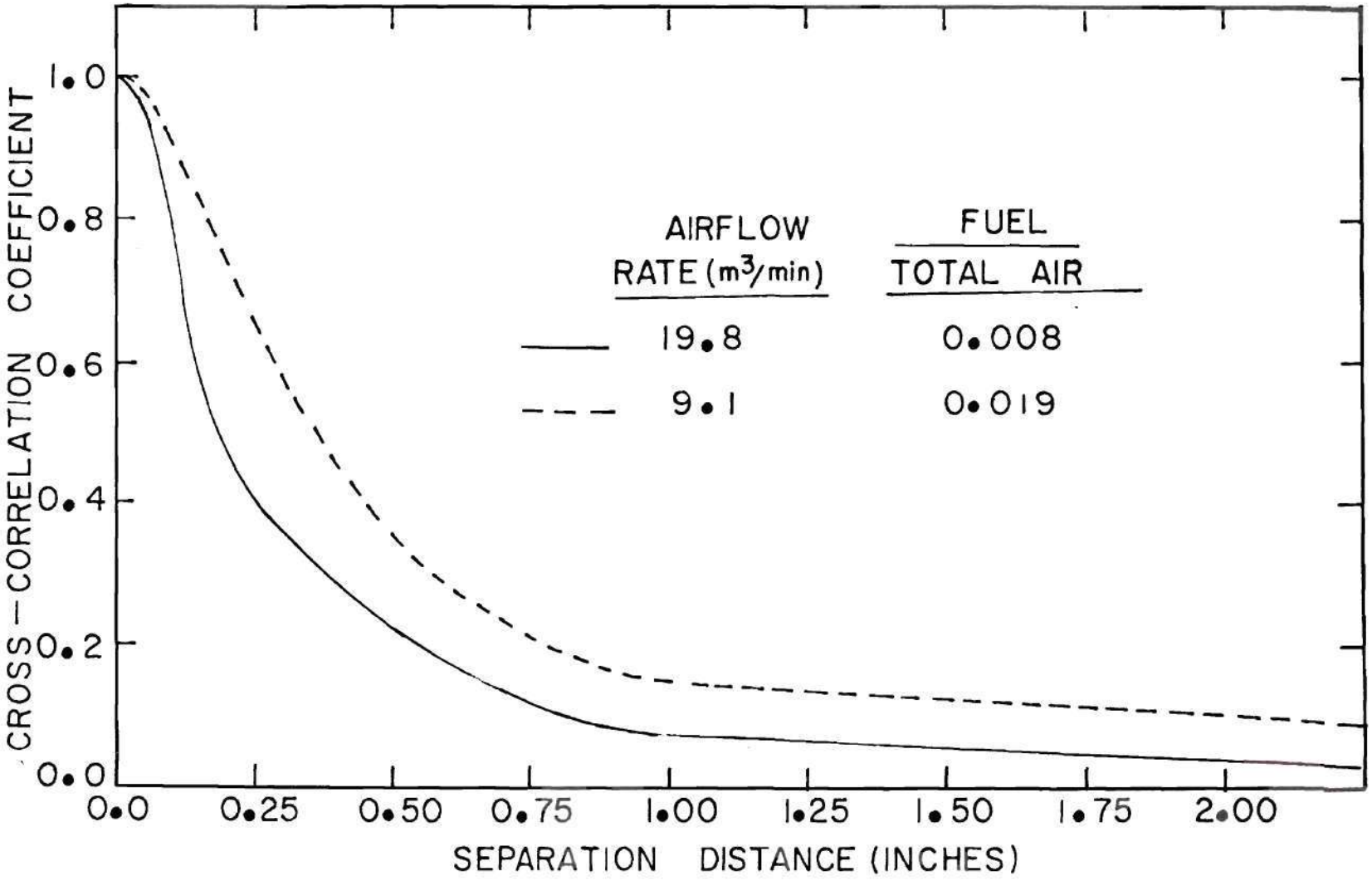

Figure 22. Cross-correlation Coefficients as a Function of Separation Distance Between Two Thermocouples for Different Operating Conditions.

exit plane. However, the entropy noise calculations require the quantities averaged over the burner exit area. The relationship between the single point thermocouple measurements and the area averaged quantities are established below.

Let T' and $\overline{T}$ represent the fluctuating and mean temperature measured at a point at the burner exit plane by a thermocouple and a ratio σ' be defined as

$$\sigma' = \frac{T'}{\overline{T}} = \frac{s'}{c_p} \tag{1}$$

where s' is the fluctuating entropy component and c_p is specific heat at constant pressure. However, the entropy noise evaluation requires $\hat{s}_\omega$ given by

$$\hat{s}_\omega = \frac{1}{A_e} \int_{A_e} \sigma_\omega \, dA \tag{2}$$

where A_e is the burner exit area, and the subscript ω represents the Fourier transform of the corresponding primed quantities. If the cross-correlation properties of the temperature fluctuations are invariant across A_e, it may be shown that

$$S_{\hat{s}\hat{s}} = \frac{A_{cor}}{A_e} S_{\sigma\sigma} \; ; \; S_{\hat{s}i} = S_{\sigma i} \; ; \; \gamma^2_{\hat{s}i} = \frac{A_e}{A_{cor}} \gamma^2_{\sigma i} \tag{3}$$

where S and γ^2 represent the spectral and coherence estimate, respectively, of the subscripted quantities and i stands for any dummy point on the burner exit plane. A_{cor} refers to the area over which the

temperature fluctuations are correlated at the burner exit plane and is given by

$$A_{cor}(\omega) = \frac{\int dA(\vec{d}) \int dA(\vec{r})\ \sigma_\omega(\vec{r})\ \sigma^*_\omega(\vec{r}+\vec{d})}{S_{\sigma\sigma} A_e} \qquad (4)$$

where $\vec{r}$ is a vector representing any point on the burner exit plane and $\vec{d}$ is a vector representing the separation distance between any two $\vec{r}$'s. It is obvious from the above expressions that the area-averaged quantities can be derived from the single point thermocouple measurements, once the correlation area as a function of frequency is evaluated through Equation (4). The variation of the normalized correlation area with the frequency, as obtained by a single radial thermocouple traverse, is shown in Figure 23. For reasons to be explained later, an average correlation area is also computed. This average one is computed from three correlation areas obtained through radial as well as circumferential thermocouple cross-correlations without any end attachment and radial cross-correlations with the orifice plate attached. The airflow rate and fuel/air ratio were kept constant at 9.1 m^3/min. and 0.019 respectively in the above three test runs. This average temperature correlation area is also shown in Figure 23. It can be seen from Figure 23 that the low frequency temperature fluctuations are correlated over a larger area compared to the high frequency fluctuations as is reasonable. Since the correlation area is a measure of the eddy size, it can be said that an eddy representing the low frequency fluctuations is larger in size compared to that of a high frequency one.

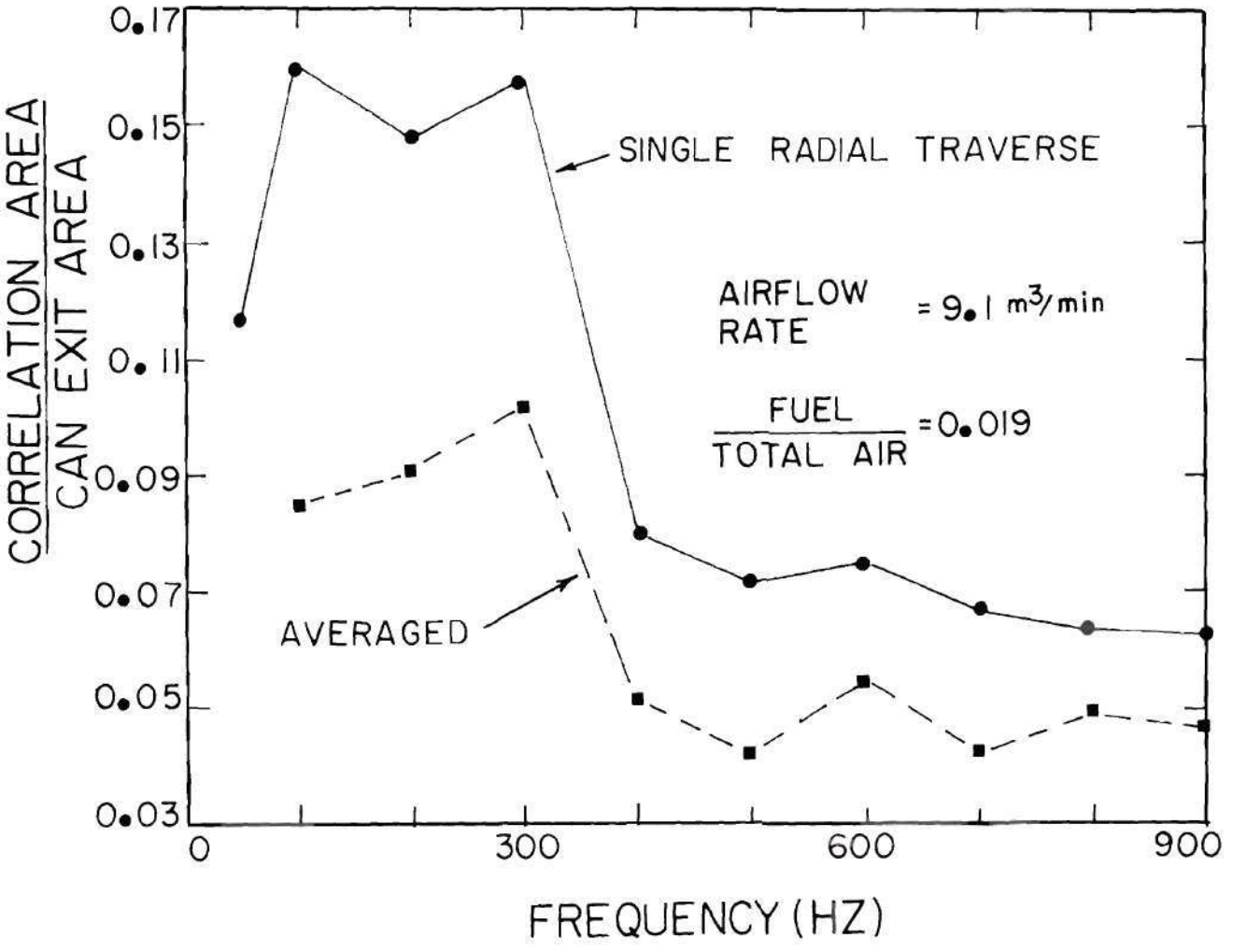

Figure 23. Frequency Distribution of Normalized Temperature Fluctuations Correlation Area.

Coherence Estimates. So far, the spectral characteristics of the individual signals have been discussed in detail. It will be expedient at this stage to look at the coherence between the various signals. As already mentioned in Chapter II, coherence estimates between two signals will bring out the true linear relationship between them. Coherence analysis among the interior, near and far field signals is explained below. Various noise sources and their associated transmission paths are illustrated in Figure 24. The near field signal is expected to contain contributions from two interior sources, namely combustion and entropy noise sources as well as from the exterior jet noise. Hence, the coherence between the interior and near field signals has to be evaluated on the basis of a multiple input problem. In such cases, the degree of linear relationship between any single cause and the effect is best revealed through the partial coherence function analysis which cancels out the effects of the other extraneous inputs. The theory of partial coherence functions and the procedures for evaluating them are described in detail in Reference 30.

The results of the coherence estimates between the interior and the near field signals are shown in Figures 25, 26, 27 and 28. It is important to note that the interior sources, namely, the interior pressure transducer and the thermocouple signals, may or may not be correlated. In either case, the coherence analysis takes care of the situation except that in the uncorrelated case, the expressions become simpler. The significance of the experimental coherence results can be best explained with the help of some analytical expressions for coherence estimates based on the model shown in Figure 24. For the purpose of

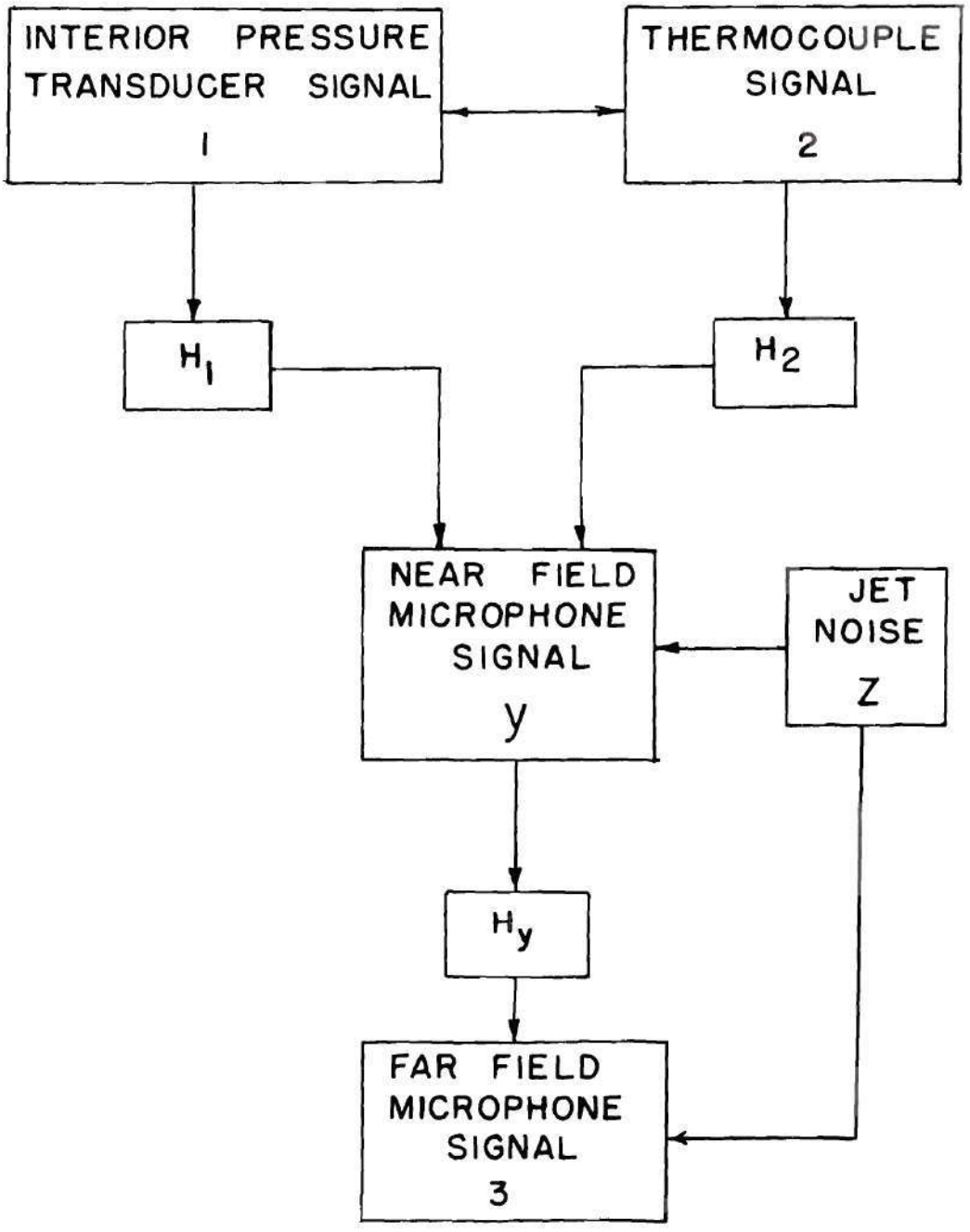

Figure 24. A Model of Noise Sources for Coherence Estimates.

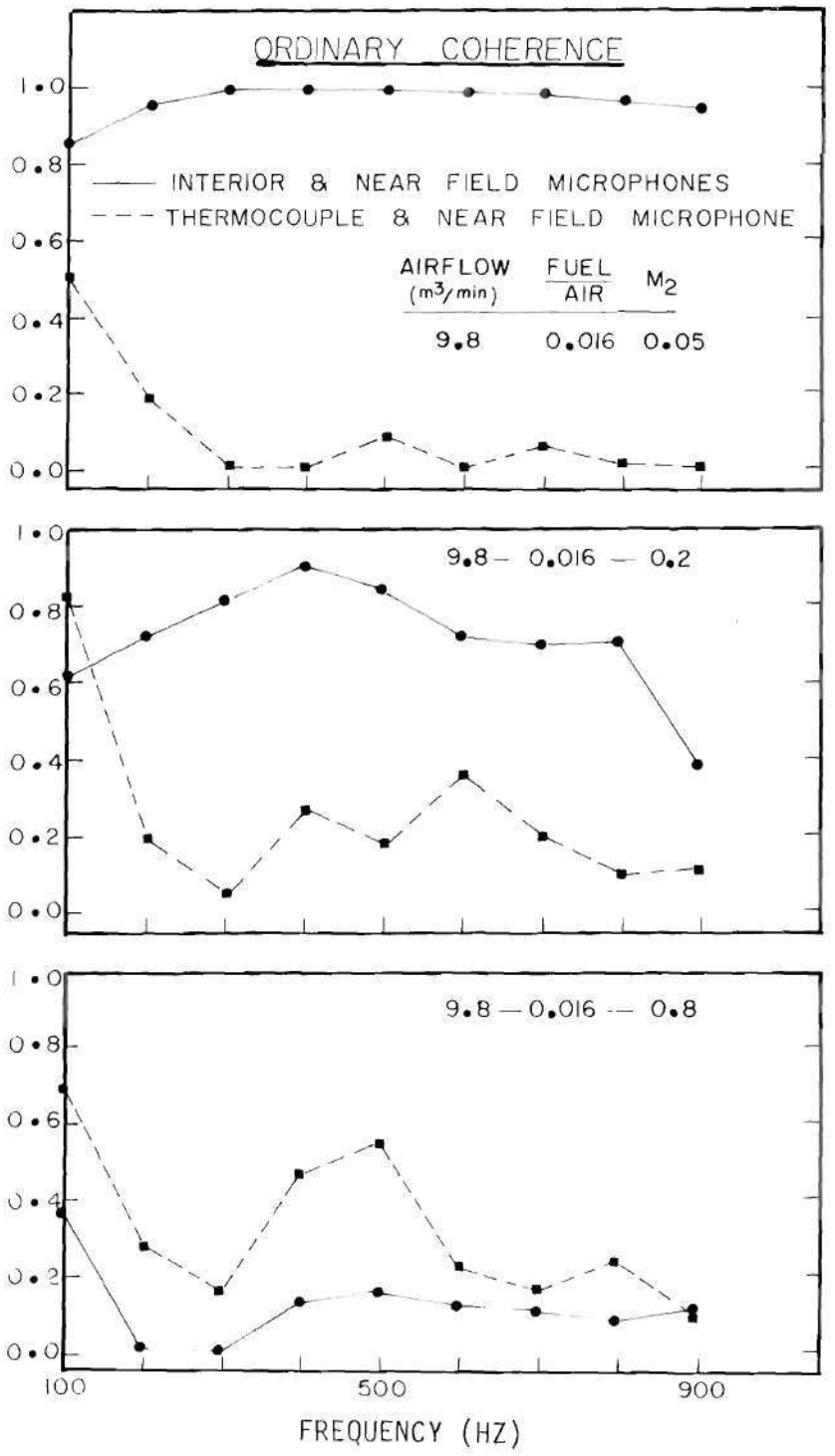

Figure 25. Ordinary Coherence Estimates Between Interior and Near Field Signals for Various Exit Mach Numbers with Different Exit Terminations.

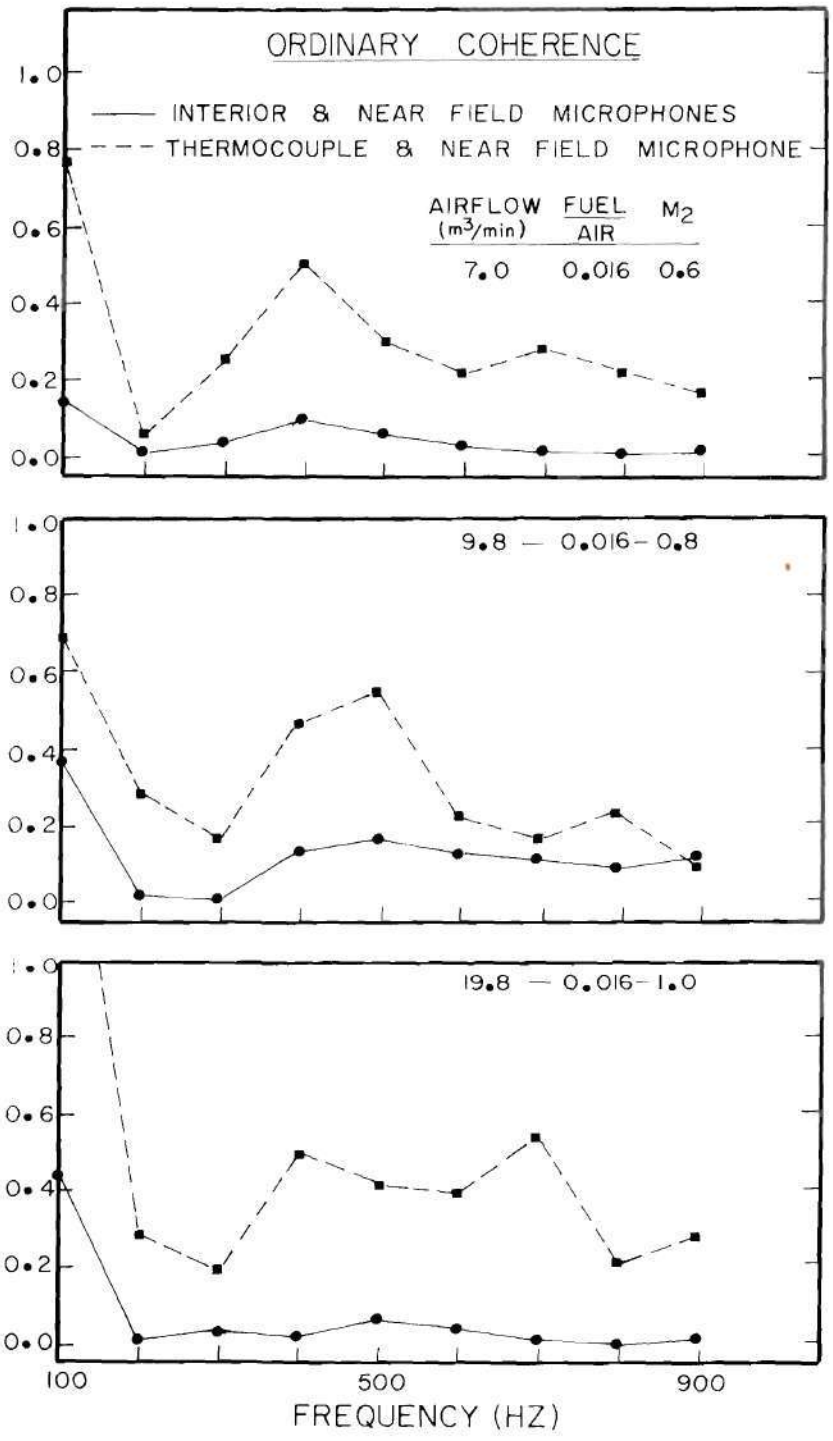

Figure 26. Ordinary Coherence Estimates Between Interior and Near Field Signals for a Fixed Exit Termination and Varying Exit Mach Numbers.

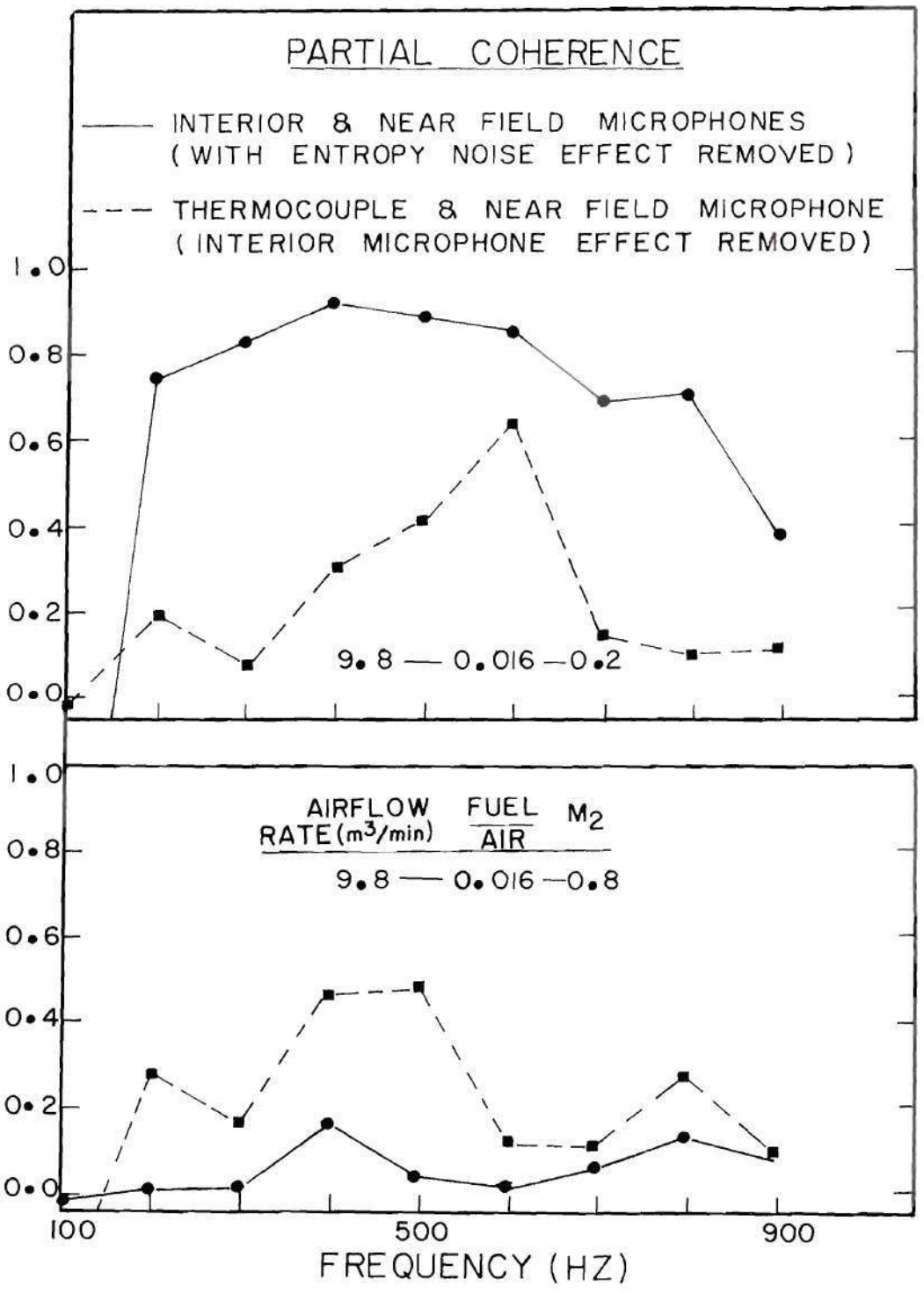

Figure 27. Partial Coherence Estimates Between Interior and Near Field Signals for Various Exit Mach Numbers with Different Exit Terminations.

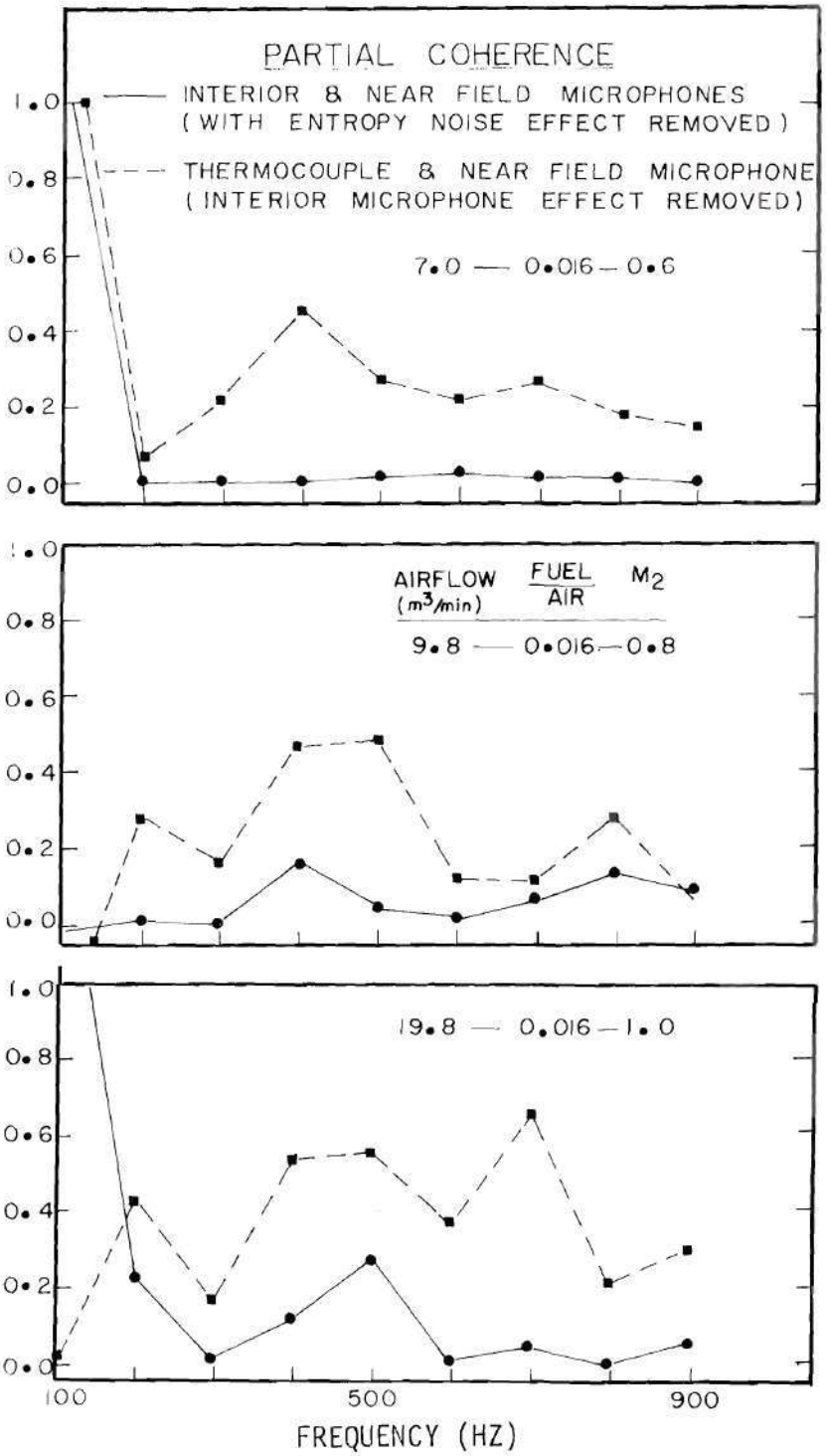

Figure 28. Partial Coherence Estimates Between Interior and Near Field Signals for a Fixed Exit Termination and Varying Exit Mach Numbers.

explanation, a model of an uncorrelated case will be assumed because of its simpler analytical expressions, although the same conclusions can be reached, even in the case of correlated inputs. For the uncorrelated *interior* sources, the model shown in Figure 24, yields the following expressions:[30]

Ordinary Coherence Estimate.

$$\text{Interior and near field microphones} = \gamma^2_{1y} = \frac{1}{1 + \left[\dfrac{|H_2|^2 \bar{S}_{22} + \bar{S}_{zz}}{|H_1|^2 \bar{S}_{11}}\right]}$$

$$\text{Thermocouple and near field microphone} = \gamma^2_{2y} = \frac{1}{1 + \left[\dfrac{|H_1|^2 \bar{S}_{11} + \bar{S}_{zz}}{|H_2|^2 \bar{S}_{22}}\right]} \quad (5)$$

Partial Coherence Estimate.

$$\text{Interior and near field microphones with entropy noise effect removed}: \quad \gamma^2_{1y,2} = \frac{1}{1 + \left[\dfrac{\bar{S}_{zz}}{|H_1|^2 \bar{S}_{11}}\right]} \quad (6)$$

$$\text{Thermocouple and near field microphone with interior microphone effect removed}: \quad \gamma^2_{2y,1} = \frac{1}{1 + \left[\dfrac{\bar{S}_{zz}}{|H_2|^2 \bar{S}_{22}}\right]}$$

where $\bar{S}$ denotes the many-sample-averaged power spectral densities of the subscripted source. Returning to the coherence results, it can be seen from Figures 25 and 26 that the ordinary coherence function level between the interior and near field microphones generally decreases with an increase in the exit Mach number, while that between the thermocouple

and the near field increases. This result, interpreted through Equations (5) suggest that the entropy noise contribution available to the near field microphone starts dominating the combustion noise contribution to the near field microphone signal, with the increase in the exit Mach number. Stated otherwise, there is a gradual transition from a combustion noise dominated situation at low Mach numbers to an entropy noise dominated one at high Mach numbers.

The partial coherence estimates, a more reliable procedure for the multiple-input problem, also confirm the above results in Figures 27 and 28. It can be seen from these figures that with the increase in the exit Mach number, the partial coherence estimate obtained between the thermocouple and the near field signals, with the interior microphone effects removed, rises above the partial coherence levels evaluated between the interior and the near field microphone signals, with the effect of the entropy noise removed. This partial coherence result, with the help of the Equations (6) reestablishes the previous result that the entropy noise starts dominating the near field signal with the increase in the exit Mach number. In other words, the partial coherence analysis also reaffirms the results of the ordinary coherence function analysis that a combustion noise domination of the near field signal at low Mach numbers yields to an entropy noise domination at high Mach numbers. It is important to note that in all the above partial coherence calculations the single point thermocouple measurements have been converted into area averaged quantities using Equations (3) and (4) which involve the ratio (A_e/A_{cor}). A look at Figure 23 reveals a significant difference in the correlation area values computed in two different ways.

The coherence results, discussed above, are based on the correlation area obtained from a single radial traverse of the thermocouple at the burner exit plane without any nozzle or orifice plate attachment. It is informative to see how sensitive the coherence estimates are to the correlation area values. Referring to Figure 24, the partial coherence estimate between 1 and y, with the effects of 2 subtracted out by a linear least-square prediction, is given as follows.[30]

$$\gamma^2_{1y,2}(f) = \gamma^2_{1y} \frac{\left(1 - \frac{A_e}{A_{cor}} \frac{\bar{S}_{1y}}{\bar{S}_{22}} \frac{\bar{S}_{2y}}{\bar{S}_{1y}}\right)}{\left(1 - \frac{A_e}{A_{cor}} \gamma^2_{12}\right)\left(1 - \frac{A_e}{A_{cor}} \gamma^2_{2y}\right)} \qquad (7)$$

The symbols used above have been explained in the previous equations and the ratio (A_e/A_{cor}) appears in the above equation to obtain the area averaged quantities from single point thermocouple measurements, as explained in Equations (3) and (4). For a given test run, the spectral and ordinary coherence estimates, after ensemble averaging and spectral smoothing have very stable values. Hence, the accurate estimation of the partial coherence estimate in Equation (7) depends heavily on the confidence with which A_{cor} can be computed for a given A_e. Figure 23 compares the correlation area obtained in two different ways. As explained in the previous section, the average correlation area is computed from the three correlation areas obtained through the radial as well as the circumferential thermocouple cross-correlations at the burner exit plane without any end attachment and the radial cross-correlations

at the burner exit plane with the orifice plate attached. The other one is obtained by a single radial traverse of the thermocouple across the burner exit plane without any end attachment. It can be seen from Figure 23 that there is about 2:1 change in the values when computed in two different ways. For a given set of spectral values, this change may drive the bracketed quantities in Equation (7) to fluctuate between very low positive values and negative ones, thereby altering the partial coherence estimates significantly. Figure 29 shows the partial coherence estimate based on this average correlation area for a few typical cases. A comparison of Figures 27 and 29 with the help of Figure 23 indicates that a decrease in the correlation area values generally increases the partial coherence estimates, with its effect being felt more on the coherence between the thermocouple and the near field signals than on the one between the interior and the near field microphones. The above arguments lead to the fact that a sufficiently accurate determination of the temperature correlation area distribution is vital for a reliable estimation of the partial coherence. This may be achieved by using a large number of thermocouples at the burner exit plane so as to obtain more details about the spatial distribution of the temperature fluctuations. The extraordinarily high coherence at about 100 Hz in the case of high Mach numbers is explained at the end of this section. It is important to note that the coherence values in some cases, even after ensemble averaging are found to be in the range of the statistical errors associated with the coherence estimates. With a view to increasing the reliability of the results, a spectral smoothing technique has been employed in which the spectral estimates corresponding to 9 adjacent

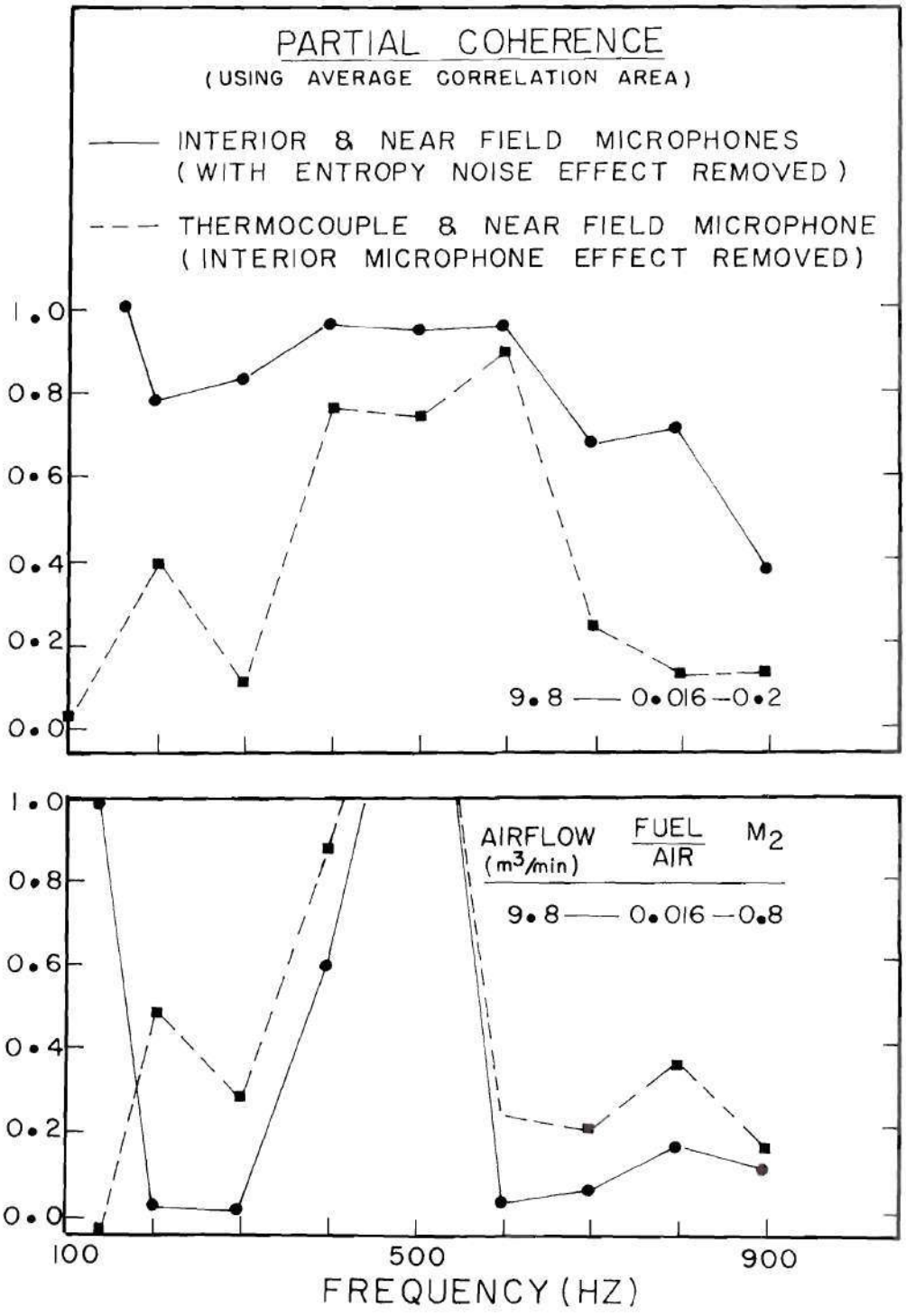

Figure 29. Partial Coherence Estimates Between Interior and Near Field Signals for Different Exit Mach Numbers Using Average Temperature Correlation Area.

frequency bands have been averaged. This process reduces the frequency resolution but improves the statistical stability.

The results of the ordinary coherence estimates between near and far field microphones are presented in Figure 30. A good coherence level exists at low exit Mach numbers. This is attributable to the fact that at these low Mach numbers, the combustion noise contribution to the exterior radiated sound is very high, and, further, its low frequency nature yields to a monopole radiation pattern. However, at high exit Mach numbers, the coherence level starts decreasing as shown in Figure 30. This may be due to the fact that with the increasing exit Mach number, the jet noise starts contaminating the core noise radiation. The far field microphone signal is contaminated to a greater degree than that of near field as the former receives the effect of the whole jet. However, the near field microphone receives a greater contribution from core noise radiation with a lesser degree of contamination by jet noise. This leads to low coherence levels between near and far field signals at high exit Mach numbers.

It can be seen from the coherence results of Figures 25 to 29 that in the high Mach number cases, the coherence suddenly jumps to a high value in the vicinity of 100 Hz. The interior and the near field microphone spectra as well as the thermocouple spectra exhibit a similar behavior at the corresponding frequencies, as shown in Figures 17, 18 and 20. Many possibilities for the occurrence of this low frequency peak have been investigated. A speculation about the contribution by the burner stand or the probe to this peak has to be discounted, because this occurs only in the high Mach number cases and, moreover, the

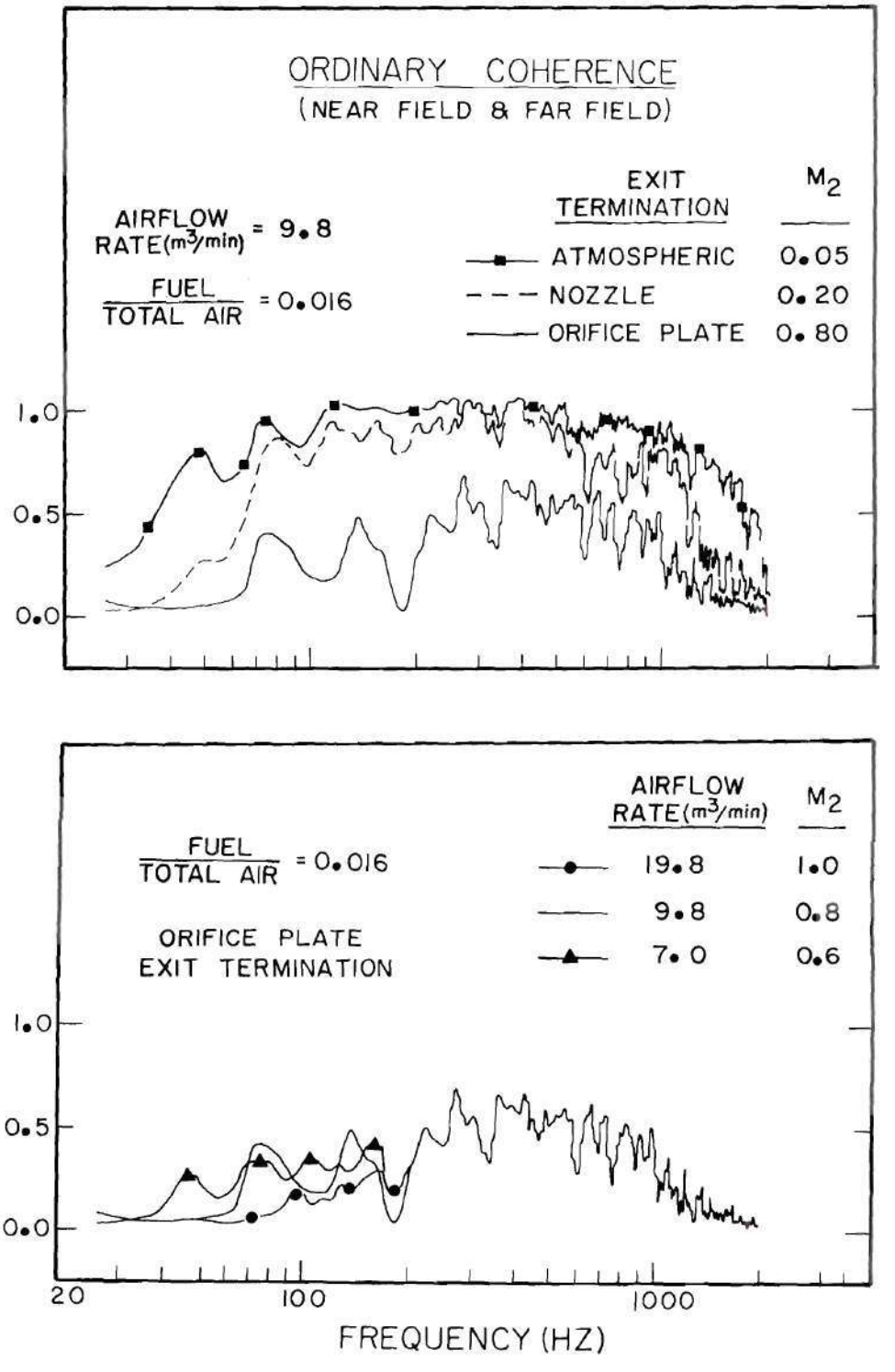

Figure 30. Ordinary Coherence Estimates Between Near and Far Field Microphone Signals for Various Exit Mach Numbers.

corresponding cold flow tests do not exhibit this trend. A suspicion on a longitudinal resonance phenomenon is ruled out because the resonant frequency of the combustor, calculated from the speed of sound within the burner rig and the length of the combustor, falls in the range of 400 - 800 Hz, depending on the nature of the exit termination, as supported experimentally by Figures 17 and B1. A strong possibility is that there may be an acoustic coupling between the interior pressure waves and the fuel/air ratio. Pressure waves traveling towards the head end of the burner will cause a change in the density of the air which results in a change in the fuel/air ratio. This changes the temperature of the fluid traveling towards the nozzle. The temperature change encountering the nozzle in turn produces a new set of pressure waves, augmenting the old set. It is believed that this acoustic feedback is mainly responsible for the observed low frequency (about 100 Hz) peak, since the frequency of the phenomenon should be governed by the flow speed and the burner length. Calculations show that this frequency falls in the range of 100 - 200 Hz. This peak, while interesting, is not too significant as far as the overall sound output is concerned in these experiments.

Finally, note from Equations (6) that the partial coherence function should be unity if there are no intervening noise sources other than the two under consideration ($S_{zz} = 0$). A partial coherence of unity is not achieved with either partial coherence function for either area correlation curve. Moreover, this is not even achieved for runs where the jet noise contamination is low. One could possibly conclude, therefore, that there are some unconsidered noise sources

which are important to the core noise problem. Unfortunately, the partial coherence function is relatively sensitive to the correlation area measurements so that this conclusion appears weak. On the other hand, the partial coherence function between the interior and near field microphones should not suffer from errors in the correlation area, and at high exit Mach number there is indeed low partial coherence between these two microphones. There is the suspicion, therefore, that at least one other noise source is present which was not investigated in this program. The most likely candidate appears to be vorticity-nozzle interaction noise, which is essentially a resistance of a nozzle to pass an axial velocity fluctuation. This deserves investigation in a future program.

CHAPTER IV

CONCLUSIONS AND RECOMMENDATIONS

Conclusions

The acoustic experiments have been conducted on a combustor, taken from a Boeing 502-7D gas turbine unit, to determine the relative importance of combustion and entropy noise in core engine noise in turbopropulsion systems. The airflow rates have been varied between 7 and 19.8 m^3/min. with the overall fuel/air ratio varying between 0.008 and 0.016. The test conditions cover a wide range of exit Mach numbers between 0.05 and 1.0, obtained either by increasing the exit contraction ratio or by varying the operating conditions. The spectral characteristics of interior, near field and far field pressure fluctuations as well as those of temperature fluctuations at the burner exit plane have been obtained. Also, ordinary and partial coherence estimates between the above signals have been evaluated. Summarizing the results of the present research investigations, the following conclusions are reached, some of which are apparatus-dependent.

1. Hydrodynamic noise, which is non-propagational pseudo-sound, dominates combustion noise in the interior of the combustor below 150 Hz, as revealed by flush mounted AVL pressure transducer measurements. For a true combustion noise propagation study, it is more appropriate to monitor the interior propagational sound from a position away from the flow field in order to keep contamination by hydrodynamic noise to a minimum.

2. The combustor used in the present program has r.m.s. temperature fluctuations at the burner exit plane varying between 9 and 14% of the mean exit temperature over the range of conditions tested here. Also, the length scales of the temperature fluctuations at the burner exit plane are found to be about 1 cm over a wide range of operating conditions.

3. *The most important* conclusion is that at low exit Mach numbers, the exterior radiated noise is mostly attributable to combustion noise whereas at high Mach numbers, entropy noise overtakes and dominates combustion generated noise. Entropy noise domination results because of the combination of high level of temperature fluctuations existing at the nozzle entrance plane and large pressure gradients being imposed on them.

4. An acoustic coupling is found to exist between interior pressure waves and the combustion process in the frequency range of 100 - 200 Hz at high exit Mach numbers.

5. The interpretation of partial coherence results suggests a possible existence of another propagational noise source, apart from combustion and entropy noise. It is inconclusive at this stage whether or not vorticity-nozzle interaction noise is a prime candidate for this.

Recommendations for Future Work

Some recommendations are made below for future investigations on the basis of present findings.

1. The partial coherence results between interior and exterior measurements of the present program lead to a suspicion on the existence

of some other unexplored propagational noise sources. Future work is needed to investigate whether or not vorticity-nozzle interaction noise is involved.

2. The significant differences, observed in the spatial correlation results of temperature fluctuations at the burner exit plane, lead to the recommendation that in future work, to achieve a good degree of accuracy, a net of thermocouples be used instead of only two thermocouple traverses used in the present program.

APPENDIX A

MEASUREMENT OF THERMOCOUPLE TIME CONSTANTS

This section describes a new method of determining the time constants associated with the thermocouples. The theoretical background of this new method has been developed by Strahle.[28] A description of the theory and the experimental procedures involved in this method is given below.

Theory

Following the same notation used in Reference 28, let x represent the true temperature fluctuation and y denote the fluctuating signal recorded by the thermocouple about the mean temperature. y can be expressed as $\tilde{y} + z$ where $\tilde{y}$ is the portion of the signal truly proportional to the temperature fluctuations and z is the background electronic noise. A heat transfer balance at the thermocouple junction yields a differential equation for $\tilde{y}$ as

$$\frac{d\tilde{y}}{dt} = \frac{1}{\tau}(\eta x - \tilde{y}) \qquad \text{(A-1)}$$

where τ is the time constant of the thermocouple, t is time and η is a factor deduced from the conduction and radiation factors and is near unity.[33] The main interest is the evaluation of time constant τ. The theoretical considerations require two thermocouples, denoted by 1 and 2, of differing time constants to be placed very close to each other in

the flow so that both register the same temperature fluctuations. However, there is a practical difficulty in keeping them very close without any damage and this small separation distance may lead to some errors, the extent of which can be assessed later through the coherence estimate.

Letting the capital letters represent the Fourier transform of the small letter quantities and taking a finite Fourier transform of Equation (A-1), it can be shown that

$$Y = \overline{Y} + Z = \frac{\eta X}{1 + i\omega\tau} + Z \qquad \text{(A-2)}$$

Using Equation (A-2), the ensemble averaged auto and cross power spectra of the signals, denoted by a bar superscript, can be derived as

$$\overline{S}_{11} = \frac{\eta^2 \overline{XX}^*}{(1 + \omega^2 \tau_1^2)} + \overline{Z_1 Z_1^*}$$

$$\overline{S}_{12} = \frac{\eta^2 \overline{XX}^*}{[1 + \omega^2 \tau_1 \tau_2 + i\omega(\tau_1 - \tau_2)]} \qquad \text{(A-3)}$$

where * denotes a complex conjugate. Equations (A-3) are obtained by assuming that the noise is incoherent with the signal and z_1 and z_2 are incoherent with each other. It is further assumed that the spurious noise for signal 1 is sufficiently small that $\overline{Z_1 Z_1^*}$ can be neglected in comparison with the first term in $\overline{S}_{11}$. Now, a ratio between $\overline{S}_{11}$ and $\overline{S}_{12}$ can be obtained as

$$R = \frac{\overline{S}_{11}}{\overline{S}_{12}} = \frac{1 + \omega^2 \tau_1 \tau_2 + i\omega(\tau_1 - \tau_2)}{1 + \omega^2 \tau_1^2} = R_r + iR_i \quad \text{(A-4)}$$

where $R_r = \frac{1 + \omega^2 \tau_1 \tau_2}{1 + \omega^2 \tau_1^2}$ and $R_i = \frac{\omega(\tau_1 - \tau_2)}{1 + \omega^2 \tau_1^2}$

Consider a limiting case, ω tending to ∞, which yields the time constant ratio as

$$\lim_{\omega \to \infty} R = \lim_{\omega \to \infty} R_r = \frac{\tau_2}{\tau_1} \quad \text{(A-5)}$$

The imaginary part R_i is more useful for present purposes. By differentiating R_i in Equation (A-4), it can be shown that for $\tau_1 \neq \tau_2$, a single extremum in R_i occurs at a frequency ω_m given by

$$\omega_m = \frac{1}{\tau_1} \quad \text{(A-6)}$$

Hence, τ_1 can be evaluated by noting the extremum frequency, ω_m, in the plot of R_i against ω. The necessary conditions for the above theoretical considerations to be valid are that both the thermocouples should be recording the same temperature fluctuations and the noise is at a sufficiently low level compared to the signal, at least in the vicinity of ω_m.

Experimental Procedures

An experiment has been designed to implement the above theoretical considerations with a view to obtain the time constants of the thermocouples. Two Chromel-Alumel thermocouples of wire diameters 0.025 mm

(TCI) and 0.075 mm (TC2) are mounted very close to each other (less than 3 mm apart) at the burner exit plane. The primary interest here is in the time constant τ_1 of TCI. Both the thermocouple signals are recorded on a magnetic tape recorder as per the procedures laid down in Chapter II. The recorded signals are then subjected to spectral analysis and coherence estimates. The thermocouple TCI is quoted to have a time constant between 1 and 10 msec by the manufacturer. Hence, a narrow frequency range of 0 - 400 Hz with a finer bandwidth of 3.1 Hz is chosen for the signal analysis. The coherence between the two thermocouple signals, as shown in Figure A1a, seems to be good, thereby satisfying the necessary conditions underlying the theoretical development of the previous section. Figure A1b shows the variation of R_r and R_i with the frequency. Equation (A-5) demands that R_r should tend to τ_2/τ_1 with increasing frequency and Figure A1b exhibits this expected behavior, yielding a value of 5.2 for τ_2/τ_1. It can be shown from heat transfer considerations that the time constant τ varies with the wire diameter D as $D^{1.5}$, thereby yielding an approximate value of $3^{1.5} = 5.2$ for τ_2/τ_1, which checks well with the experimental value. From the plot of R_i in Figure A1b the frequency, ω_m, corresponding to an extremum in R_i, is obtained as 40 Hz which yields a time constant $\tau_1 = 1/(2\pi 40) = 4$ msec, through Equation (A-6). Figure A2 shows the fixed bandwidth spectra of the two uncompensated thermocouple signals and also the true spectrum, after compensation for time constant. It is assumed in the development of Equation (A-1) that the time constant τ primarily depends on the convective heat transfer rate which in turn involves flow velocity of the hot exhaust gases. It can be shown mathematically that the value

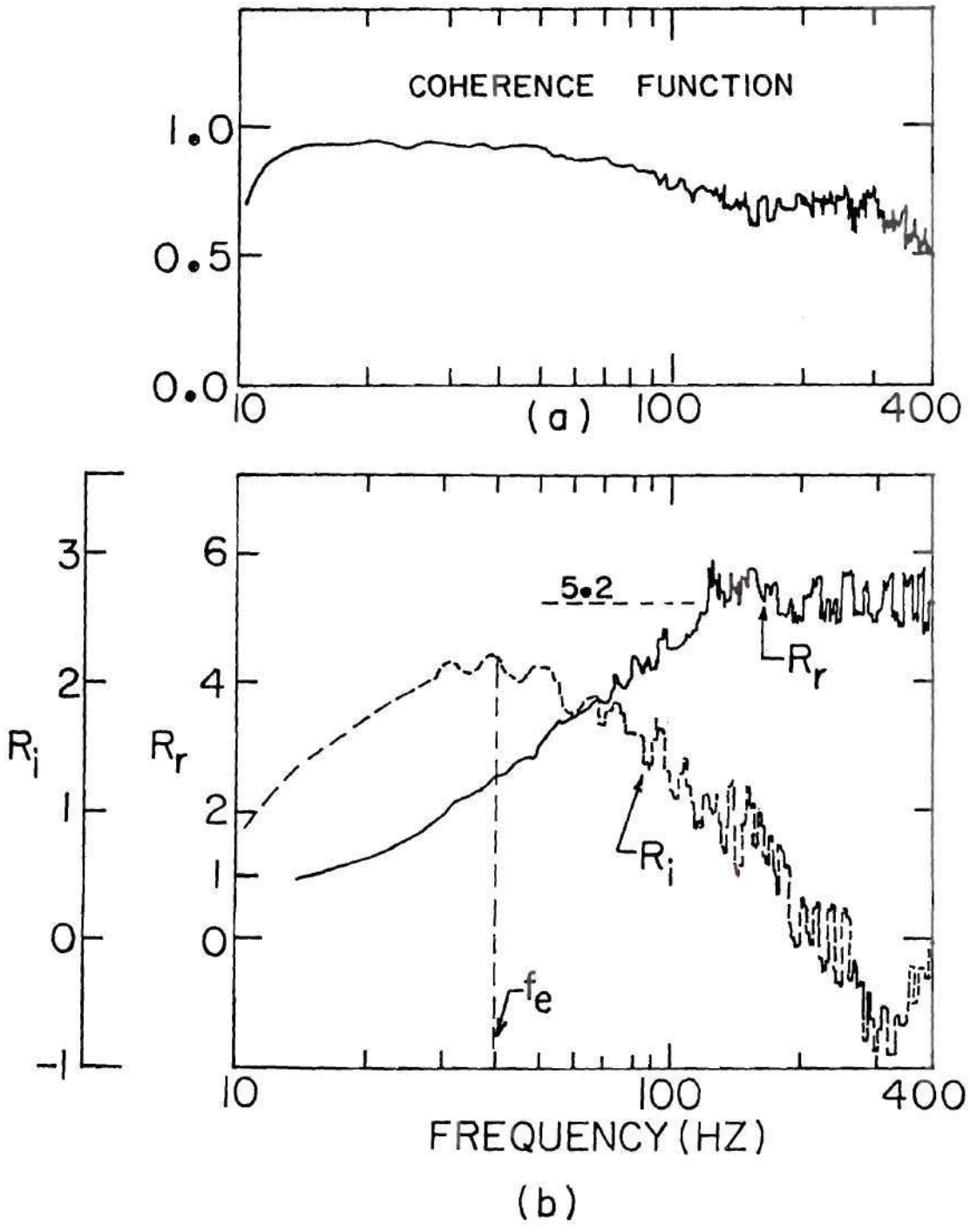

Figure A1. a) Coherence Estimate Between Two Thermocouple Signals and b) Time Constant Determination for the Thermocouples.

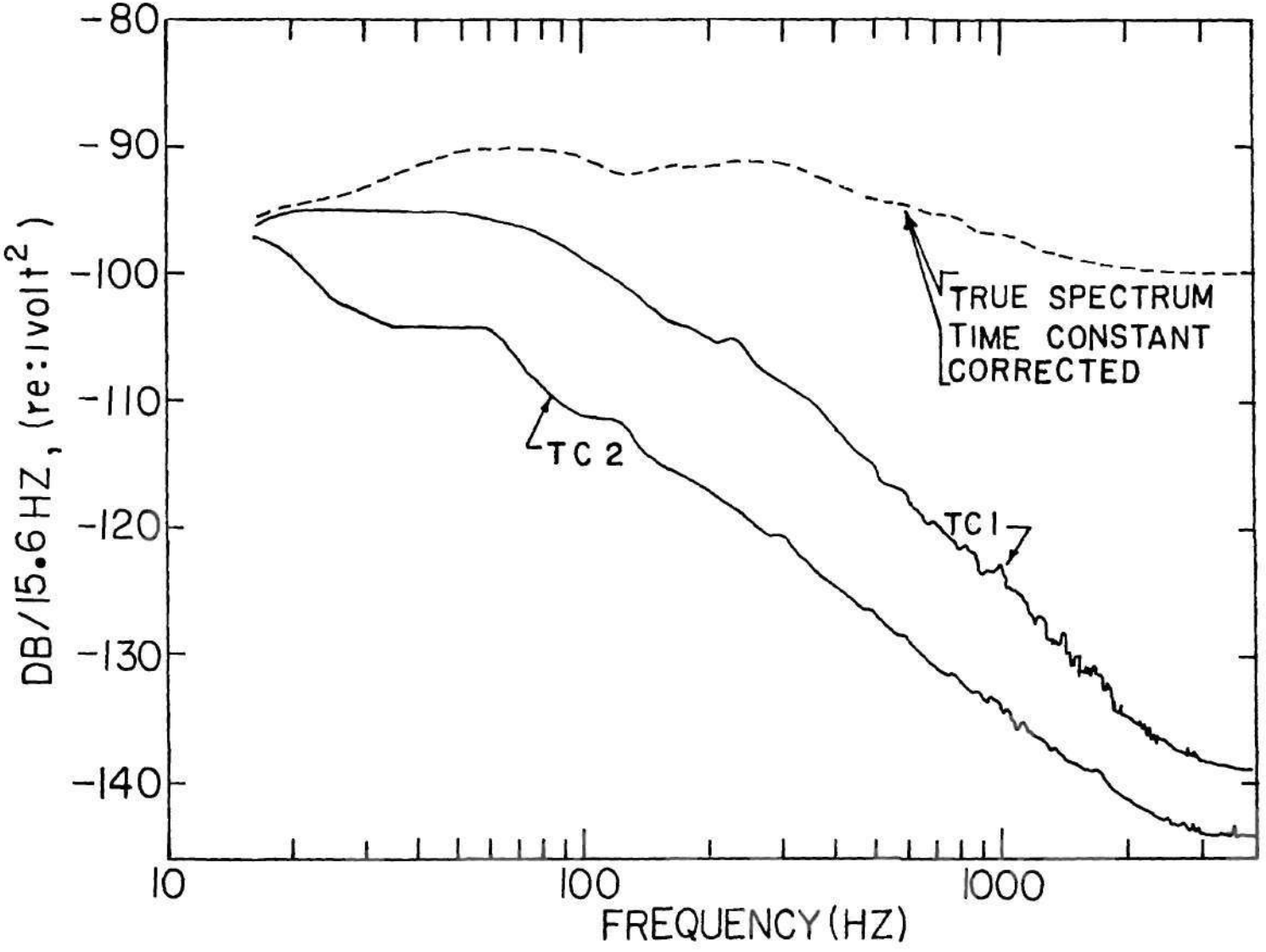

Figure A2. Temperature Fluctuations Spectra for Two Different Thermocouples (both uncompensated and compensated).

of τ is determined mostly by mean flow velocity and the fluctuations in velocity about the mean cause only insignificant changes in τ.

In the present method, the thermocouple signal is compensated for the time constant during data analysis through the Fourier Analyzer system. A look at the Equation (A-2) suggests that as long as the noise level is low, the Fourier transform of the true temperature fluctuations can be obtained from the Fourier transform of the thermocouple signal by multiplying the latter by a factor $(1 + i\omega\tau)$. This multiplication can be very easily effected through a simple programming step in the Fourier Analyzer system.

The main problem encountered in this method is that the maximum in R_i is somewhat broad and this leads to some uncertainty in the computed values of time constants. For example, in the present case, an error of less than 10% may be expected in the value of τ_1. It appears that this must be accepted as a limitation of the method.

APPENDIX B

ADDITIONAL MEASUREMENTS AND RESULTS

It has been established in Chapter III that a study of interior propagational sound sources can be best achieved by monitoring the interior pressure fluctuations from a position displaced from the flow field. This arrangement helps to keep hydrodynamic noise contamination of the interior signals to a minimum. The results of such measurements conducted with a photocon pressure transducer, have been reported in Chapter III. However, initially a series of exploratory tests, covering a wide range of exit Mach numbers, have been carried out with the flush mounted AVL pressure transducer measuring the interior pressure fluctuations. The results of these AVL measurements, not reported in Chapter III, are presented below, as a matter of additional information.

In the present series of tests, the airflow rates vary between 7.0 and 19.8 m^3/min. with the overall fuel/air ratio varying between 0.017 and 0.019. An exit Mach number, $M_2 = 0.05$, represents the burner can operating without a nozzle while, $M_2 = 0.21$, belongs to the convergent nozzle case and $M_2 = 0.6$, 0.8 and 1.0 come through the use of orifice plate. Figure B1 shows the spectra of interior pressure fluctuations measured with flush mounted AVL pressure transducer. Figure B1a illustrates spectral changes with the increasing pressure drop across the combustor as the exit termination is changed whereas Figure B1b shows the spectral behavior with increasing pressure drop across the orifice

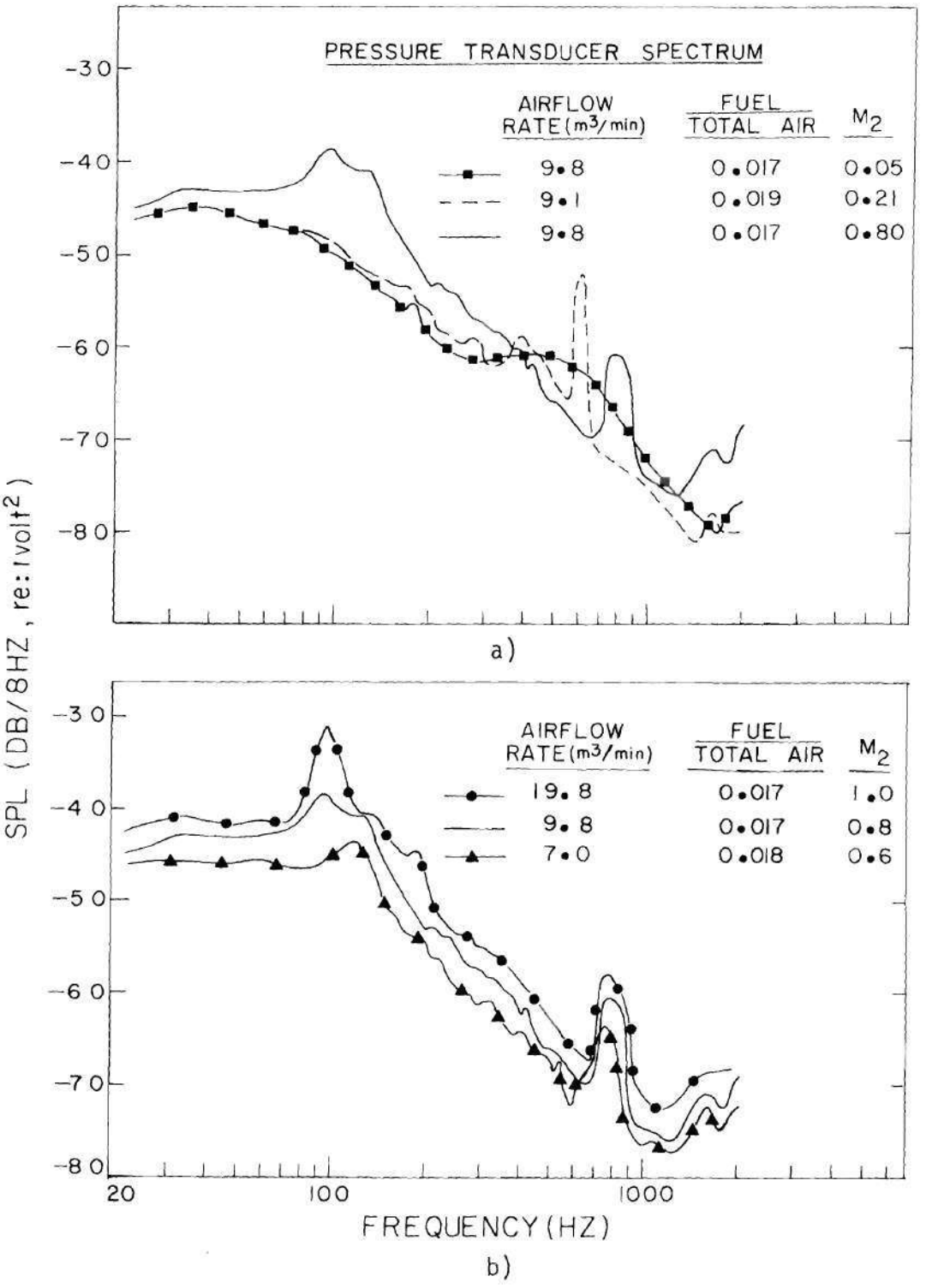

Figure B1. Interior AVL Spectra for Various Exit Mach Numbers.

plate for varying operating conditions. All the interior spectra exhibit a general trend of maintaining an almost constant level up to about 100 Hz and then falling off rapidly. Figure B1a brings out the shift in the resonance peaks from 500 through 800 Hz as the quarter wave burner can resonance tends towards half wave, with increasing exit contraction ratio. However, it is surprising to note that the resonance peaks corresponding to high Mach number cases are totally absent in the spectra obtained with photocon measurements as seen from Figure 17 in Chapter *III*.

The results of near and far field measurements corresponding to the above cases are not reported here because they have identical behavior with those described in Figures 18 and 30 of Chapter III, as expected.

The results of ordinary and partial coherence estimates between interior AVL and near field microphone signals, for the above cases, are brought out in Figures B2, B3, B4 and B5. The general interpretation of these results is the same as the one mentioned in Chapter III under the entropy noise section. The general conclusion, arrived at there, also remains valid. Namely, at low Mach numbers, core noise is mostly attributable to combustion noise while at high Mach numbers, entropy noise is a prime contributor to core noise. The major difference between the present coherence results obtained with interior AVL measurements and those described in Chapter III with photocon measurements is that the AVL measurements have been contaminated with non-propagational hydrodynamic noise, resulting in poor coherence in the frequency range of 0 - 150 Hz.

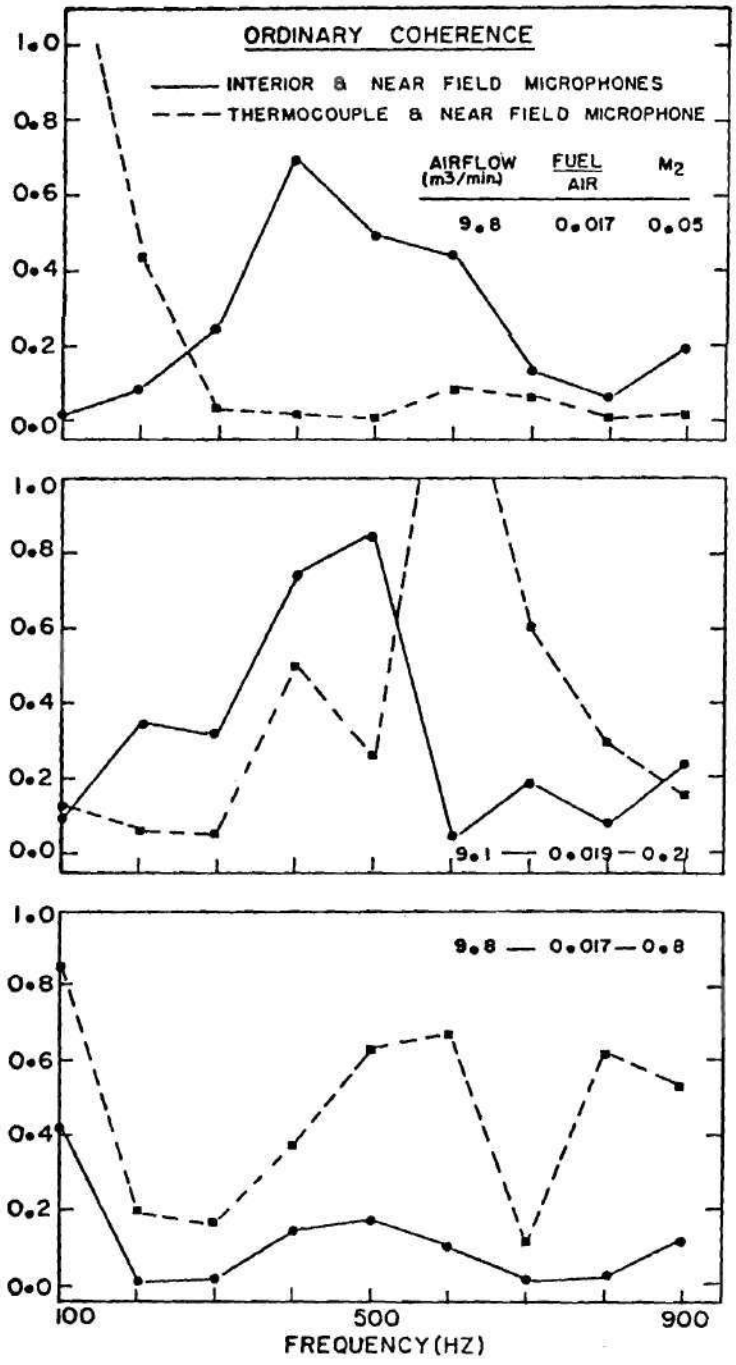

Figure B2. Ordinary Coherence Estimates Between Interior and Near Field Signals for Various Exit Mach Numbers with Different Exit Terminations.

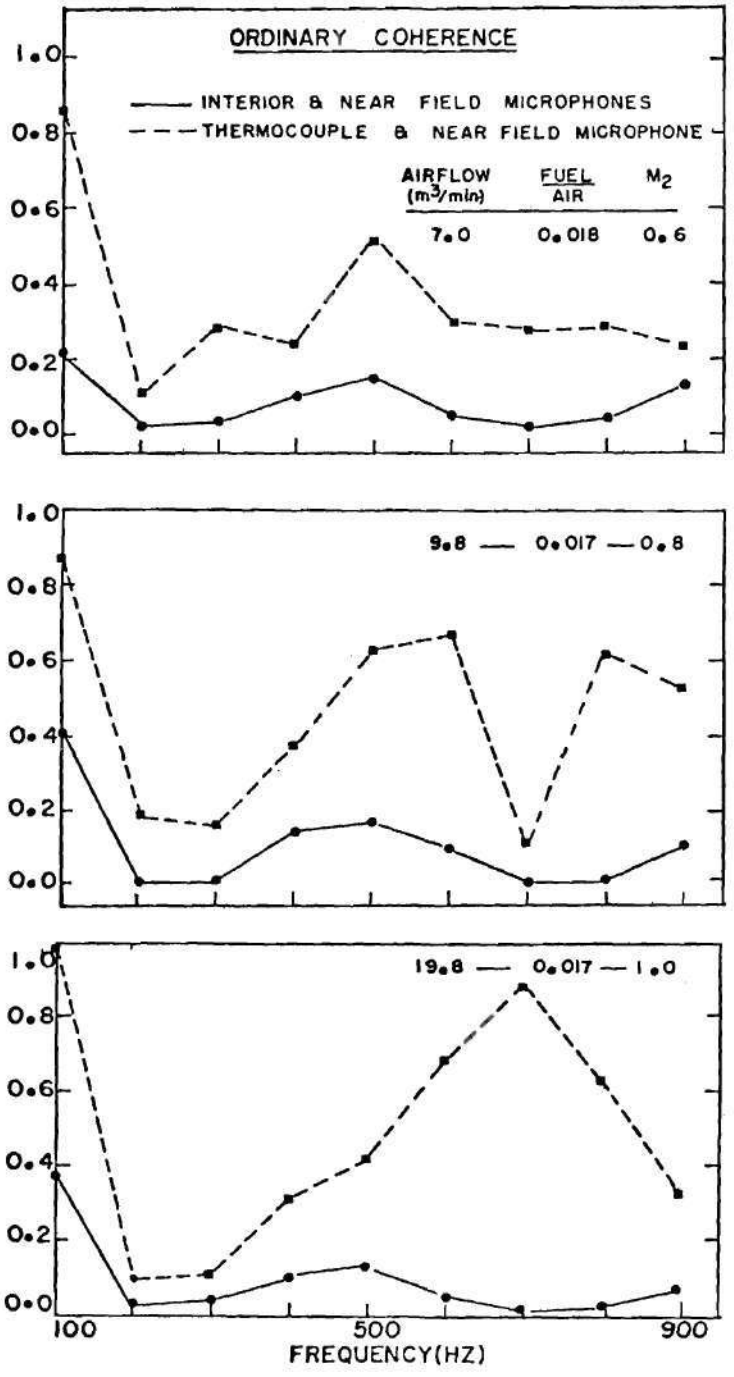

Figure B3. Ordinary Coherence Estimates Between Interior and Near Field Signals for Various Exit Mach Numbers and a Fixed Exit Termination.

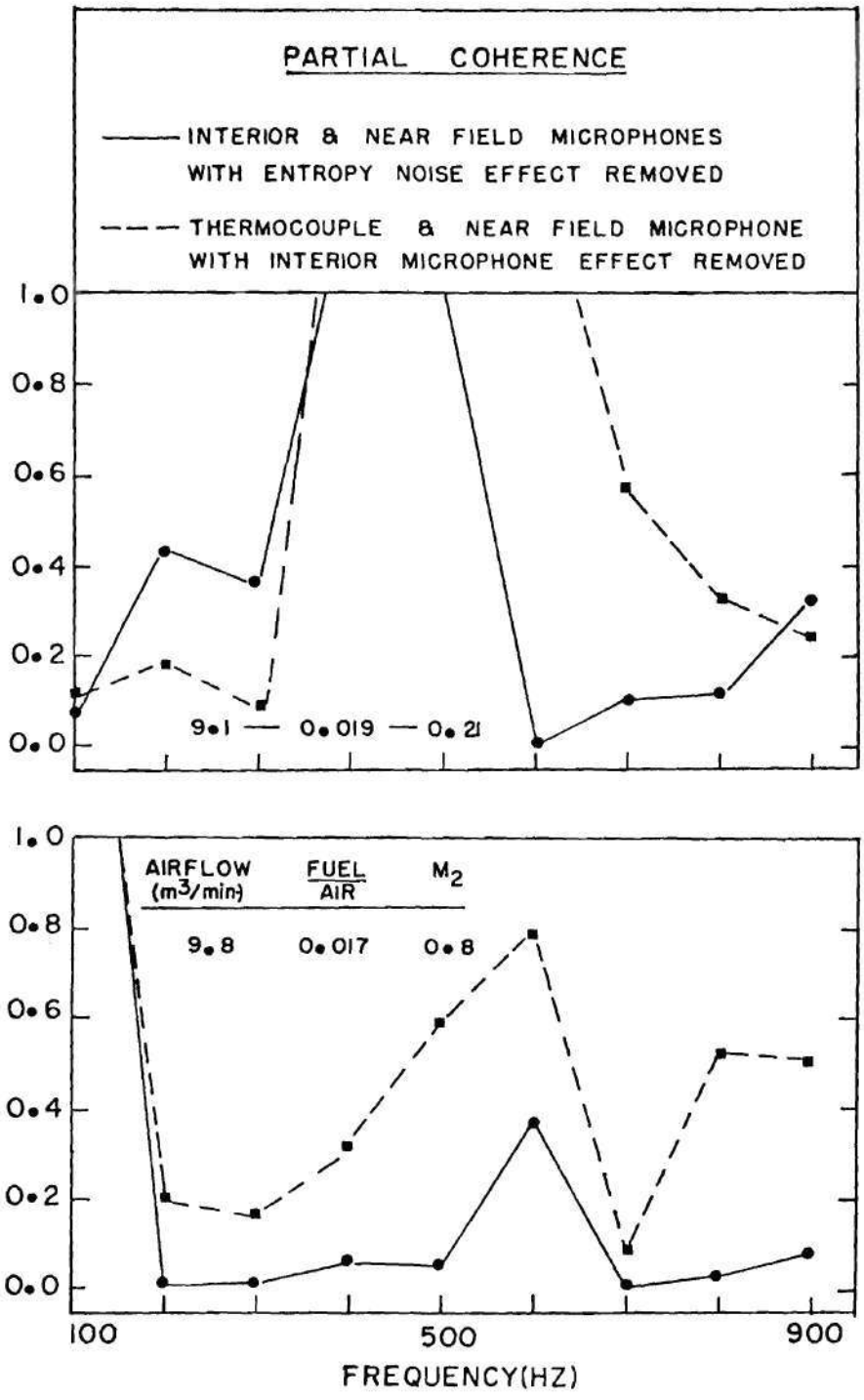

Figure B4. Partial Coherence Estimates Between Interior and Near Field Signals for Various Exit Mach Numbers with Different Exit Terminations.

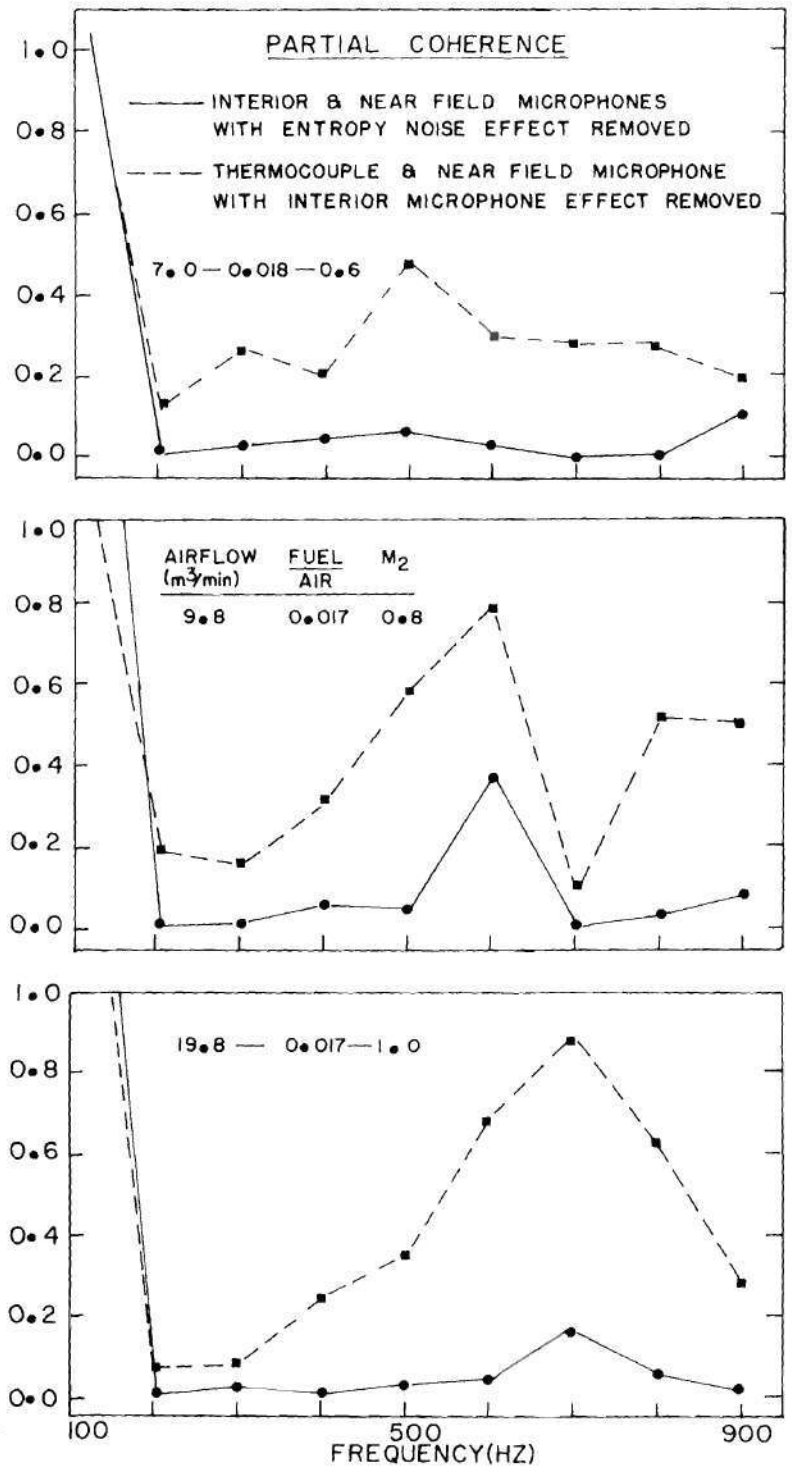

Figure B5. Partial Coherence Estimates Between Interior and Near Field Signals for Various Exit Mach Numbers and a Fixed Exit Termination.

Returning to the other exploratory tests, experiments have been conducted on the nozzle configuration to study the effects of variations in overall fuel/air ratio on the exterior radiated noise characteristics. The main idea here is to check whether or not a significant variation in fuel/air ratio will produce large changes in temperature fluctuations and affect a transition from combustion noise dominance to entropy noise domination. The airflow rate was maintained constant at 9.1 m^3/min. with overall fuel/air ratio varying between 0.01 and 0.019. The interior AVL and near field microphone spectra, shown in Figure B6 for extreme conditions, exhibit characteristics similar to those described in Figures B1 and 18. A shift in the resonance peak in the near field spectra with an increase in fuel/air ratio is seen clearly in Figure B6. The spectral characteristics of temperature fluctuations at the nozzle entrance plane are very similar to those described in Figure 20 of Chapter III. Since no significant changes have been observed either with spectral characteristics or r.m.s. levels of temperature fluctuations, even with 2:1 change in fuel/air ratio, it is believed that a study of transitional characteristics may not be feasible by varying the fuel/air ratio alone. This fact is confirmed through Figure B6 wherein the near field microphone spectra, corresponding to the extreme conditions, display very similar combustion noise characteristics. Hence, in the main body of this dissertation, the study of entropy noise has been facilitated by subjecting the exhaust gases to different pressure gradients, brought out by varying the exit contraction ratios. These results have been already presented in Chapter III.

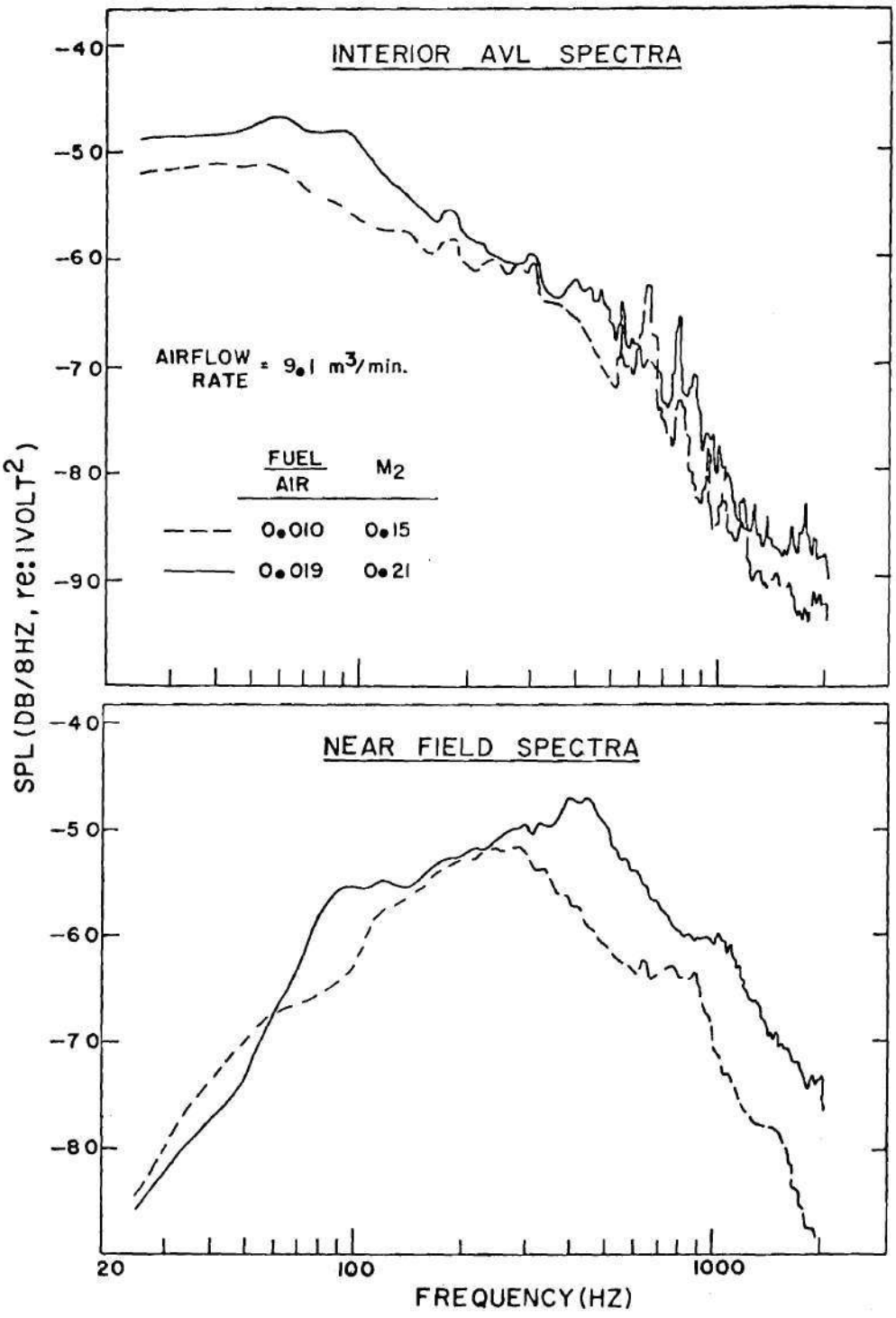

Figure B6. Interior AVL and Near Field Microphone Spectra for a Fixed Airflow Rate and Varying Overall Fuel/air Ratios.

Some of the early exploratory tests have been conducted with a different nozzle of area reduction 5.9:1. Results pertaining to two cases with this nozzle are reported here. The airflow rates are 12 and 11.2 m^3/min. with overall fuel/air ratios being 0.008 and 0.015 respectively. The corresponding exit Mach numbers are 0.37 and 0.45. Figure B7 shows the interior AVL and near field microphone spectra for these two cases. The interior spectra have characteristics similar to those described in Figures B1 and B6. But, the near field spectra exhibit a peak around 1000 Hz which is not observed in the combustion noise spectra. This looks more like a jet noise spectrum. A check of the near field noise scaling laws with velocity gives an exponent of 5 which is higher than a combustion noise exponent of 2 to 4, but falling below the jet noise exponent of 8. This leads to the strong suspicion that there is significant jet noise contamination of the near field signal even at moderate exit Mach numbers with this nozzle. An attempt to reach low Mach numbers was met with some practical difficulties in monitoring the flow systems. Hence, this nozzle has been modified to yield an area reduction of 3:1 to carry out tests with less jet noise interference at least in low Mach number cases. The results, obtained with this modified nozzle, have been reported in Chapter III.

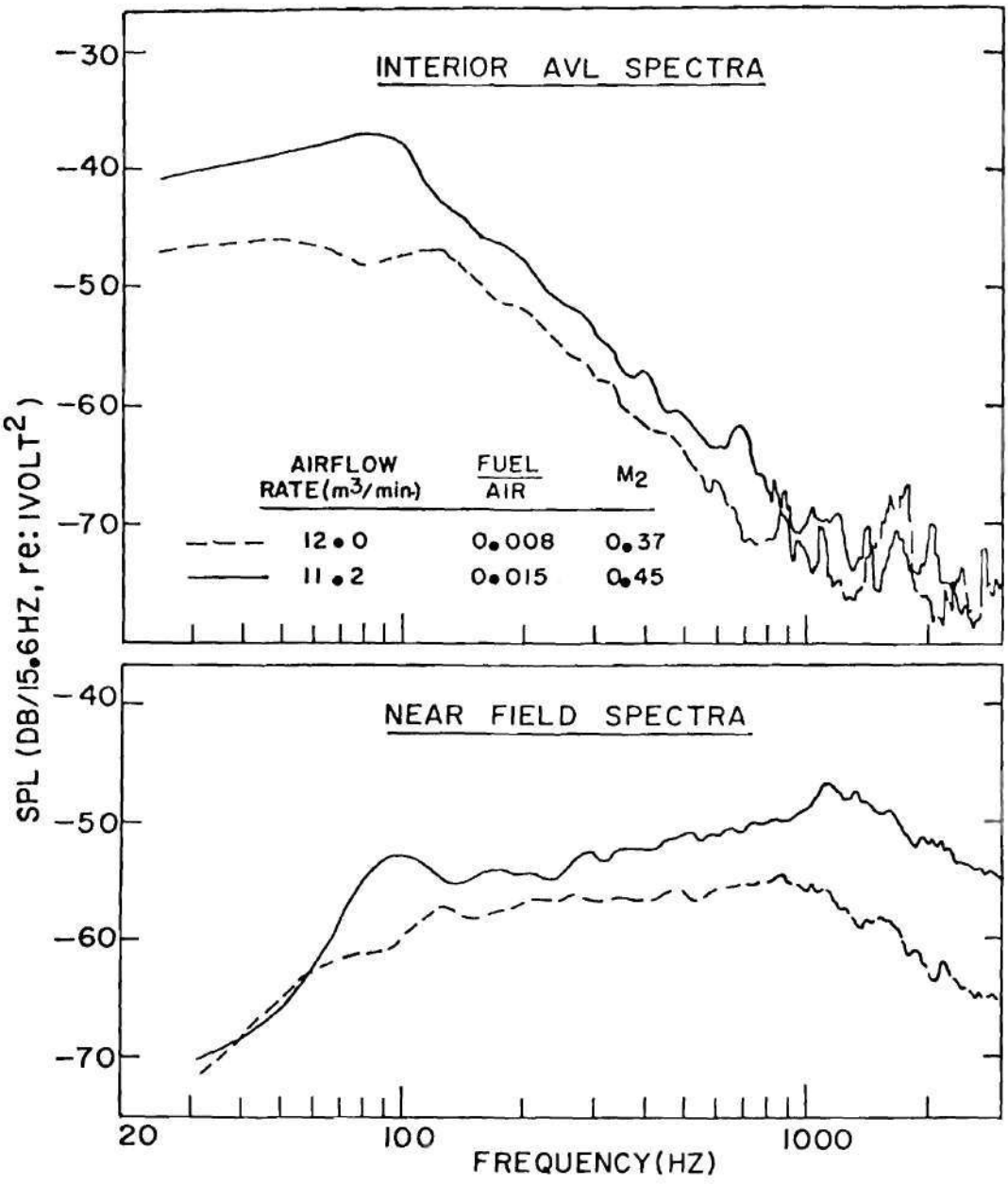

Figure B7. Interior AVL and Near Field Microphone Spectra for Different Operating Conditions with a Long Nozzle of Area Reduction 5.9:1.

REFERENCES

1. Bushell, K. W., "A Survey of Low Velocity and Coaxial Jet Noise with Application to Prediction," Journal of Sound and Vibration, Vol. 17, No. 2, 1971, pp. 271-282.

2. Mathews, D. C. and Peracchio, A. A., "Progress in Core Engine and Turbine Noise Technology," AIAA Paper No. 74-948, 1974.

3. Hoch, R. G., Thomas, P., and Weiss, E., "An Experimental Investigation of the Core Engine Noise of a Turbofan Engine," AIAA 2nd Aero-Acoustics Conference, Paper No. 75-526, 1975.

4. Huff, R. G., Clark, B. J., and Dorsch, R. G., "Interim Prediction Method for Low Frequency Core Engine Noise," NASA TMX-71627, 1974.

5. Motsinger, R. E. and Emmerling, J. J., "Review of Theory and Methods for Combustion Noise Prediction," AIAA Paper No. 75-541, 1975.

6. Mathews, D. C., Nagel, R. T., and Kester, J. D., "Review of Theory and Methods for Turbine Noise Prediction," AIAA Paper No. 75-540, 1975.

7. Strahle, W. C., "On Combustion Generated Noise," Journal of Fluid Mechanics, Vol. 49, No. 1, Sept. 1971, pp. 339-414.

8. Strahle, W. C., "Some Results in the Combustion Generated Noise," Journal of Sound and Vibration, Vol. 23, No. 1, July 1972, pp. 113-125.

9. Strahle, W. C. and Shivashankara, B. N., "A Rational Correlation of Combustion Noise Results from Open Premixed Turbulent Flames," Fifteenth Symposium (International) On Combustion, The Combustion Institute, Pittsburg, 1975.

10. Chiu, H. H. and Summerfield, M., "Theory of Combustion Noise," Acta Astronautica, Vol. 1, Nos. 7-8, July-August 1974, pp. 967-984.

11. Shivashankara, B. N., Strahle, W. C., and Handley, J. C., "Combustion Noise Radiation by Open Turbulent Flames," Aeroacoustics: Jet and Combustion Noise; Duct Acoustics, Ed. H. Nagamatsu, AIAA, New York, 1975, p. 277.

12. Muthukrishnan, M., Strahle, W. C., and Handley, J. C., "The Effects of Flameholders on Combustion Generated Noise," AIAA Paper No. 76-39, 1976.

13. Chiu, H. H., Plett, E. G., and Summerfield, M., "Noise Generation by Ducted Combustion Systems," AIAA Paper No. 73-1024, 1973.

14. Abdelhamid, A. N., Harrje, D. T., Plett, E. G., and Summerfield, M., "Noise Characteristics of Combustion Augmented Jets at Mid-subsonic Speeds," AIAA Journal, Vol. 12, No. 3, 1974, pp. 336-342.

15. Strahle, W. C. and Shivashankara, B. N., "Wall Reflection Effects in Combustion Generated Noise," AIAA Paper No. 75-127, 1975.

16. Strahle, W. C. and Shivashankara, B. N., "Combustion Generated Noise in Gas Turbine Combustors," NASA CR-134843, August 1974.

17. Cuadra, E., "Acoustic Wave Generation by Discontinuities Flowing Past an Area Change," The Journal of the Acoustical Society of America, Vol. 42, No. 4, 1967, pp. 725-732.

18. Crocco, L. and Sirignano, W. A., "Behavior of Supercritical Nozzles Under Three-Dimensional Oscillatory Conditions," AGARDograph No. 117, Nato, 1967.

19. Candel, S. M., "Analytical Studies of Some Acoustic Problems of Jet Engines," Ph.D. Thesis, California Institute of Technology, 1972.

20. Wahbah, M. M., "Analysis Related to Combustion Noise Research, Ph.D. Thesis, Georgia Institute of Technology, 1975.

21. Pickett, G. F., "Core Engine Noise due to Temperature Fluctuations Convecting through Turbine Blade Rows," AIAA Paper No. 75-528, 1975.

22. Cumpsty, N. A., "Excess Noise from Gas Turbine Exhausts," ASME Paper No. 75-GT-61, 1975.

23. Strahle, W. C., "Noise Produced by Fluid Inhomogeneities," AIAA Journal, Vol. 14, No. 7, July 1976, pp. 985-987.

24. Grande, E., "Core Engine Noise," AIAA Paper No. 73-1026, 1973.

25. Mathews, D. E. and Nelson F. Rekos, Jr., "Direct Combustion Generated Noise in Turbopropulsion Systems - Prediction and Measurement," AIAA Paper No. 76-579, 1976.

26. Strahle, W. C., Muthukrishnan, M., Neale, D. H. and Ramachandra, M.K., "An Investigation of Combustion and Entropy Noise," NASA CR-135220, July 1977.

27. Carbon, M. W., Kutsch, H. J., and Hawkins, G. A., "The Response of Thermocouples to Rapid Gas-Temperature Changes," ASME Trans., July 1950, pp. 655-657.

28. Warren C. Strahle and Muthukrishnan M., "Thermocouple Time Constant Measurement by Cross Power Spectra," AIAA Journal, Vol. 14, No. 11, November 1976, pp. 1642-1644.

29. Hewlett-Packard Fourier Analyzer System 5451A Operating Manual, Hewlett-Packard (1972).

30. Bendat, J. S. and Piersol, A. G., Random Data: Analysis and Measurement Procedures, Wiley-Interscience, New York, 1971.

31. Warren C. Strahle, M. Muthkrishnan, and Douglas H. Neale," Coherence Between Internal and External Noise Generated by a Gas Turbine Combustor," AIAA Journal, Vol. 15, No. 7, July 1977, pp. 1018-1024.

32. Vernon H. Gray, Orlando A. Gutierrez and David Q. Walker, "Assessment of Jets as Acoustic Shields by Comparison of Single and Multitube Suppressor Nozzle Data," Aeroacoustics: Jet and Combustion Noise; Duct Acoustics, ed. H. Nagamatsu, AIAA, New York, 1975, p. 153.

33. Scadron, M. D. and Warshawsky, S., "Experimental Determination of Time Constants and Nusselt Numbers for Bare-Wire Thermocouples in High-Velocity Air Streams and Analytical Approximation of Conduction and Radiation Errors," NACA TN 2599, 1952.